

Alma Mater Studiorum – Università di Bologna

DOTTORATO DI RICERCA IN

CHIMICA

Ciclo XXIX

Settore Concorsuale di afferenza: 03/C2

Settore Scientifico disciplinare: CHIM/04

***Coolant Chemistry Control in Heavy Liquid Metal
cooled Nuclear Systems***

Presentata da: Serena Bassini

Coordinatore Dottorato

Prof. Aldo Roda

Relatore

Prof.ssa Carla Martini

Co-Relatore

Dr. Mariano Tarantino

Esame finale anno 2017

ACKNOWLEDGEMENTS

The present PhD work have been performed in the frame of several funded projects. I am grateful to the Italian Framework Program ENEA-MiSE (ADP ENEA-MiSE, LP2) and the European projects SEARCH (EURATOM FP7, n°295736) and MAXSIMA (EURATOM FP7, n°323312) for the financial support.

Special thanks are for all the people who gave me scientific, technical and moral support during my PhD activity.

I wish to thank my supervisor Prof. Carla Martini for having assisted me also during the PhD program and for her useful and valuable advice, and Dr. Mariano Tarantino for his inspiring guidance which has made me passionate about the heavy liquid metals and the nuclear energy, a world almost unknown for me until few years ago.

I am grateful to Dr. Ivan Di Piazza for all the encouragement and the support in the experimental activities, to Dr. Alessandro Gessi for the scientific guidance at the beginning, and Prof. Alessandro Paglianti for the academic support on the interpretation of some chemical-physical mechanisms playing in heavy liquid metals.

I wish to thank all the colleagues of the Experimental Engineering Division at ENEA Brasimone who contributed to the experimental activities of this PhD thesis. Thanks to Massimo Valdiserri and Daniel Gianotti for the electric support in the operation of the experimental capsules of RACHEL laboratory, Stefano Cati for the technical support in the operation of HELENA facility storage tank, Giuseppe Polazzi and Valerio Sermenghi for the support in the operation of NACIE-UP facility. And a special thank goes to the colleague and friend Andrea Antonelli, for the irreplaceable and valuable help in all the experiment activities and for the continuous moral support.

Thanks also to all my colleagues and friends for the lovely times spent at ENEA Brasimone. Thanks to Andrea Malavasi, Dario Diamanti and Fabiano Serra for the pleasant walks along the lake, and thanks to the friends living in the “Palazzina Ingresso”, Emanuela, Graziella, Bruno, Roberto, Simona and Aldo, for the laughs and the funny chats and for their friendship.

Finally, I sincerely thank my friends for the generous moral support (and for putting up with me during the writing of the thesis!), and my parents Gualtiero and Luisa, whose unconditional love and endless support were essential for the achievement of this goal.

Thank you all.

Serena Bassini

ABSTRACT

Heavy liquid metals (HLMs) such as lead and lead-bismuth eutectic are considered as primary coolants in Lead-cooled Fast Reactor and Accelerator Driven System. A major issue in HLM-cooled nuclear reactors concerns the HLM chemistry and the dissolved oxygen, which has to be balanced within an optimal concentration range to prevent HLM oxidation and minimize corrosion of steels in contact with the HLM via formation of a protective Fe-Cr oxide layer.

In this framework, the present research focused on the development of oxygen sensors based on solid-electrolyte and the control of the oxygen concentration in HLM via gas phase. A baseline study about the performance of different sensors was carried out in laboratory scale. Solid electrolytes such as Yttria Partially and Totally Stabilized Zirconia were considered as well as internal references such as the Pt-air, Bi/Bi₂O₃ and Cu/Cu₂O. The sensors were calibrated in HLM in a wide temperature range to assess the minimum reading temperature and the accuracy. In parallel, the development and the test of a sensor for large HLM pools was performed.

The sensors so manufactured were used to study the HLM deoxygenation with Ar-H₂ gas in different conditions of H₂ concentration, HLM temperature and HLM fluid-dynamic regime. A gas control system was implemented to create safe gas mixtures with flexible H₂ concentration and to obtain easy HLM deoxygenation in small steel capsules and HLM storage tanks. The HLM deoxygenation in dynamic condition was performed with success in a loop facility by injecting Ar-3%H₂ and the effect of metal-oxygen interactions in the HLM was analysed. The results here obtained helped in identifying the factors influencing the process and led to a preliminary and qualitative interpretation of the deoxygenation mechanism.

INDEX

ACKNOWLEDGEMENTS	i
ABSTRACT	ii
ACRONYMS AND ABBREVIATIONS	vi
1. SUMMARY	1
2. INTRODUCTION TO HLM-COOLED NUCLEAR SYSTEMS.....	3
2.1 GENERAL CONTEXT.....	3
2.2 LEAD AND LEAD-BISMUTH PROPERTIES.....	4
2.3 ALFRED AND MYRRHA.....	7
2.4 AIMS AND NEEDS	8
2.5 REFERENCES	9
3. FUNDAMENTALS OF HLM CHEMISTRY.....	12
3.1 GENERAL PRINCIPLES	12
3.2 OXYGEN CONCENTRATION IN HLM.....	15
3.2.1 Maximum Oxygen Concentration	15
3.2.2 Minimum Oxygen Concentration	16
3.2.3 Optimal Oxygen Range	19
3.3 OXYGEN CONTROL METHODS.....	21
3.3.1 Injection of H ₂ and O ₂	21
3.3.2 Injection of H ₂ /H ₂ O mixture	22
3.3.3 PbO mass exchanger	24
3.3.4 Oxygen getters	25
3.4 CHEMISTRY CONTROL IN START-UP OPERATIONS.....	26
3.5 HLM CORROSION AND PROTECTION	27
3.5.1 Fundamentals of HLM corrosion.....	27
3.5.2 Materials protection.....	29
3.6 REFERENCES	33
4. OXYGEN SENSORS FOR HLM	37
4.1 GENERALITY.....	37
4.2 THE ELECTRIC POTENTIAL.....	37
4.3 FEATURES	41
4.3.1 Manufacturing and Use.....	41
4.3.2 Operating Temperature	42

4.3.3	Ceramic Failure and Protection	42
4.3.4	Effect of Impurities	43
4.4	CALIBRATION	44
4.5	OXYGEN SENSORS FOR LARGE HLM POOL	45
4.6	REFERENCES	45
5.	EXPERIMENTAL PART I: DEVELOPMENT OF OXYGEN SENSORS	48
5.1	ASSESSMENT OF THE PERFORMANCE OF OXYGEN SENSORS	48
5.1.1	Aim of the work	48
5.1.2	Experimental Setup	48
5.1.3	Calibration Results.....	51
5.1.4	Error analysis	55
5.1.5	Discussion	56
5.2	OXYGEN SENSORS FOR LARGE HLM POOL FACILITY	58
5.2.1	Aim of the work	58
5.2.2	Experimental Setup	59
5.2.3	Calibration Results.....	61
5.3	EFFECT OF METALLIC IMPURITIES ON SENSOR OUTPUT	64
5.3.1	Experimental Setup	64
5.3.2	Results	64
5.4	CONCLUSIVE REMARKS	66
5.5	REFERENCES	67
6.	EXPERIMENTAL PART II: EXPERIENCES IN OXYGEN CONTROL WITH GAS MIXTURES	69
6.1	OXYGEN CONTROL IN SMALL EXPERIMENTAL CAPSULES (RACHEL LAB)	69
6.1.1	Introduction.....	69
6.1.2	Experimental Setup	69
6.1.3	Results	72
6.2	OXYGEN CONTROL IN HLM STORAGE TANK (HELENA LOOP)	74
6.2.1	Goal of the work.....	74
6.2.2	Experimental Setup	75
6.2.3	Results	76
6.3	OXYGEN CONTROL IN HLM LOOP FACILITY (NACIE-UP).....	79
6.3.1	Goal of the work.....	79
6.3.2	Description of NACIE-UP facility	80
6.3.3	Experimental Setup	81

6.3.4	Results	84
6.4	CONCLUSIVE REMARKS	88
6.5	REFERENCES	89
7.	CONCLUSIONS AND FUTURE WORK.....	91
	LIST OF PUBLICATIONS	93

ACRONYMS AND ABBREVIATIONS

AdP ENEA-MiSE	Framework Program ENEA - Italian Ministry of Economic Development
ADS	<u>A</u> ccelerator <u>D</u> riven <u>S</u> ystem
AFA	<u>A</u> ustenitic <u>F</u> orming <u>A</u> ustenite steel
AISI	<u>A</u> merican <u>I</u> ron and <u>S</u> teel <u>I</u> nstitute
ALFRED	<u>A</u> dvanced <u>L</u> ead <u>F</u> ast <u>R</u> eactor <u>E</u> uropean <u>D</u> emonstrator
ALLEGRO	European Helium-cooled Gas Fast Reactor
ASTRID	<u>A</u> dvanced <u>S</u> odium <u>T</u> echnological <u>R</u> eactor for <u>I</u> ndustrial <u>D</u> emonstration
BID1	<u>B</u> rasimone gas- <u>I</u> njection <u>D</u> evice 1 (LBE-cooled small pool facility at ENEA Brasimone)
BREST	Russian Lead-cooled Fast Reactor
CEA	<u>C</u> ommissariat à l' <u>É</u> nergie <u>A</u> tomique et aux <u>É</u> nergies Alternatives (France)
CRAFT	LBE-cooled loop facility at SCK·CEN
CIRCE	<u>C</u> irculation <u>E</u> utectic (LBE-cooled large pool facility at ENEA Brasimone)
CVR	<u>C</u> entrum <u>V</u> ýzkumu <u>Ř</u> ež (Czech Republic)
DACS	<u>D</u> ata <u>A</u> cquisition and <u>C</u> ontrol <u>S</u> ystem
DELTA	<u>D</u> evelopment of <u>L</u> ead alloy <u>T</u> echnical <u>A</u> pplications (LBE-cooled loop facility in LANL)
DHR	<u>D</u> ecay <u>H</u> eat <u>R</u> emoval
EDS	<u>E</u> nergy <u>D</u> ispersion <u>S</u> pectroscopy
ELSY	<u>E</u> uropean <u>L</u> ead-cooled <u>S</u> ystem (EU Lead-Fast Reactor concept)
ENEA	Italian National Agency for New Technologies, Energy and Sustainable Economic Development (Italy)
ESNII	<u>E</u> uropean <u>S</u> ustainable <u>N</u> uclear <u>I</u> ndustrial <u>I</u> nitiative
EURATOM	European Atomic Energy Community
F/M	<u>F</u> erritic/ <u>M</u> artensitic steel
FAC	<u>F</u> low <u>A</u> ccelerated <u>C</u> orrosion
FALCON	<u>F</u> ostering <u>A</u> lfred <u>C</u> ONstruction (European Consortium)
FPS	<u>F</u> uel <u>P</u> in <u>S</u> imulator
FR	<u>F</u> ast <u>R</u> eactor
GDC	<u>G</u> adolinium- <u>D</u> oped <u>C</u> eria
GESA	<u>G</u> epulste <u>E</u> lektronen <u>S</u> trahl <u>A</u> nlage (German coating deposition technology)
GFR	<u>G</u> as <u>F</u> ast <u>R</u> eactor
GIF	<u>G</u> eneration IV <u>I</u> nternational <u>F</u> orum
HAD	<u>H</u> ot <u>D</u> ipping <u>A</u> luminizing (coating deposition technology)

HELENA	<u>H</u> Heavy <u>L</u> iquid metal <u>E</u> xperimental loop for advanced <u>N</u> uclear <u>A</u> pplications (Pb-cooled loop facility at ENEA Brasimone)
HELIOS	LBE-cooled small pool facility in South Korea
HLM	<u>H</u> heavy <u>L</u> iquid <u>M</u> etal (Pb and LBE)
HX	<u>H</u> eat <u>e</u> Xchanger
ICN	<u>I</u> nstitutul de <u>C</u> ercetari <u>N</u> ucleare (Romania)
IPPE	<u>I</u> nstitute of <u>P</u> hysical and <u>P</u> ower <u>E</u> ngineering (Russia)
KIT	<u>K</u> arlsruhe <u>I</u> nstitute of <u>T</u> echnology (Germany)
KOCOS	LBE-cooled small pool facility at KIT
LANL	<u>L</u> os <u>A</u> lamos <u>N</u> ational <u>L</u> aboratory
LBE	<u>L</u> ead- <u>B</u> ismuth <u>E</u> utectic
LEADER	<u>L</u> ead-cooled <u>E</u> uropean <u>A</u> dvanced <u>D</u> emonstration <u>R</u> eactor (7 th Framework Program EU)
LECOR	<u>L</u> ead <u>C</u> ORrosion (Pb-cooled loop facility at ENEA Brasimone)
LFR	<u>L</u> ead <u>F</u> ast <u>R</u> eactor
LPSS	<u>L</u> ow <u>P</u> ressure <u>P</u> lasma <u>S</u> pray (coating deposition technology)
LSM	<u>L</u> anthanum <u>S</u> trontium-doped <u>M</u> anganite
MA	<u>M</u> inor <u>A</u> ctinide
MAXSIMA	<u>M</u> ethodology, <u>A</u> nalysis and <u>e</u> Xperiments for the <u>S</u> afety <u>I</u> n <u>M</u> YRRHA <u>A</u> ssessment (7 th Framework Program EU)
MOX	<u>M</u> ixed <u>O</u> X fuel
MRS	<u>M</u> olten <u>S</u> alt <u>R</u> eactor
MYRRHA	<u>M</u> ulti-purpose <u>h</u> ybrid <u>R</u> esearch <u>R</u> eactor for <u>H</u> igh-tech <u>A</u> pplications
NACIE-UP	<u>N</u> atural <u>C</u> irculation <u>E</u> xperiment <u>U</u> P-grade (LBE-cooled loop facility at ENEA Brasimone)
P&ID	<u>P</u> iping & <u>I</u> nstrumentation <u>D</u> igram
PID	<u>P</u> roportional <u>I</u> ntegral <u>D</u> erivative
PLC	<u>P</u> rogrammable <u>L</u> ogic <u>C</u> ontroller
PLD	<u>P</u> ulsed <u>L</u> aser <u>D</u> eposition (coating deposition technology)
R&D	<u>R</u> esearch & <u>D</u> evelopment
RACHEL	<u>R</u> eaction and <u>A</u> dvanced <u>C</u> HEmistry of <u>L</u> ead (chemical laboratory at ENEA Brasimone)
SCK-CEN	<u>S</u> tudiecentrum voor <u>K</u> ernenergie - <u>C</u> entre d'Étude de l'énergie <u>N</u> ucléaire (Belgium)
SEARCH	<u>S</u> afe <u>E</u> xploitAtion <u>R</u> elated <u>C</u> HEmistry for HLM reactors (7 th Framework Program EU)
SET-Plan	<u>S</u> trategic <u>E</u> nergy <u>T</u> echnology <u>P</u> lan
SFR	<u>S</u> odium <u>F</u> ast <u>R</u> eactor

SNETP	<u>S</u> ustainable <u>N</u> uclear <u>E</u> nergy <u>T</u> echnology <u>P</u> latform
SOFC	<u>S</u> olid <u>O</u> xide <u>F</u> uel <u>C</u> ell
SS	<u>S</u> tainless <u>S</u> teel
SSTAR	<u>S</u> mall <u>S</u> ecure <u>T</u> ransportable <u>A</u> utonomous <u>R</u> eactor (USA Lead-Fast Reactor concept)
STELLA	LBE-cooled loop facility at CEA
SCWR	<u>S</u> upercritical <u>W</u> ater <u>R</u> eactor
TC	<u>T</u> hermo <u>c</u> ouple
VHTR	<u>V</u> ery <u>H</u> igh <u>T</u> emperature <u>R</u> eactor
YPSZ	<u>Y</u> ttria <u>P</u> artially <u>S</u> tabilized <u>Z</u> irconia
YTSZ	<u>Y</u> ttria <u>T</u> otally <u>S</u> tabilized <u>Z</u> irconia

1. SUMMARY

Heavy Liquid Metals (HLMs) such as liquid lead and lead-bismuth eutectic (LBE) are candidate coolants in Generation IV Fission Nuclear Reactors thanks to their nuclear, thermo-physical and chemical properties particularly suitable for this purpose. Specifically, liquid lead and lead-bismuth are considered as primary coolants in the Lead-cooled Fast Reactor (LFR) and Accelerator Driven System (ADS).

One of the major issue in the development of future HLM-cooled nuclear reactors regards the control of the HLM chemistry, which is strongly related to the issue of the dissolved oxygen in the melt. Indeed, the oxygen dissolved can have both a beneficial and negative effect depending on its concentration in the liquid metal. Oxygen enables the formation of a self-healing Fe-Cr oxide layer above steel surfaces, acting as a barrier against the HLM and reducing the corrosion of structures and components as well as the release of corrosion products in the HLM. On the other hand, oxygen is detrimental when its concentration reaches the solubility level. In such conditions, coolant oxides may form and deposit above the inner walls of structures and components with degradation of the heat transfer or even plugging of the circulation. Thus oxygen has to be balanced within an optimal concentration range by means of adequate operative procedures and on-line devices aimed at achieving and keeping constant the target oxygen concentration. In addition, high-strength oxygen sensors are required to monitor the oxygen concentration with reliability and accuracy in the HLM environment.

The present PhD thesis describes the research activity carried out over three years about the topic of the HLM chemistry. The activity was performed at the ENEA Research Centre of Brasimone (Camugnano, Italy) and was divided in two experimental parts:

- 1) study and development of oxygen sensors for various HLM environments;
- 2) control and reduction of the oxygen concentration in HLM with H₂ containing gas mixtures.

Prior to the experimental activity, an intensive study of the chemical-physical behaviour of HLM and a deep review about the state of the art of oxygen sensors and oxygen control methods was performed and reported in this thesis.

Then, potentiometric oxygen sensors based on solid electrolytes were developed for the measurement of the oxygen concentration. First, a baseline study on the performance of different oxygen sensors was carried out in small amounts of static HLM. Solid electrolytes such as Yttria Partially Stabilized Zirconia (YPSZ) and Yttria Totally Stabilized Zirconia (YTSZ) were considered in the study as well as different internal references such as the Pt-air, Bi/Bi₂O₃ and Cu/Cu₂O systems. The oxygen sensors so manufactured were calibrated in HLM in a wide temperature range to evaluate their minimum reading temperature and the accuracy. The effect of dissolved metal impurities on the sensor electric potential was also analysed. In parallel, the development of a sensor prototype for large HLM pool facility was performed. The scope of this activity is to equip the large HLM pool facility CIRCE (CIRCulation Eutectic) in Brasimone with reliable and accurate oxygen sensors to monitor the oxygen distribution in the pool configuration during the operation. High mechanical and thermal strength and excellent tightness are mandatory for this type of sensor in order to bear the huge pressures exercised by the HLM in the pool. Several configuration of the sensor were considered and the selected final configuration was calibrated and tested with success at different temperatures in the HLM storage tank of the loop facility HELENA (HEavy Liquid metal Experimental loop for advanced Nuclear Applications) in Brasimone.

Concerning the control of the oxygen concentration, the effect of argon mixtures with H₂ on the deoxygenation of the HLMs was investigated from a qualitative point of view in different conditions of H₂ concentration, HLM temperature, HLM amount and HLM fluid-dynamic regime (static and flowing). First, a dedicated gas control system was implemented in the chemical laboratory RACHEL

(Reaction and Advanced CHEmistry of Lead) in Brasimone to create gas mixtures with different H₂ concentrations and with the purpose to obtain rapid deoxygenation of small amounts of static HLM inside small experimental capsules. Then, the same gas control system was used to perform the deoxygenation in larger scale experiments inside HELENA HLM storage tank, which represents an important step in start-up operations of an experimental facility. The oxygen sensor prototype developed for the application in HLM pools was used to monitor the trend of the oxygen concentration over time during the tests. Finally, the deoxygenation of the HLM was performed in dynamic conditions in the thermal-hydraulic loop facility NACIE-UP (NAtural Circulation Experiment UP-grade) in Brasimone by injecting Ar-3%H₂ mixture in the riser column. An oxygen sensor with Cu/Cu₂O reference system was manufactured for the purpose and installed in the expansion vessel of the loop. The magnitude of the deoxygenation achieved was analysed and compared with results obtained in static conditions and the effect of metal-oxygen interactions established in the melt was considered. The experimental results allowed to identify the factors influencing the HLM deoxygenation process with H₂ gas, even if the data are preliminary and the chemical-physical interpretation of the process still qualitative. In addition, the experiment performed in NACIE-UP loop highlighted some critical aspects concerning the oxygen control in experimental facility and the information obtained will be useful in future to develop a complete and efficient oxygen control system for HLM-cooled facility.

2. INTRODUCTION TO HLM-COOLED NUCLEAR SYSTEMS

2.1 GENERAL CONTEXT

According to the forecast by the International Energy Agency, the current increase of world population will require a growth of the global energy demand of 37 % by 2040 [1].

Today, the major share of energy needs is covered by fossil fuel resources. Indeed, around 80 % of the worldwide energy sources is shared between oil, coal and natural gas and the remaining % is covered by renewable and nuclear energy sources [1]. With a growing world population and a growing energy consumption per capita, fossil fuel resources are becoming scarce while global ecological impacts due to greenhouse gas emissions is increasing day by day.

Aiming at cutting greenhouse gas emissions and facing the large foreseen energy demand, the EU has launched in 2007 a coordinated strategy to deliver new safe, competitive and low-carbon technologies to the European market. The Strategic Energy Technology Plan (SET-Plan) was defined by the European Commission to speed up the development of clean, efficient and low-carbon energy technologies between now and 2050 [2,3]. The energy technologies that have been identified by EU as a priority are six: wind, solar, smart electricity grids, bioenergy, CO₂ capture and storage and nuclear fission [2,3].

In the framework of the European SET-Plan, the Sustainable Nuclear Energy Technology Platform (SNETP) was launched to support the nuclear fission research and innovation [4]. Within SNETP, the European Sustainable Nuclear Industrial Initiative (ESNII) constitutes one of the three structural pillars. The purpose of ESNII is to support the technological development of the Fast Reactor (FR) and Accelerator Driven System concept [5]. Thanks to a closed-fuel cycle and an high efficiency of fuel use and burning, these technologies possess high sustainability, safety and reliability features, making them completely innovative.

The reactor concepts considered within ESNII are the following [5]:

- Sodium-cooled Fast Reactor (SFR), fast neutron reactor cooled by liquid sodium. The reactor concept is represented by ASTRID reactor (Advanced Sodium Technological Reactor for Industrial Demonstration), to be built in France and whose development is supported by a consortium led by CEA (Commissariat à l'Énergie Atomique et aux Énergies Alternatives, France) [5,6].
- Lead-cooled Fast Reactor (LFR), fast neutron reactor cooled by liquid lead. The reactor concept is represented by ALFRED reactor (Advanced Lead Fast Reactor European Demonstrator), which shall be built in Pitesti (Romania). The development is supported by the FALCON Consortium (Fostering ALfred CONstruction), which is composed of ANSALDO NUCLEARE and ENEA (Italy), ICN (Institutul de Cercetari Nucleare, Romania) and CVR (Centrum Výzkumu Řež, Czech Republic) [5,7].
- Accelerator Driven System (ADS), critical or sub-critical reactor cooled with LBE aimed at demonstrating the feasibility of transmutation of long-lived radioactive waste. The European irradiation facility MYRRHA (Multi-purpose hYbrid Research Reactor for High-tech Applications) should act as pilot plant for LFR and demonstrator for ADS, being able to operate both in critical and sub-critical mode. MYRRHA will also support the technology development of the fast reactor concept, in particular for material, components and fuel irradiation tests. MYRRHA is developed under the leadership of SCK-CEN (Belgium) [5,8,9].
- Gas-cooled Fast Reactor (GFR), fast neutron reactor cooled by helium and represented by the small-power demonstrator ALLEGRO supported by Slovakia, Czech Republic, Hungary, Poland and CEA [5,10].

The technological roadmap regarding the development and construction of the four reactor concepts supported by ESNII is depicted in Fig. 2.1. In these context, MYRRHA acts as both ADS and a supporting facility to perform irradiation tests about structural materials and components.

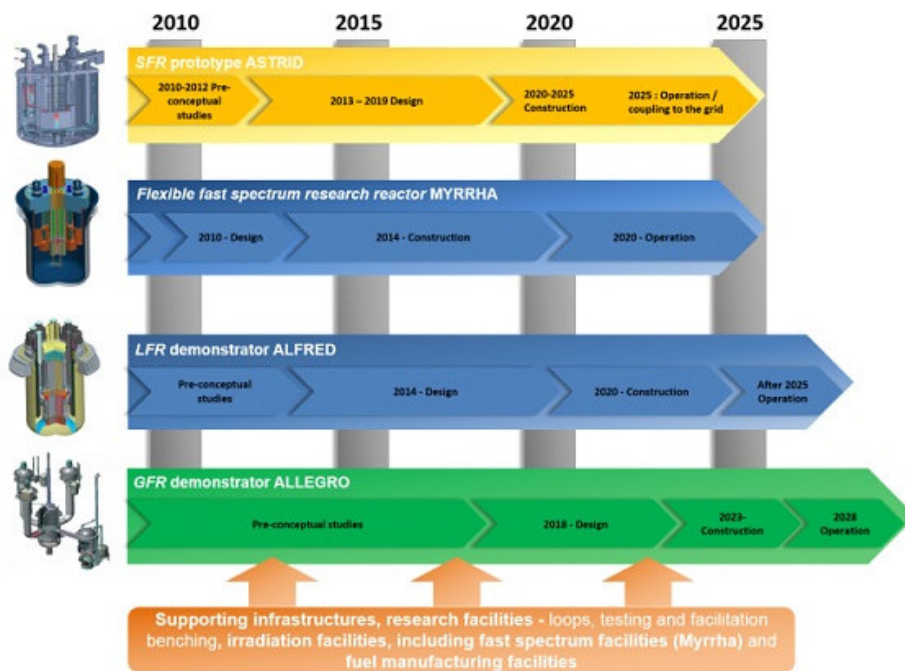


Fig. 2.1: Technological Roadmap of FR and ADS according to ESNII [5].

SFR, LFR and GFR concepts are included in the “Generation IV”, which constitutes the future generation of nuclear systems aimed at replacing previous generation II and III of thermal neutron reactors cooled by water. Besides the three FR concepts, Generation IV includes also thermal reactors such as the Molten Salt Reactor (MSR), the Supercritical Water-cooled Reactor (SWCR) and the Very-High-Temperature Reactor (VHTR) [11-13]. Generation IV nuclear systems are supported by the Generation IV International Forum (GIF), an initiative founded in 2000 and that today has 13 members worldwide (among which EU through the European Atomic Energy Community, EURATOM) [11]. Important R&D activities on FRs and other innovative thermal reactors are currently coordinated worldwide through GIF. Europe, through SNETP and ESNII, has defined its own strategy based on FRs, considered the most likely to meet Europe’s energy needs in terms of safety, sustainability, proliferation resistance and economic competitiveness.

In this framework, Italy is involved in the development of Lead-cooled systems only, i.e. MYRRHA and in particular ALFRED, being Italy among the first to join the FALCON Consortium through ANSALDO NUCLEARE and ENEA. Several R&D activities in support of the design and development of MYRRHA and ALFRED are performed in the context of European projects as well as the Italian Framework Program between ENEA and the Italian Ministry of Economic Development (MISE).

2.2 LEAD AND LEAD-BISMUTH PROPERTIES

The study of lead as nuclear coolant started in 1950s at the Institute of Physics and Power Engineering (IPPE) in Russia (USSR at the time) under the supervision of A.I. Leipunsky [14]. In those years, USA and USSR concurrently began the development of a liquid metal cooled nuclear power facility to be employed as a propulsion system for nuclear submarines [14]. In USSR LBE was chosen as coolant, while in USA sodium was chosen for the superior thermal-hydraulic properties.

The research carried out by Leipunsky led to the operation of the 27/VT LBE-cooled reactor prototype in 1958 [15]. Following that success, eight nuclear submarines cooled with LBE were built afterwards. K-27 submarine, known with the Russian designation “project 645”, was commissioned in 1963. The seven other submarines, known with the Russian designation “project 705”, were commissioned in 1977-1981. The latter submarines were also known as “Alpha class” according to NATO designation. The hull of the Alpha submarines was made of titanium and so extremely light. Thanks to the use of titanium and lead technology, these submarines were and are still the fastest submarines ever developed [15]. Conversely the operation of sodium-cooled nuclear submarines (known as “Sea Wolf class”) led to several accidents caused by the contact of sodium with water and air. Sodium-cooled reactors were so quickly dismantled by USA and replaced by pressurized water ones [14].

Sustainability and safety features of the LFR are mainly due to neutron, physical and chemical properties of lead and LBE (eutectic composition: 45.5% Pb, 55.5% Bi), which some are listed in Tab. 2.1 [16-18]. The properties of sodium coolant are reported for comparison. The physical and chemical features of coolants determine the maximal potential non-nuclear energy per volume unit stored in the system (including thermal energy, coolant compression energy and chemical energy) which may be released in case of accident [18]. Lead and LBE have a significantly lower maximal potential energy factor (around 1) compared to sodium and water coolant (equal to 10 and 21.9 respectively), which means higher intrinsic safety for lead and LBE cooled nuclear plants and simplification for safety measures [18].

Tab. 2.1: Neutron, physical and chemical properties of lead, LBE and sodium coolants [16-18].

Coolant	Pb	LBE	Na
Melting Point (°C)	327	125	98
Boiling Point (°C)	1745	1670	883
Relative Moderating Power	1.0	0.8	1.8
Neutron absorption cross-section (1MeV)	6.00	1.42	0.23
Density at 450°C (kg/m ³)	10520	10150	845
Heat Capacity at 450°C (kJ/kg·K)	147.3	146	1.3
Thermal Conductivity at 450°C (W/m·K)	17.1	14.2	68.8
Kinematic Viscosity at 450°C (m ² /s)	$1.9 \cdot 10^{-7}$	$1.4 \cdot 10^{-7}$	$3 \cdot 10^{-7}$
Chemical Reactivity with O ₂ and H ₂ O	negligible	negligible	very high
Maximal Potential Energy (GJ/m³)	≈ 1.1	≈ 1.1	≈ 10

Lead and LBE coolants have low neutron absorption cross-section and moderating power (unlike water), which allows to design reactor cores working with fast neutron spectrum. Fast neutrons increase the sustainability of the nuclear fuel usage thanks to the conversion of fertile uranium into fissile material (formation of Pu-239 from U-238 by neutron capture) and also to the improvement of the performance of fuel burning and transmutation of long-life fission products and minor actinides (MAs) when compared to current Generation II and III reactors [15,19,20].

LFRs also contribute to the reduction of radioactive waste volume thanks to a closed-fuel cycle. Pu and MAs (mainly Np, Am and Cm) are the main responsible for the high radiotoxicity of nuclear waste in Generation II and III, requiring storage times in geological sites of million years. In a closed fuel cycle, nuclear wastes produced in LFRs do not contain Pu and MAs as they are recycled and reused [9,20,21]. Thanks to the closed-fuel cycle and the high transmutation performance, the waste volumes from a LFR and the relative radiotoxicity are significantly reduced, allowing the storage for only 300-400 years (see Fig. 2.2).

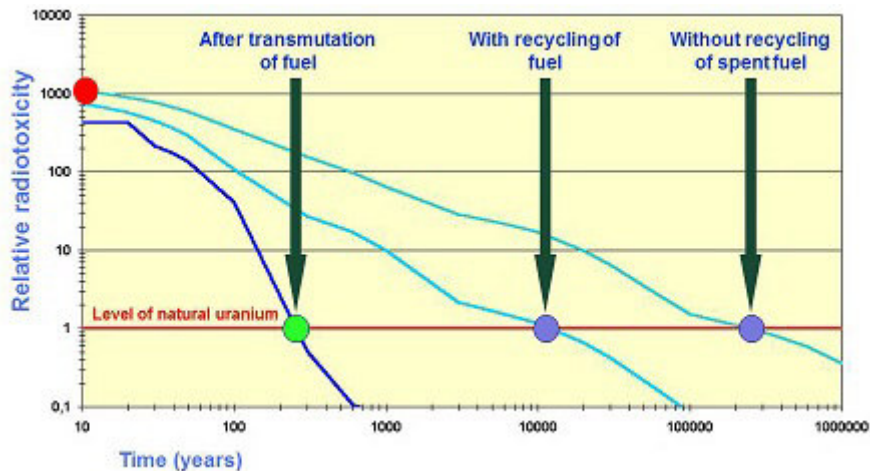


Fig. 2.2: Radiotoxicity of nuclear waste with and without transmutation and closed-fuel cycle [9].

From the point of view of safety, lead and LBE are characterized by high thermal conductivity and heat transport capability which provides an excellent heat transfer efficiency during normal operating conditions, transient regimes, as well as during decay heat removal [15,19]. Lead and LBE have also high boiling point and low vapour pressure even at high temperatures. These features allows the operation of a LFR at atmospheric pressure (unlike current water-cooled reactors, working at hundreds of bar) [14,20-23]. Moreover, the high boiling point of lead alloys excludes the probability of voids formation within the core (probability as not to exclude in SFR) [19,20,22,23]. The high density of lead and LBE significantly reduces the risk of fuel compaction in case of core melting (even if unlikely) [20,23]. Conversely, this scenario is not negligible for water and sodium cooled reactors, for which the risk of partial or complete core melting is less reduced than for a LFR. Lead has also the capability to shield γ radiations and trap volatile fission products such as Iodine and Cesium reducing the risk of exposure for operators [23]. Finally, lead and LBE have very low chemical reactivity with air and water (unlike sodium) excluding strong criticality such as fires and explosions in case of coolant leakage from the primary system [21-23]. This aspect introduces also an economic advantage since an intermediate coolant circuit is not needed for the heat removal [21-23].

Concerning the proliferation resistance and the public safety, the use of mixed U and Pu oxides (MOX) and MAs in the fuel makes the LFR unemployable for the production of weapon-grade plutonium [21]. The neutron properties of lead allow also the design of long-live cores hindering the Pu production. In addition, the use of a coolant with high boiling point, operating at low pressure and chemically inert with air and water increases the physical protection of the population living in the surrounding areas of the nuclear site, thus reducing the need for complex protection systems in case of terrorist attacks [19,21].

Comparing lead and LBE, the latter has a lower melting point (125°C), which reduces the problems connected with freezing [20,22]. A critical drawback with the use of LBE is the formation of Po-210 from Bi-209 by neutron capture. Po-210 is toxic and a strong α emitter ($T_{1/2} = 138$ days) and forms volatile compounds when in contact with air or water [14,19]. This issue requires specific devices for Po treatment and safety systems in case of leakage. Lead instead is more available on earth crust, is less expensive and produces lower amount of Po-210 (by a factor of 10^4) [14,19]. For this reason most of the civil reactor projects under development (e.g. BREST, STAR, ELSY) are based on pure lead as coolant. LBE is mainly reserved to experimental reactors thanks to the lower freezing temperature and for the large power density that can be obtained even at low operating temperature [23]. The drawback of pure lead is the high melting point (327°C), which requires engineering strategies to prevent freezing anywhere in the system, particularly during reactor shut down, maintenance and refuelling steps [20,22,23].

2.3 ALFRED AND MYRRHA

ALFRED and MYRRHA are the two reactor concepts cooled with HLM (lead and lead-bismuth eutectic) supported in Europe through ESII. ALFRED aims to be the European LFR demonstrator, with the purpose to show the viability of the LFR technology for the employment in future commercial power plants. MYRRHA aims to be the ADS pilot with the goal to demonstrate the feasibility of the transmutation of fuel and MAs but also to provide scientific support to the study of materials and components operating under a fast spectrum regime.

ALFRED has been conceptualized under the leadership of ANSALDO NUCLEARE in the framework of the European project LEADER (Lead-cooled European Advanced DEMonstration Reactor, 7th Framework Program EU) [24]. ALFRED is a pool-type reactor cooled with lead. The pool-type concept involves the containment of all the primary coolant in the reactor vessel, thus excluding issues related to circulation of the coolant outside the main vessel. Consequently, the configuration provides that all the components of the primary loop (fuel assemblies, pumps, steam generators, etc.) are introduced in the main vessel [7,24]. The design of ALFRED reactor (as conceptualized during the LEADER project) is shown in Fig. 2.3.

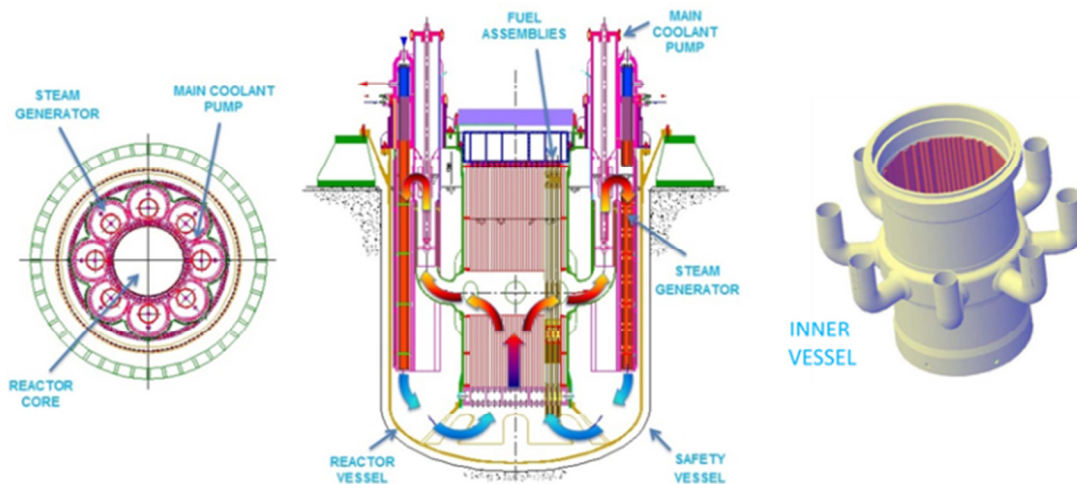


Fig. 2.3: Configuration and specifications of ALFRED LFR. Power: 300 MWth; Core inlet-outlet temperature: 400-480°C; max. fuel cladding temperature: 550°C [7,24].

MYRRHA ADS consists of a high-power proton accelerator, a HLM spallation target able to produce neutrons when bombarded by a high-power proton beam, and a sub-critical core [8,9]. When the proton-beam from the accelerator hits the spallation target, several spallation reactions occur, generating a large number of fast neutrons. These neutrons are in charge to sustain the nuclear chain reaction. The ADS is designed with the purpose to burn fuel containing MAs, which instability may generate problems in maintaining the critical mode. Furthermore, the ADS provides an important benefit from the point of view of safety: the power is modulated by controlling the beam current and the nuclear system can be shut down in any moment by cutting off the proton beam [8,9]. The design of MYRRHA is shown in Fig. 2.4: basically, it is a LBE-cooled pool-type reactor with the components of the primary loop all introduced in the main vessel. An external accelerator generates a proton-beam which is directly sent to the spallation target (consisting always in LBE) to start and sustain the nuclear chain reaction.

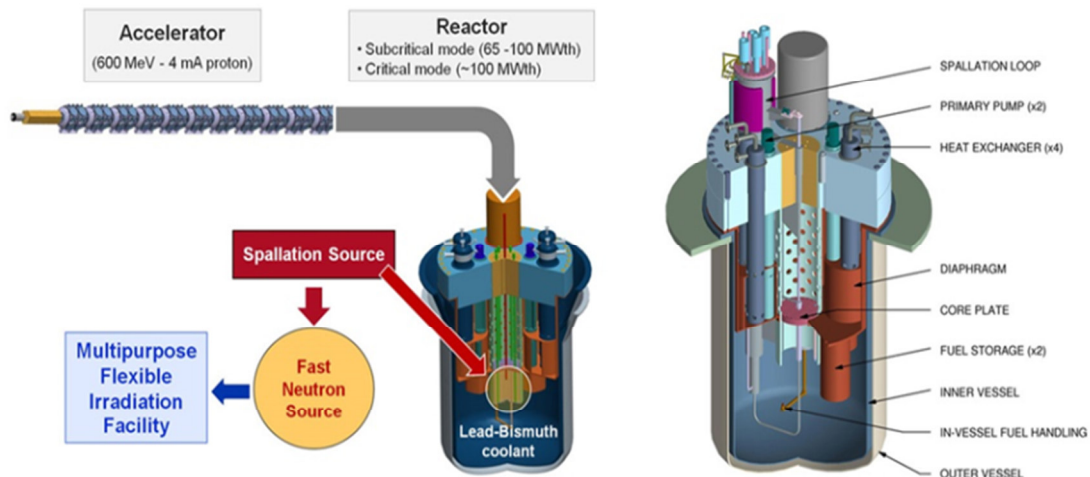


Fig. 2.4: Configuration and specifications of MYRRHA ADS. Power: 100 MWth; Core inlet-outlet LBE temperature: 270-410°C; max. fuel cladding temperature: 470°C [8,9].

2.4 AIMS AND NEEDS

The main technological issues in the development of lead-cooled nuclear system are related to the chemistry of the lead coolant and its interaction with structural materials.

Lead and LBE absorb oxygen forming different Pb and Bi oxides according to the level of oxygen contamination in the coolant. Such oxides are very critical, being able to deposit above the reactor components and thus to affect coolant thermal-hydraulic features (circulation and heat transfer). This situation occurred during the operation of Russian K-27 nuclear submarine in 60', where the plugging of piping and components due to the deposition of coolant oxides and corrosion products led to a severe damage of the core. There is a broad agreement inside the scientific community about the need to control the oxygen concentration at values far from the oxygen solubility in order to avoid the risk of plugging.

In addition, lead and LBE are highly aggressive towards conventional structural steels (even if pure lead is less corrosive than LBE at the same temperature). The corrosion by flowing lead and LBE is a major issue and protection strategies are mandatory to avoid severe damage of structures, especially those one that are exposed to the highest temperature and neutron irradiation doses (e.g. the fuel cladding and fuel assemblies at 500-550°C) [23,25]. Among the various methods considered for the protection in HLM, the most viable options for the short-term include the use of coatings for structures exposed above 480°C and the control of the oxygen dissolved in the coolant to preserve the structures at lower temperatures [23,25].

The oxygen control takes place through the balancing of the oxygen concentration to a target level which is sufficient to ensure the passivation of steel structures by formation of Fe-Cr oxide layer above the surface. The ploy is realized to reduce steel corrosion at an acceptable value, even if its effectiveness is limited to structures exposed up to 480°C due to the loss of protectiveness of the oxide layer at high temperature. One of the technological gaps is then associated with fuel cladding structures, which requires high resistance in terms of HLM corrosion, fretting, thermal creep, irradiation embrittlement and swelling [23,25]. In such conditions, the oxygen control technology is no more effective and the development of high-performance coatings are mandatory to face all these issues.

Fig. 2.5 shows the R&D needs for lead-cooled nuclear reactors [23]. A deep qualification of candidate materials is needed in terms of HLM corrosion, fretting, thermal creep resistance, irradiation embrittlement and swelling. In parallel, the coolant chemistry control and, in particular, the oxygen control technology requires deep investigations about suitable devices, able to control the oxygen

concentration in pool reactors. The oxygen control also needs oxygen sensors able to operate in HLM with accuracy and reliability. Sensors based on solid electrolytes have been developed in the last decade but their application mostly involves small scale systems (small pools and loops) and a technology sufficiently resistant for large HLM pools is not yet available. Aiming at reducing the technological gap about the topic of the HLM chemistry and the oxygen control technology, the present thesis was focused on the development of oxygen sensors for small scale experiments and also for large HLM pools, and the control of the oxygen concentration with H₂ gas was studied and implemented for several HLM environments.

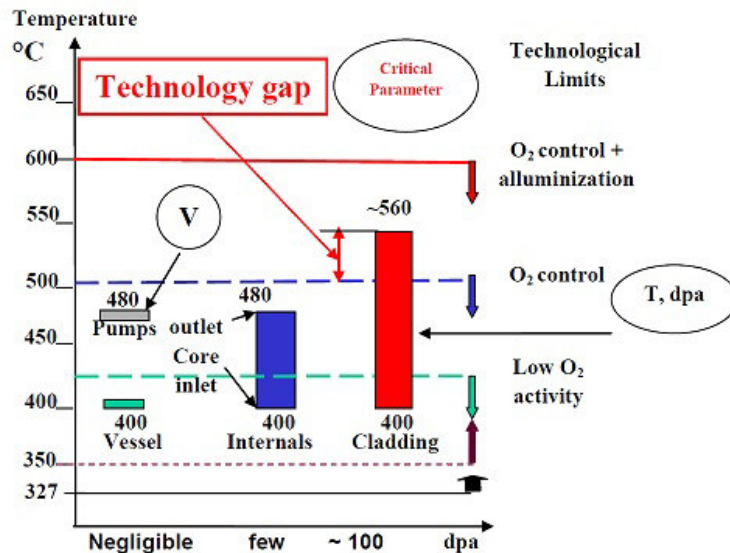


Fig. 2.5: R&D needs and technological gaps in the development of Lead-cooled nuclear reactors [23].

2.5 REFERENCES

- [1] OECD/IEA, "World Energy Outlook", 2014, available at: www.iea.org/publications/freepublications/publication/WEO_2014_ES_English_WEB.pdf
- [2] "Towards a European Strategic Energy Technology Plan", COM(2006) 847.
- [3] "An energy policy for Europe", COM(2007) 1, SEC(2007) 12, 10, January 2007.
- [4] EURATOM Directorate-General for Research, "The Sustainable Nuclear Energy Technology Platform. A vision report", Report n° EUR22842, 2007, available at: www.snetp.eu/wp-content/uploads/2014/05/sne-tp_vision_report_eur22842_en.pdf
- [5] Sustainable Nuclear Energy Technology Platform (SNETP) Secretariat, "ESNII: The European Sustainable Nuclear Industrial Initiative. A contribution to the EU Low Carbon Energy Policy: Demonstration Programme for Fast Neutron Reactors", Concept Paper, October 2010, available at: www.snetp.eu/publications/
- [6] C. Latgé, "ASTRID (Advanced Sodium Technological Reactor for Industrial Demonstration) project: Status and main challenges", Workshop on Thermal-hydraulics and Thermo-mechanical Issues for Safety, 12-13 May 2016, Brasimone, Italy.
- [7] A. Alemberti, "ALFRED: The European Lead Fast Reactor Demonstrator", 5th Annual International Conference on Sustainable Development through Nuclear Research and Education, 16-18 May 2012, Pitesti, Romania.
- [8] H. Aït Abderrahim, P. Baeten, D. De Bruyn, R. Fernandez, "MYRRHA - A multi-purpose fast spectrum research reactor", *Energ. Convers. Manage.* 63 (2012) 4-10.

- [9] M. Schyns, H. Aït Abderrahim, P. Baeten, R. Fernandez, D. De Bruyn, "The MYRRHA ADS Project in Belgium Enters the Front End Engineering Phase", Proceedings of the 2nd International Symposium on Science at J-PARC - Unlocking the Mysteries of Life, Matter and the Universe, JPS Conf. Proc. 8, 001001 (2015).
- [10] P. Vácha, "ALLEGRO project: Status and perspectives", Workshop on Thermal-hydraulics and Thermo-mechanical Issues for Safety, 12-13 May 2016, Brasimone, Italy.
- [11] OECD Nuclear Energy Agency for the Generation IV International Forum, "Technology Roadmap Update for Generation IV Nuclear Energy Systems", January 2014, available at: www.snetp.eu/wp-content/uploads/2014/05/sne-tp_vision_report_eur22842_en.pdf
- [12] T. Abram, S. Ion, "Generation-IV nuclear power: A review of the state of the science", Energ. Policy 36 (2008) 4323-4330.
- [13] G. Locatelli, M. Mancini, N. Todeschini, "Generation IV nuclear reactors: Current status and future prospects", Energ. Policy 61 (2013) 1503-1520.
- [14] B. F. Gromov, Yu. S. Belomitcev, E. I. Yefimov, M. P. Leonchuk, P. N. Martinov, Yu. I. Orlov, D. V. Pankratov, Yu. G. Pashkin, G. I. Toshinsky, V. V. Chekunov, B. A. Shmatko, V. S. Stepanov, "Use of lead-bismuth coolant in nuclear reactors and accelerator-driven systems", Nucl. Eng. Des. 173 (1997) 207-217.
- [15] A. V. Zrodnikov, V. I. Chitaykin, B. F. Gromov, O. G. Grigoryv, A. V. Dedoul, G. I. Toshinsky, Yu. G. Dragunov, V. S. Stepanov, "Use of Russian technology of ship reactors with lead-bismuth coolant in nuclear power", Proceedings of an Advisory Group Meeting in Obninsk, Russian Federation, 20-24 July 1998, IAEA-TECDOC-1172 (2000).
- [16] IAEA "Liquid metal coolants for Fast Reactors cooled by sodium, lead and lead-bismuth eutectic", Nuclear Energy Series n° NP-T-1.6, 2012, Vienna, Austria.
- [17] OECD/NEA, "Handbook on lead-bismuth eutectic alloy and lead properties, materials compatibility, thermal-hydraulics and technologies", 2015.
- [18] G. I. Toshinsky, O. G. Komlev, I. V. Tormyshev, V. V. Petrochenko, "Effect of Potential Energy Stored in Reactor Facility Coolant on NPP Safety and Economic Parameters", World Journal of Nuclear Science and Technology 3, (2013) 59-64.
- [19] G. I. Toshinsky, O. G. Grigoryev, E. H. Pylchenkov, D. E. Skorikov, O. I. Komkova, "Comparative analysis of coolants for FBR of future nuclear power", Proceeding of the 9th International Conference On Nuclear Engineering (ICONE-9), 8-12 Apr 2001, Nice, France.
- [20] A. Alemberti, V. Smirnov, C. F. Smith, M. Takahashi, "Overview of lead-cooled fast reactor activities", Prog. Nucl. Energ. 77 (2014) 300-307.
- [21] A. Alemberti, "The Lead Fast Reactor: An opportunity for the future?", Engineering 2 (2016) 59-62.
- [22] K. Tucek, J. Carlsson, H. Wider, "Comparison of Sodium and Lead-cooled Fast Reactors regarding reactor physics aspects, severe safety and economic issues", Nucl. Eng. Des. 236 (2006) 1589-1598.
- [23] M. Tarantino, L. Cinotti, D. Rozzia, "Lead-cooled Fast Reactor (LFR) development gaps", IAEA Technical Meeting to Identify Innovative Fast Neutron Systems Development Gaps, IAEA Headquarters, 29 February - 2 March 2012, Vienna, Austria.
- [24] M. Frogheri, A. Alemberti, L. Mansani, "The Lead Fast Reactor: Demonstrator (ALFRED) and ELFR design", IAEA Proceedings of the International Conference on Fast Reactors and Related Fuel Cycles: Safe Technologies and Sustainable Scenarios (FR13), Vol. 1, 4-7 March 2013, Paris, France.

- [25] K. Tucek, S. Hermsmeyer, L. Ammirabile, D. Blanc, E. Wattelle, L. Burgazzi, M. Frogheri, L. Mansani, S. Ehster-Vignoud, B. Carlucci, Th. Aoust, C. Niculae, Zs. Elter, I. Toth, "Identification and categorisation of safety issues for ESNII reactor concepts. Part I: Common phenomena related to materials", *Ann. Nucl. Energy* 87 (2016) 411-425.

3. FUNDAMENTALS OF HLM CHEMISTRY

3.1 GENERAL PRINCIPLES

The chemistry of Pb and LBE is a key topic to be addressed for the development of lead-cooled nuclear reactors for two main reasons: HLM oxidation and corrosion of structural steels. The activation of the coolant due to corrosion, spallation and fission products also constitutes an important issue which requires specific control procedures to ensure the safe management of the operative and maintenance phases [1]. However, the latter topic is not objective of this work and thus it will not describe below.

HLM oxidation - Pb and LBE solubilize significant amount of oxygen. When oxygen is dissolved up to the solubility level, coolant oxides formation (mainly PbO) and their consequent deposition may occur. Coolant oxides affect HLM thermal-hydraulics and cause the plugging of the structures, thus leading to potential safety risks. Some solubility value for oxygen in liquid Pb and LBE are reported in Tab. 3.1 [1].

Tab. 3.1: Solubility of oxygen in Pb and LBE in the range 400-600°C [1].

T (°C)	Pb		LBE	
	C _{O,sat} (% wt.)	C _{O,sat} (ppmw)	C _{O,sat} (% wt.)	C _{O,sat} (ppmw)
400	$5.5 \cdot 10^{-5}$	0.5	$1.3 \cdot 10^{-4}$	1.3
450	$1.8 \cdot 10^{-4}$	1.8	$3.5 \cdot 10^{-4}$	3.5
500	$5.1 \cdot 10^{-4}$	5.1	$8.2 \cdot 10^{-4}$	8.2
550	$1.3 \cdot 10^{-3}$	13	$1.7 \cdot 10^{-3}$	17
600	$2.8 \cdot 10^{-3}$	28	$3.4 \cdot 10^{-3}$	34

Steel Corrosion - Pb and LBE have high capability to dissolve the alloy elements of conventional steels (Fe, Cr and Ni) damaging the structures especially subjected to the highest temperature (e.g. core). Also, dissolved chemical elements contribute to the plugging since they tend to deposit in the cooling loop when they reach the solubility level. Tab. 3.2 reports some solubility values for Fe, Cr and Ni in Pb and LBE in the range 400-550°C [1]. LBE dissolves higher amount of elements than pure Pb and this is ascribable to the presence of Bi, which is more aggressive towards steels. In addition, Ni is highly soluble in Pb and LBE. This aspect has a primary influence on the corrosion resistance of Ni-enriched steels (e.g. austenitic steels) and detrimental selective leaching of Ni from the outer surface is usually detected for such steels during the exposure in liquid Pb and LBE [2].

Coolant oxides and corrosion products, either in the form of oxides or dissolved, have long-term cumulative effects in a non-isothermal system (as the nuclear reactor). This is ascribable to mass transfer, which occurs from the hot part to the cold part and from the HLM bulk to the structural walls (see Fig. 3.1), generating operating risks for long-term operation. An examples of this problem is given by the accident of the LBE-cooled K-27 Nuclear Submarine in 1968: during the operation, the deposition of slugs composed of coolant oxides, dissolved metal elements and oily residue from the primary pump occurred above the structures and components of the system (see Fig. 3.2), causing a loss of power with partial melting of the core [3].

Tab. 3.2: Solubility values of Fe, Cr and Ni in Pb and LBE in the range 400-550°C [1].

Element	T (°C)	Pb		LBE	
		C _{sat} (% wt.)	C _{sat} (ppmw)	C _{sat} (% wt.)	C _{sat} (ppmw)
Fe	400	$2.2 \cdot 10^{-6}$	0.022	$2.9 \cdot 10^{-5}$	0.29
	450	$7.7 \cdot 10^{-6}$	0.077	$8.3 \cdot 10^{-5}$	0.83
	500	$2.2 \cdot 10^{-5}$	0.22	$2.0 \cdot 10^{-4}$	2.0
	550	$5.8 \cdot 10^{-5}$	0.58	$4.5 \cdot 10^{-4}$	4.5
Cr	400	$5.5 \cdot 10^{-7}$	0.0055	$3.8 \cdot 10^{-4}$	3.8
	450	$2.7 \cdot 10^{-6}$	0.027	$7.8 \cdot 10^{-4}$	7.8
	500	$1.1 \cdot 10^{-5}$	0.11	$1.4 \cdot 10^{-3}$	14
	550	$3.5 \cdot 10^{-5}$	0.35	$2.5 \cdot 10^{-3}$	25
Ni	400	$1.9 \cdot 10^{-1}$	1939	1.0	10013
	450	$2.7 \cdot 10^{-1}$	2697	2.0	20170
	500	$3.6 \cdot 10^{-1}$	3595	2.5	24828
	550	$4.6 \cdot 10^{-1}$	4627	3.0	29800

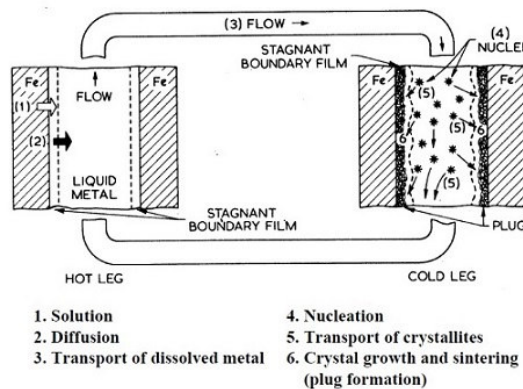


Fig. 3.1: Scheme depicting thermal mass transfer processes in a HLM-cooled nuclear reactor [1].

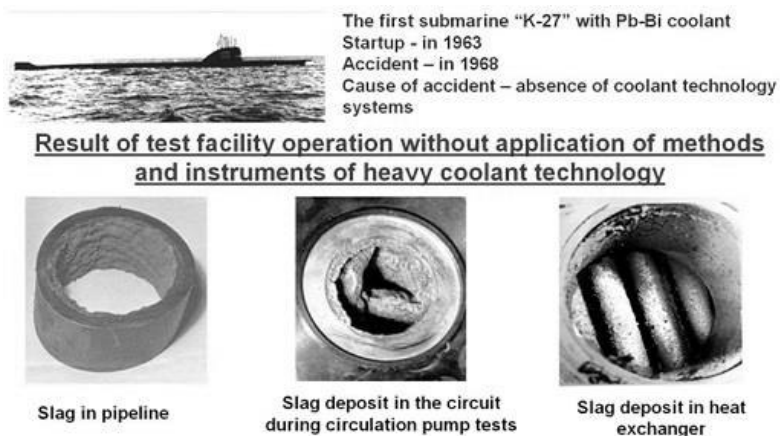


Fig. 3.2: Slag formation (coolant oxides, dissolved metal elements and oily residues) and plugging of structures and components in LBE-cooled K-27 Soviet Nuclear Submarine in 1960s [3].

The oxygen dissolved in HLMs plays a fundamental role. In fact, a too high oxygen concentration in the HLM is potentially dangerous, since it may generate coolant oxides (mainly PbO) in stagnant and coldest area of the reactor. On the other hand, a sufficient and optimal oxygen concentration in the HLM allows the self-passivation of the steel structures by formation of a double-oxide layer (external Fe_3O_4 + internal Fe-Cr spinel oxide), which is able to reduce the dissolution as well as the release of corrosion products in the HLM. Experimental data about the compatibility of steels with HLMs have shown that three different corrosion regimes exist as function of the oxygen concentration (see Fig. 3.3). If the oxygen concentration is too low for the formation of a stable oxide layer, steel dissolution occurs. At high oxygen concentration, fast detrimental steel oxidation occurs. Between these two extremes, there is a transition zone where dissolution and oxidation are concomitant and where the overall corrosion rate is low [4].

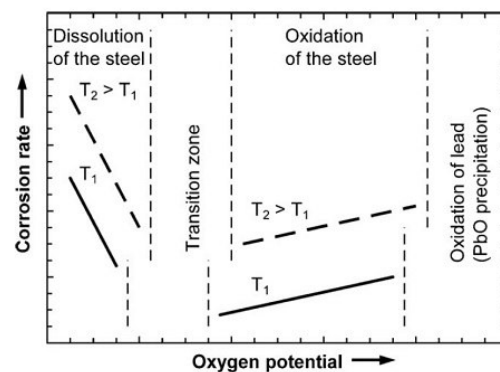


Fig. 3.3: Qualitative behaviour of steels versus oxygen potential (oxygen concentration) in Pb and LBE [4].

Considering the contamination behaviour of oxygen and its influence on steel corrosion resistance, it is of paramount relevance to control the oxygen concentration within a well-defined range in order to reduce both the dangerous formation of coolant oxides and the dissolution of steel structures. The oxygen control technology in HLM thus constitutes a key research area in the development of Pb-cooled fast reactors.

The oxygen control technology can involve different approaches about the optimal oxygen content dissolved in the coolant. However, the different strategies have the common point to work with a low oxygen content in the HLM to avoid dangerous plugging and operate in safe. This approach requires an oxygen content at least lower than the solubility at the minimum operating temperature of the reactor.

Oxygen is naturally dissolved in HLM and comes from start-up operations, maintenance phases as well from possible incidental contaminations during the normal operation [5,6]. The strategy of working with a low oxygen concentration implies the adoption of procedures and on-line devices aimed at achieving and keeping constant a fixed oxygen concentration in the HLM during start-up and operational phases, as well as design solutions able to guarantee a good tight sealing of the nuclear system. Furthermore, the control of the oxygen concentration in HLM involves the employment of accurate and reliable oxygen sensors able to detect the actual oxygen concentration and identify possible deviations.

Concerning the steel structures, it is important to mention that the low oxygen approach might enhance the corrosive effect if the dissolved oxygen concentration is not sufficient to ensure the steel passivation via formation of the oxide layer. In addition, the passivation cannot be considered an effective protection for steels exposed above 450-480°C. In such conditions localized depletion of Ni and Cr is anyway observed in austenitic steels and strong oxidation is detected in ferritic/martensitic (F/M) steels, both ascribable to the low protective features of the oxide above these temperatures [2,7]. This issue mandatorily requires the use of further protection strategies at

least for steel structures exposed to the highest temperature in the reactor (e.g. fuel cladding and fuel assemblies at 500-550°C in LFR). For instance, the protection strategy for ALFRED LFR demonstrator consists in coatings [8]. To the opposite, the low temperature operating conditions of MYRRHA ADS (270-450°C) may not require further protection in addition to the passivation method.

3.2 OXYGEN CONCENTRATION IN HLM

3.2.1 Maximum Oxygen Concentration

To prevent HLM oxidation and guarantee self-passivation of steels at the same time, the oxygen concentration has to be lower than the maximum oxygen concentration limit (saturation) and higher than the minimum required for the formation of the Fe-Cr oxide layer on steel surfaces at a given temperature. This requirement must be ensured in the whole operating temperature range and in any point of the primary system.

When oxygen dissolves in the HLM, the main oxide that forms is PbO since it is the most stable one compared to other Pb and Bi oxides. For Pb and LBE, the oxygen saturation is then linked to the following reaction:



and the oxygen solubility is defined by the following equations recommended in [1] and valid in the ranges 400-1100°C and 400-740°C for Pb and LBE respectively:

$$\log C_{O,sat}^{Pb} = 3.23 - \frac{5043}{T} \quad \text{Eq. 3.2}$$

$$\log C_{O,sat}^{LBE} = 2.25 - \frac{4125}{T} \quad \text{Eq. 3.3}$$

where $C_{O,sat}$ is expressed in % wt. and T is expressed in K. Some oxygen solubility values in Pb and LBE calculated from Eq. 3.2 and Eq. 3.3 are reported in Tab. 3.1.

The maximum oxygen concentration to avoid HLM oxidation is then defined by PbO solubility, even if both Pb and Bi oxides can form in case of large oxygen contamination. Then the general operating requirement to avoid PbO precipitation is $C_O < C_{O,sat}$, where $C_{O,sat}$ is defined by the oxygen solubility at the coldest point of the system (where oxide formation and deposition is more favoured).

The oxygen concentration is related to the oxygen partial pressure in the atmosphere above the HLM surface. The determination of the dissolved oxygen concentration starting from the oxygen partial pressure is based on the hypothesis that the HLM behaves as a dilute solution and the Henry's law can be applied to the dissolved oxygen [1,9].

Considering Henry's law valid up to the saturation concentration of the solute $X_{O,sat}$, it is possible to state that:

$$a_O = \frac{x_O}{x_{O,sat}} \cong \frac{C_O}{C_{O,sat}} \quad \text{Eq. 3.4}$$

where a_O is the oxygen activity, x_O and C_O the oxygen concentration in the HLM and $x_{O,sat}$ and $C_{O,sat}$ the oxygen concentration at saturation in mole fraction (% mol) and mass concentration (% wt.) respectively. According to the equation, $a_O=1$ for oxygen-saturated HLM solutions and $a_O<1$ for unsaturated HLM solutions.

Assuming also that molecular oxygen dissolves atomically in the HLM and the square root of pO_2 is proportional to the oxygen concentration according to Sievert's law, and assuming also that the law is valid up to the oxygen saturation concentration $x_{O,sat}$ [9], the oxygen partial pressure is linked to the oxygen concentration in the HLM according to the following equation:

$$a_{O} = \frac{x_{O}}{x_{O,sat}} = \sqrt{\frac{p_{O_2}}{p_{O_2,sat}}} \cong \frac{C_{O}}{C_{O,sat}} \quad \text{Eq. 3.5}$$

where p_{O_2} is the oxygen partial pressure in the gas atmosphere above the HLM surface and $p_{O_2,sat}$ the oxygen partial pressure in the gas atmosphere required to saturate the HLM with oxygen. The equation shows that the oxygen concentration in the HLM depends on oxygen partial pressure of the gas phase, suggesting that the oxygen can be controlled by adjusting the oxygen partial pressure in the cover gas above the HLM surface.

3.2.2 Minimum Oxygen Concentration

Any metallic element in contact with oxygen-containing environments is characterized by a physical-chemical equilibrium which involves the oxidation of the metal according to the following reaction [10,11]:



The standard Gibbs' free energy of formation of the metal oxide ΔG° (referred to the consume of one mole of oxygen) is expressed as [10,11]:

$$\Delta G_{M_xO_y}^\circ = -RT \cdot \ln K_{eq} = -RT \cdot \ln \left(\frac{a_{M_xO_y}^{\frac{2}{y}}}{a_M^{\frac{2x}{y}} \cdot p_{O_2}} \right) = RT \cdot \ln p_{O_2} \quad \text{Eq. 3.7}$$

where R is the gas constant (in J/mol), T is the temperature (in K), K_{eq} is the equilibrium constant of the reaction, a_M and $a_{M_xO_y}$ the activity of the metal and the metal oxide respectively and p_{O_2} is the equilibrium oxygen partial pressure (in bar). The equation is true considering a_M and $a_{M_xO_y}$ equal to 1.

According to Eq. 3.7, the thermodynamic stability of the oxide is ensured when $\Delta G > \Delta G^\circ$, i.e. when the oxygen partial pressure in the environment is higher than the equilibrium oxygen partial pressure.

Pb and LBE are oxygen-containing environments since several ppm of oxygen are dissolved in the HLM. In such conditions, the stability of a given metal-oxide depends on the oxygen activity in the HLM, which is related to the oxygen partial pressure in the gas phase and the oxygen concentration in the HLM according to Eq. 3.5.

To find out the thermodynamic stability of oxides in HLMs, standard Gibbs' free energies of formation of oxides $\Delta G_{M_xO_y}^\circ$ are graphically represented as a function of temperature in the Ellingham diagrams, where the oxygen partial pressure in the gas or the oxygen concentration in the HLM can be depicted as iso-lines. Ellingham diagrams depicting the stability of oxides as function of the oxygen partial pressure (expressed in bar) and the oxygen concentration (in % wt.) for liquid Pb and LBE are reported in Fig. 3.4 and Fig. 3.5.

The Ellingham diagram is a helpful tool to evaluate the thermodynamic stability of metal-oxides in different conditions as well as to make comparison about the stability of different oxides. When the operating parameters T and C_O correspond to points above a given M/M_xO_y equilibrium line, the oxidation of the metal M is favoured. To the opposite, when T and C_O have values below the M/M_xO_y equilibrium line, the oxide decomposition is favoured and the metal reduction occurs. In addition, a given metal can reduce all the metal-oxides whose M/M_xO_y equilibrium lines are placed in the upper zone of the diagram.

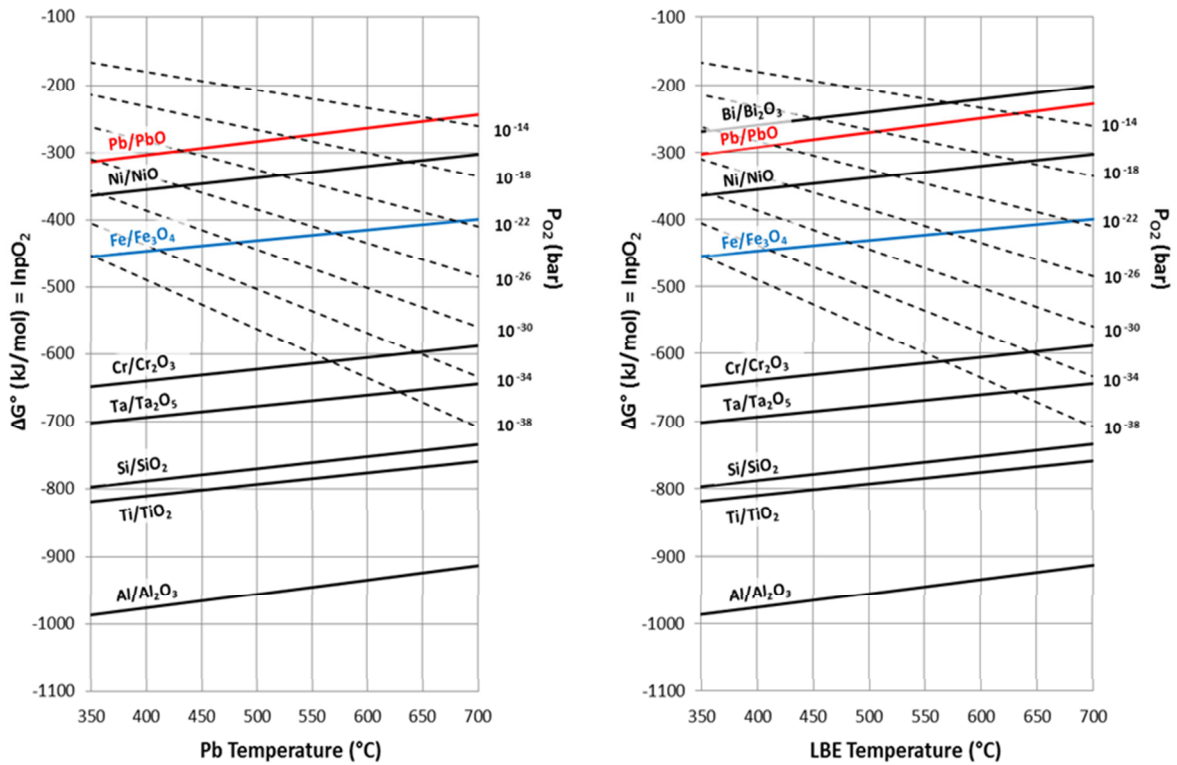


Fig. 3.4: Ellingham diagrams showing the stability of various metal oxides as a function of the oxygen partial pressure in the gas for Pb (left) and LBE (right).

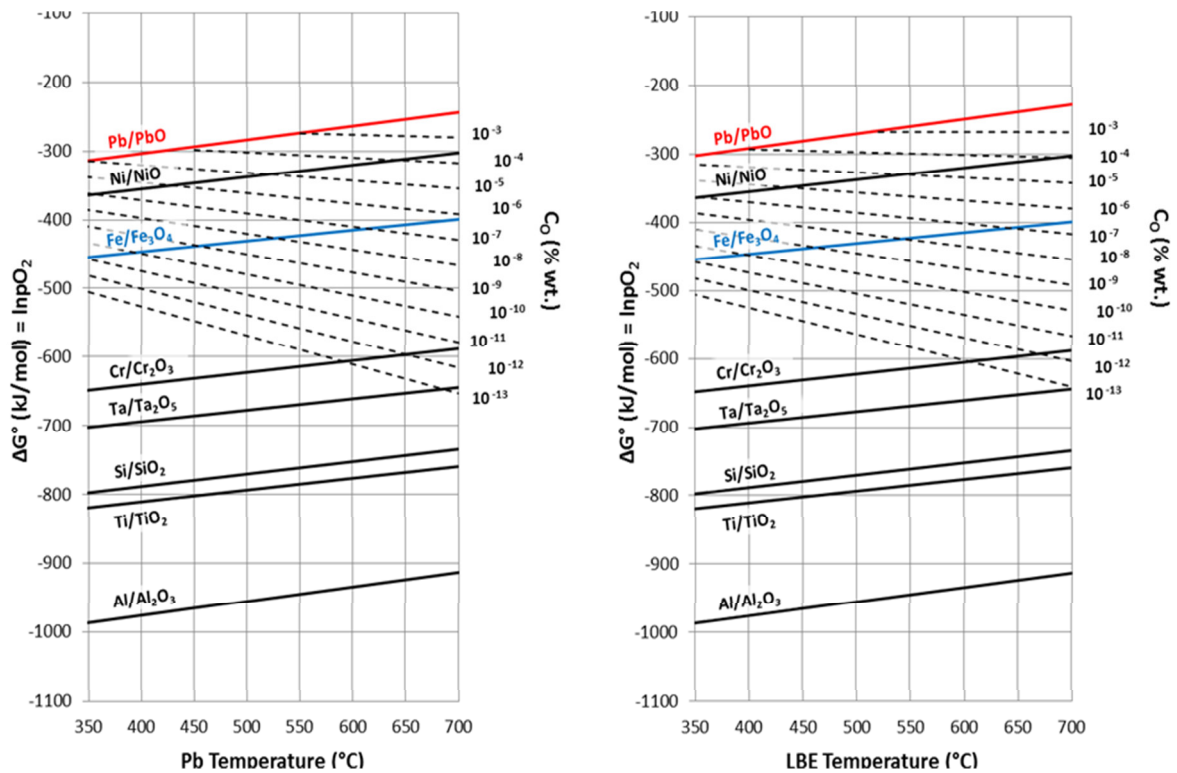


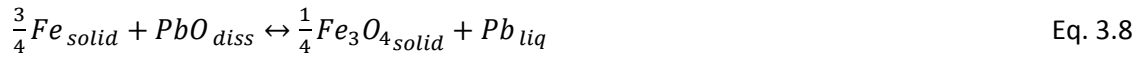
Fig. 3.5: Ellingham diagrams showing the stability of various metal oxides as a function of the oxygen concentration in Pb (left) and LBE (right).

For Fe-Cr steel in contact with liquid Pb and LBE, Fe_3O_4 (magnetite) is the least stable oxide that constitutes the passivation layer (usually composed of external Fe_3O_4 and Fe-Cr internal spinel oxide). Then Fe_3O_4 equilibrium formation defines the minimum oxygen concentration in HLMs required for

steel self-protection. Observing Ellingham diagrams, we see that Fe_3O_4 is more stable than PbO and, consequently, it is possible to promote the formation of Fe_3O_4 on steels by ensuring oxygen content in the HLM higher than the minimum required for its formation. In particular, it is to note that the window for steel corrosion protection corresponds to the narrow area delimited by Fe/Fe_3O_4 equilibrium line and Pb/PbO equilibrium line (oxygen saturation equilibrium in Pb alloys). Differently to Fe_3O_4 , oxides of other alloy elements such as Cr_2O_3 , Ta_2O_5 , SiO_2 , TiO_2 , Al_2O_3 are stable over the whole range of oxygen concentration in practice achievable in HLMs.

However, it is to note that Ellingham diagrams in Fig. 3.4 and Fig. 3.5 are plotted considering the activity of all metals equal to 1 (except for Pb in LBE where $a_{Pb} < 1$), meaning that all elements are dissolved in the HLM up to their solubility. This is unlikely to happen in non-isothermal nuclear systems where dissolved alloy elements as well as dissolved oxygen are subjected to mass transfer. According to that, the actual activity of dissolved metals is likely far from 1 and their M/M_xO_y equilibrium lines are placed a little upper with respect to the corresponding in Fig. 3.4 and Fig. 3.5.

To calculate the minimum oxygen concentration required for the formation of Fe_3O_4 on steels in contact with HLMs, the following reaction concerning Fe oxidation in the HLM is assumed:



where oxygen is supposed to be below its saturation limit in the form of dissolved PbO .

According to Eq. 3.7, the standard Gibbs' free energy of formation of Fe_3O_4 is expressed as:

$$\Delta G_{Fe_3O_4}^\circ = -RT \cdot \ln \frac{a_{Fe_3O_4}^{1/4} \cdot a_{Pb}}{a_{Fe}^{3/4} \cdot a_{PbO}} \quad \text{Eq. 3.9}$$

which, considering $a_{Fe_3O_4} = 1$ and $a_{PbO} = a_O$, is approximated as:

$$\Delta G_{Fe_3O_4}^\circ = -RT \cdot \ln \frac{a_{Pb}}{a_{Fe}^{3/4} \cdot a_{PbO}} \quad \text{Eq. 3.10}$$

where $a_{Pb} = 1$ for pure liquid Pb and $a_{Pb} < 1$ for LBE.

The standard Gibbs' free energy associated to Eq. 3.8 is calculated as follows:

$$\Delta G_r^\circ \left(\frac{j}{mol} \right) = \Delta H_r^\circ - T \cdot \Delta S_r^\circ = -57190 - 21.1 \cdot T \quad \text{Eq. 3.11}$$

which is valid in the temperature range 127-727°C [1].

Eq. 3.10 shows that the stability of Fe_3O_4 depends both on iron and oxygen activity in the HLM. Applying Henry's law for the dissolved oxygen and assuming the law valid also for dissolved iron, oxygen and iron activities in the HLMs are respectively defined as:

$$a_O = \frac{C_O}{C_{O,sat}} \quad \text{Eq. 3.12}$$

$$a_{Fe} = \frac{C_{Fe}}{C_{Fe,sat}} \quad \text{Eq. 3.13}$$

where the concentrations are expressed in % wt.

$C_{O,sat}$ in Pb and LBE is calculated from Eq. 3.2 and Eq. 3.3 whereas $C_{Fe,sat}$ is calculated from the following equations by Gossè [1]:

$$\log C_{Fe,sat}^{Pb} = 2.11 - \frac{5225}{T} \quad \text{Eq. 3.14}$$

$$\log C_{Fe,sat}^{LBE} = 2.00 - \frac{4399}{T} \quad \text{Eq. 3.15}$$

which are valid in Pb and LBE in the ranges 327-900°C and 126-900°C respectively [1].

Assuming that $a_{Fe} < 1$ (i.e. no mass transfer in the HLM system), the minimum oxygen concentration for the formation of stable Fe_3O_4 is evaluated as follows:

$$\ln C_O = \frac{\Delta G_{Fe_3O_4}^\circ}{RT} + \ln C_{O,sat} + \ln a_{Pb} \quad \text{Eq. 3.16}$$

where $a_{Pb} = 1$ for pure Pb and $a_{Pb} < 1$ for LBE. In the latter case, Pb activity in LBE can be calculated as a function of temperature using the following equation available in [1] and recommended by Zhang in the range 350-550°C [12]:

$$\ln a_{Pb} = -\alpha - \frac{\beta}{T(K)} \quad \text{Eq. 3.17}$$

where $\alpha = 0.8598$ and $\beta = 135.21$.

The minimum oxygen concentration in the nuclear system is defined by the minimum oxygen concentration required for the formation of Fe_3O_4 at the hottest point of the nuclear system, i.e. at the point where the formation of the Fe-oxide is less thermodynamically favoured. However, since in a nuclear reactor mass transfer phenomena are likely, $a_{Fe} < 1$ and the minimum oxygen concentration for the formation of stable Fe_3O_4 has even higher values and defined as:

$$\ln C_O = \frac{\Delta G_{Fe_3O_4}^\circ}{RT} + \ln C_{O,sat} - \frac{3}{4} \ln C_{Fe} + \frac{3}{4} \ln C_{Fe,sat} + \ln a_{Pb} \quad \text{Eq. 3.18}$$

3.2.3 Optimal Oxygen Range

The requirement for the oxygen concentration in HLMs needed to ensure both no contamination by PbO and corrosion protection of steels is the following:

$$C_{O,magnetite} < C_O < C_{O,sat} \quad \text{Eq. 3.19}$$

where C_O is the oxygen concentration dissolved in the HLM, $C_{O,sat}$ is the maximum oxygen concentration limit (saturation) and $C_{O,magnetite}$ is minimum oxygen concentration required for the formation of Fe_3O_4 above the steels. Fig. 3.6 illustrates a general oxygen concentration range for a Pb-cooled system (the so-called “active oxygen” range): the blue line corresponds to Pb/PbO equilibrium and $C_{O,sat}$ while full and dashed red lines corresponds to Fe/ Fe_3O_4 equilibria and $C_{O,magnetite}$ when $a_{Fe}=1$ and $a_{Fe}<1$ respectively. The optimal oxygen concentration is framed between Pb/PbO and Fe_3O_4 equilibria within the “steel passivation” area.

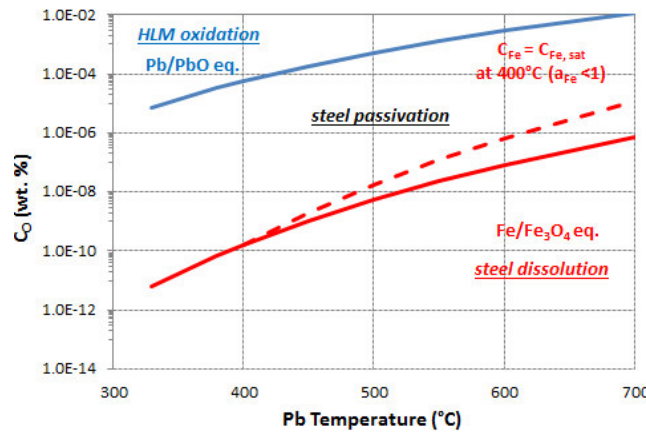


Fig. 3.6: “Active oxygen” for a Pb-cooled system represented by the “steel passivation” area.

In general, the first requirement $C_O < C_{O,sat}$ is considered mandatory for any nuclear system to avoid dangerous plugging of structures and components. The second one $C_O > C_{O,magnetite}$ is preferable but optional and its adoption depends on the strategy chosen for the specific system. In addition, the comply of the first requirement is important also for experimental facilities in order to assess a correct thermal-hydraulics of the coolant and to reduce the frequency of cleaning operations of the structures.

For MYRRHA reactor, the strategy consists in working with a fixed oxygen concentration in the LBE able to guarantee the requirements of both no contamination by PbO and steel passivation in the working range 270-450°C. To this aim, the oxygen concentration has been set at around 10^{-7} % wt. [13]. Fig. 3.7 (left) illustrates the general oxygen concentration range (dashed black box) and the fixed oxygen concentration (full black box) for the operation of MYRRHA.

For ALFRED reactor, the strategy for the oxygen control aims to work with an oxygen concentration in the liquid Pb coolant much lower than the saturation at the minimum operating temperature of the reactor (lower than $3 \cdot 10^{-5}$ % wt., which is the saturation level at the refuelling temperature of 380°C). In particular, the preferred oxygen concentration range is reported to be between 10^{-6} and 10^{-8} % wt. in order to reduce the chance of PbO formation even in case of local heterogeneities and potential deviations [8]. Fig. 3.7 (right) depicts the general oxygen concentration range (dashed black box) and the preferred oxygen concentration (full black box) for ALFRED operation. It can be noticed that the oxygen concentration is positioned further down than the range required to ensure both steel self-passivation and no HLM oxidation. As a matter of fact, the oxygen concentration chosen can in principle guarantee the self-protection of the structures exposed to the lowest temperatures (e.g. the vessel exposed at 400°C) but not the other structures exposed to higher temperatures. However, since the passivation method is not completely effective for steels exposed above 450-480°C, the use of other protection strategies are mandatory in Pb-cooled reactors even in presence of a sufficient amount of dissolved oxygen. For instance, in the case of ALFRED demonstrator, the protection strategy followed consists in coatings, which have the advantage to protect the structures maintaining the mechanical and irradiation properties of the steel substrate (in particular, the swelling and the creep properties for fuel cladding tubes) [8].

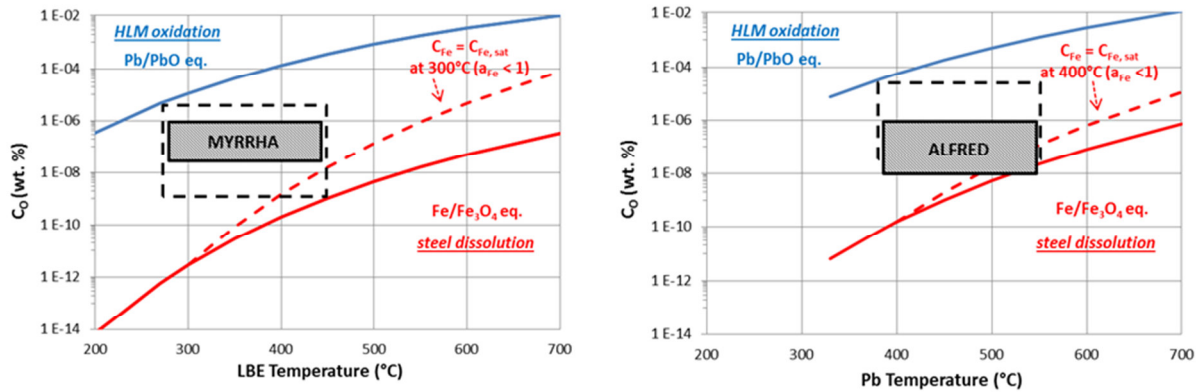


Fig. 3.7: General oxygen concentration range (dashed black box) and fixed oxygen concentration (full black box) for MYRRHA (left) and ALFRED operation (right).

3.3 OXYGEN CONTROL METHODS

The oxygen control technology represents an important field of research for mitigating both HLM oxidation and corrosion of steels in HLM systems. As discussed before, contamination and corrosion issues can be minimized by using oxygen concentrations included between the oxygen solubility at the coldest point and the minimum oxygen required for the formation of Fe_3O_4 at the hottest point. These requirements are achieved by using methods and devices able to control the oxygen concentration within a narrow range and eventually to compensate for possible deviations.

The main oxygen control methods studied and employed to date are divided in two main groups: “gas-phase oxygen control” and “solid-phase oxygen control” methods. Tab. 3.3 lists the oxygen control methods with their advantages and disadvantages according to the literature. Another less common method (not reported in the table) is the vacuum technique [14].

Tab. 3.3: Main oxygen control methods for HLM systems.

Type	Method	Advantages	Disadvantages
Gas-phase	Injection of O_2 and H_2 gases (oxygen supply and removal)	Simple operation; rapid adjustment of C_o	Potential PbO contamination during O_2 supply; precise control is difficult
	Injection of H_2/H_2O mixture	Set the desired oxygen concentration by controlling H_2/H_2O ratio in the gas	Long time to reach the equilibrium; difficulty in restoring large deviations
Solid-phase	PbO mass exchanger (oxygen supply)	Simple operation; efficiency due to solid/liquid contact; no PbO contamination of the coolant	Replenishment after the consume; poor experience in large scale experiments
	Oxygen getters addition (oxygen removal)	Simple operation; efficiency due to solid/liquid contact	HLM contamination with metal-oxides; replenishment after the consume; poor experience

3.3.1 Injection of H_2 and O_2

Injection of H_2 and O_2 has been used in experimental facilities such as DELTA, LECOR, HELIOS and CORRIDA [5,15-17]. Oxygen and hydrogen are usually diluted with inert gas (argon or helium) and

supply to the HLM through bubbling lines to oxidize or reduce the HLM according to Eq. 3.1 and the following reaction:



The efficiency of the reactions can be enhanced by increasing the exchange area (i.e. reducing the bubbles area using spargers or impellers), and the HLM temperature as investigated by Ricapito (see Tab. 3.4) [18].

The direct injection of O₂ and H₂ is a simple procedure and required easy plant implementation. Gas injection does not involve HLM contamination with solid products but PbO may form in case of large addition of O₂. For this reason, some authors recommended the use of O₂ only in case of abrupt decrease of the oxygen concentration [19]. To the opposite, the use of H₂ easily restores the correct oxygen concentration after a large HLM contamination with PbO and allows the purification of the HLM from the excess of oxygen in storage tanks before the filling procedure [5].

Tab. 3.4: PbO reduction rate in oxygen-saturated LBE using Ar-3%H₂ gas [18].

T _{LBE} (°C)	PbO reduction rate (g/m ² ·h)
250	9
300	28
350	94
400	288

3.3.2 Injection of H₂/H₂O mixture

The requirement of stable low oxygen concentrations in HLMs could be achieved by using the H₂/H₂O gas mixtures [20-22]. The low oxygen partial pressure to reach the low oxygen concentration in HLMs can be set considering the following reaction:



The oxygen partial pressure (in bar) expressed by Eq. 3.21 is defined as:

$$p_{O_2} = \left(\frac{p_{H_2O}}{p_{H_2}} \right)^2 \cdot \exp\left(\frac{2\Delta G_{H_2O}^\circ}{RT} \right) \quad \text{Eq. 3.22}$$

where $\Delta G_{H_2O}^\circ$ the Gibbs free energy of formation of water vapour.

Combining then Eq. 3.22 with Eq. 3.5, it follows that:

$$\frac{p_{H_2}}{p_{H_2O}} = \frac{c_{O,sat}}{c_O \cdot \sqrt{p_{O_2,sat}}} \cdot \exp\left(\frac{\Delta G_{H_2O}^\circ}{RT} \right) = \frac{c_{O,sat}}{c_O} \cdot \exp\left(\frac{\Delta G_{H_2O}^\circ - \Delta G_{PbO}^\circ}{RT} \right) \quad \text{Eq. 3.23}$$

So it is possible to control the oxygen concentration in the HLM by setting a specific H₂/H₂O ratio in the gas mixture. The influence of the H₂/H₂O ratio on the stability of metal-oxides in liquid Pb is depicted in the Ellingham diagram of Fig. 3.8 [23].

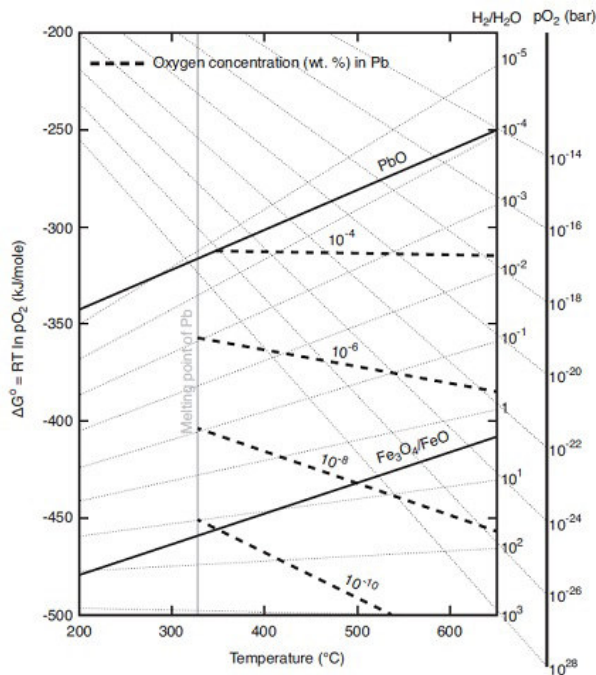


Fig. 3.8: Ellingham diagram showing the stability of metal-oxides in liquid Pb as a function of temperature, H_2/H_2O ratio, oxygen partial pressure and oxygen concentration [23].

H_2/H_2O mixture is usually diluted with inert gas such as argon and it is prepared by bubbling argon- H_2 mixture into water at a given temperature in order to create a H_2O -saturated Ar- H_2 mixture [24,25]. For this purpose, a tank containing water at the correct temperature can be used to create the Ar- H_2/H_2O mixture. By varying the H_2/H_2O ratio in the mixture (used as bubbling or cover gas), different oxygen concentrations in the HLM can be obtained. Fig. 3.9 shows the P&ID for the oxygen control in LBE via Ar- H_2 - H_2O gas mixture in KOCOS facility at KIT (Karlsruhe Institute of Technology) [24].

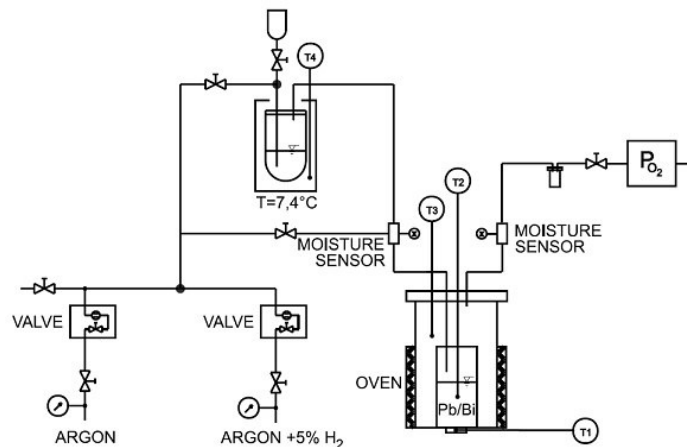


Fig. 3.9: Scheme of oxygen control via Ar- H_2/H_2O gas mixture in LBE in KOCOS facility [23].

A good control of the oxygen concentration in the HLM by using a proper mixtures of Ar- H_2/H_2O have been obtained in stagnant conditions (e.g. COSTA), small pools (e.g. KOCOS, HELIOS III) and loops (e.g. CORRIDA, DELTA, COLONRI) [24-26]. According to Russian experience in LBE chemistry, the Ar- H_2/H_2O gas mixture provides an efficient HLM purification from PbO into ΔT loop facility ensuring at the same time the protection of structural steels [19,27,28]. However, the method requires high

gas/liquid exchange area to have good process efficiency and this method could be not effective in large HLM pools where the ratio “exchange area/HLM volume” may be not high enough to promote mass transfer in large volumes. More experimental investigations are needed for such application.

3.3.3 PbO mass exchanger

PbO mass exchanger is proposed as oxygen supply device to contrast a too low oxygen concentration in HLMs [3,21,26,29-31]. The device contains solid PbO, usually in the form of spheroids, which are dissolved in the HLM when the oxygen concentration is low. The dissolution reaction is the following:



The mass transfer occurs mainly at PbO/HLM interface, i.e. in the boundary layer surrounding the solid PbO spheroids, even if internal transfer by diffusion within the porous solid can occur. Considering only external mass transfer in the boundary layer, the flow of the solid material dissolved in the HLM can be generically expressed as follows [25]:

$$\phi = k_d \cdot A \cdot \Delta C = k_d \cdot A \cdot (C_o^* - C_o) \quad \text{Eq. 3.25}$$

where Φ is the flow of the dissolved material (expressed in kg/s), k_d is the mass transfer coefficient for the dissolution process (in m/s), A is the exchange area (in m^2) and ΔC is the oxygen concentration gradient (in kg/m^3) corresponding to the difference between the oxygen concentration in the HLM above the spheroid surface ($C_o^* = C_{o, sat}$) and that one in the external liquid covering the PbO spheroids (C_o). The mass transfer coefficient k_d is specific to the transfer and depends on the temperature (through several physical constants), HLM flow rate and PbO spheroid size [3,25]. Temperature and HLM flow rate are the main parameters for the control of the oxygen concentration with a PbO mass exchanger device.

PbO mass exchanger has the advantage to shun gas circuits in the nuclear system, thus enhancing the confinement of activated volatile products and the overall safety. This is particularly important for LBE-cooled nuclear systems, where the formation of hazardous Po volatile products from Bi is a major safety issue. In addition, this process has been demonstrated its efficiency on small scale loop presenting an outstanding stability in controlling oxygen (see Fig. 3.10) [3,20]. For such device, the next step is to assess the feasibility in a large HLM pools, where the huge surface of steel structures may require a great amount of oxygen for the passivation.

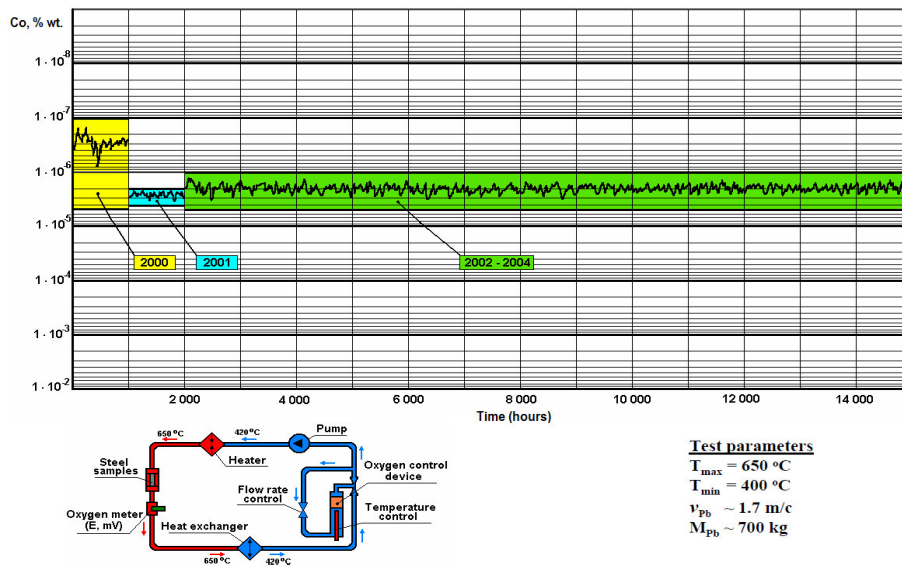


Fig. 3.10: Continuous oxygen regulation in Pb with PbO mass exchanger on “SM-2” test rig at IPPE [3,20].

An example of PbO mass exchanger for HLM pool system developed by IPPE is described in Fig. 3.11 [30]. The device consists in a stainless steel cylindrical vessel containing two slot grids filled with PbO spheroids ($d_{sp}=9-11$ mm). During a working cycle, inert gas is extracted from the facility cover gas and supplied through a gas pipeline to the mass exchanger, so that pressurized inert gas can push an oxygen-enriched HLM into the facility pool via an header. Switching off the gas injection, the HLM is drawn back to mass exchanger vessel via the header mixing with the rest of the oxygen-enriched HLM in the bottom section. The amount of oxygen inserted into the facility pool depends on the HLM volume flowing out from the device, which is regulated modifying the differential pressure between the one in the cover gas and the one in the vessel.

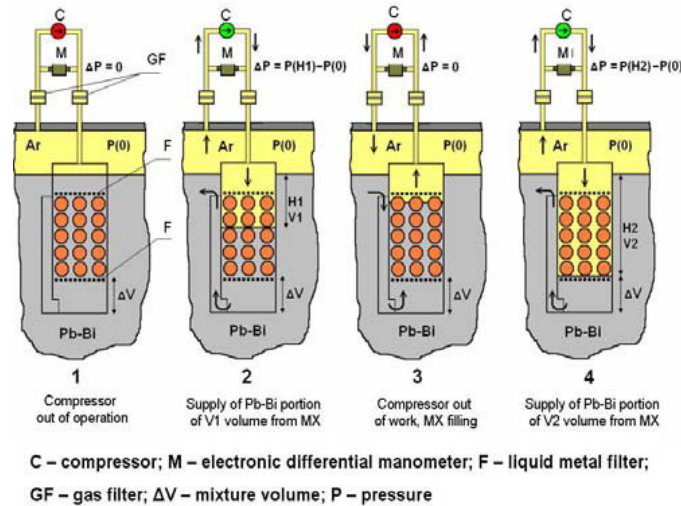


Fig. 3.11: Working principle of a PbO mass exchanger for HLM pool facility developed by IPPE [30].

3.3.4 Oxygen getters

Oxygen getters are metallic elements able to remove oxygen from an high-temperature environment by oxidation of the metallic elements themselves.

Ti, Zr alloys are commonly used as getters for the purification of inert gases at high-temperature [33-37]. Concerning liquid metals, Mg and Zr and Ti-based alloys have been used as oxygen getters in liquid Na [38,39] and only Mg has been used as oxygen getter for liquid Pb and Bi in small scale experiments [15,40-42]. The reaction involving the use of Mg in liquid Pb alloys is the following:



The efficiency of an oxygen getter material depends on several parameters:

- 1) propensity to oxidation (thermodynamic and kinetic issues);
- 2) surface area;
- 3) temperature.

Considering the case of Mg as oxygen getter, MgO formation of according to Eq. 3.26 is thermodynamically favoured since MgO is largely more stable than PbO [10,11]. The efficiency of Mg as oxygen getter is enhanced by its very low resistance to high-temperature oxidation, involving the whole consuming of Mg by oxidation over time [10,11].

Oxygen getters are not so much employed in HLM facilities and further investigations about the efficiency of other getter materials may be performed. The major drawback associated with the use of oxygen getters is the formation of oxide solid products, which implies the use of containment devices (such as cartridges) to entrap the oxide powders and avoid the HLM contamination.

3.4 CHEMISTRY CONTROL IN START-UP OPERATIONS

During initial start-up of HLM facility, the main source of contamination is oxygen. Oxygen comes from Pb and LBE ingots, from adsorbed gases on steel structural walls and traces of oxygen and moisture in the circuits before the HLM load. Accurate start-up operations are required to ensure fairly good oxygen conditions in the HLM before the operation, simplifying the oxygen and the impurities control procedures during the real operation.

In general, the main contamination sources in start-up procedures are [5]:

- Intrinsic contaminations of the Pb alloy. The ingots contain several metal impurities and oxides resulting from casting operations. In particular, the oxides above the ingot surface, as well as air bubbles entrapped within the solid ingots, contribute greatly to the oxygen contamination of the HLM.
- Gases adsorbed on the structures inner surface. New structures contains adsorbed gases such as H_2 , O_2 and H_2O which tend to desorb when in contact with the HLM.
- Traces of impurities in the circuits before the filling. Such impurities are usually O_2 and H_2O and are transferred to the HLM during the filling procedure.
- Casual impurities, such as oil, grease, welding and oxide scale remaining above the structures after the assembly. Cleaning procedures (degreasing and pickling) are needed to reduce these contaminations.
- Incidental contaminations, such as air inlets due to a loss of tightness of the system.

According to the various contamination sources, star-up operations should include specific procedures aimed at reducing the oxygen contaminations as well as oxygen monitoring devices. The following procedures are in general recommended [5,6]:

- 1) Intrinsic oxygen contaminations in the ingots are managed by using appropriate filtering procedures to remove the oxides above the ingots surface. The complete procedure to guarantee a high-purity HLM involves the melting of the ingots into a melting tank where metal impurities and oxides can float above the melt surface. The HLM is then transferred to a storage tank by passing through a filtering section which prevents the ingress of impurities and oxides. Once transferred in the storage tank, the HLM is treated with an argon/ H_2 gas to reduce the oxygen content. The level of oxygen in the HLM is monitored with oxygen sensors in the storage tank. The scheme of the procedure is illustrated in Fig. 3.12.
- 2) Oxygen contamination from the new structures has to be taken into account by loading HLM with an oxygen content far lower than that one strictly required, in order to take some margin.
- 3) Traces of O_2 and H_2O in the system are reduced by applying degassing procedures consisting in: a) washing the inner structures with inert gas at room temperature and then at higher temperatures or b) applying vacuum and then filling the facility with inert gas, repeating the procedures several times first at room temperature and then at increasing temperatures.

In general, if the purification procedures are carefully performed during start-up phases, a high oxygen contamination is not likely to occur during the facility operation, at least if a good tightness of the system is maintained and the risk of large contamination avoided. In such conditions, the gradual consume of oxygen from the structural steel for the passivation (as well as from the spallation products in nuclear systems) becomes the major issue to address to keep on ensuring the requirement of steel self-protection [6]. Here, corrosion products continuously form with a rate depending on the operating conditions (temperature, HLM flow rate, type of material, etc...) and have potential blockage effects on long-term operation due to the mass transfer. At this stage, oxygen supply may be required in order to restore the correct oxygen concentration for Fe_3O_4 formation.

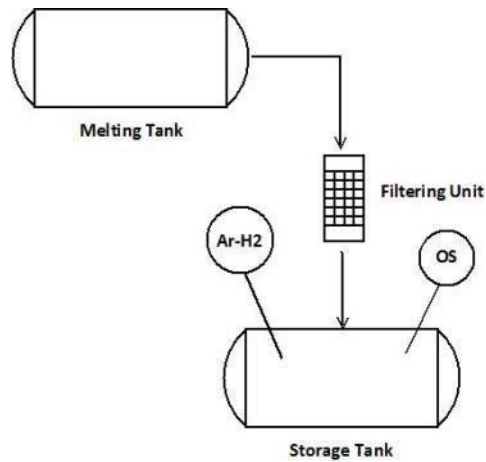


Fig. 3.12: Scheme for the purification of Pb alloy ingots before the filling of the facility with HLMs (OS = oxygen sensor, Ar-H₂ = reducing gas injection).

3.5 HLM CORROSION AND PROTECTION

3.5.1 Fundamentals of HLM corrosion

Lead and LBE have high capability to corrode (dissolve) conventional steels and the protection of structural materials is one of the most critical point to be assessed for the operation of future Pb-cooled nuclear reactors. Presently, reference materials for ALFRED and MYRRHA reactors are 316L and 15-15Ti austenitic steels and T91 F/M steel [43]. In this context, deep investigations concerning the assessment of corrosion mechanisms, as well as the identification of protection strategies, are carried by the European scientific community to keep under control the corrosion issue in HLMs.

316L austenitic steel (18% Cr, 10% Ni, 2% Mo) is now considered for the most of the structures and components of Pb-cooled reactors (main vessel, inner vessel, steam generator, decay heat removal heat exchanger, primary pumps) while 15-15Ti steel (15 % Cr, 15% Ni, 2% Mo) is considered mostly for fuel cladding and fuel assemblies thanks to its good swelling resistance under neutron irradiation and excellent creep resistance [8,43]. T91 F/M steel (9% Cr, 1% Mo) possesses excellent swelling properties and it is considered as reference materials for wrapper and spallation target window [43,44]. However, T91 (as well as F/M steels in general) forms very thick and less protective oxide layer and are highly susceptible to HLM embrittlement [43-45], meaning that long-term application of this steel may be problematic.

The corrosion of structural steels has two main effects on the operation of the nuclear reactor. First of all, the loss of material due to the corrosion process affects the integrity of structures and components, especially for thin components exposed to high temperature such as the fuel cladding (550°C) and the heat exchanger tubes (480°C). In addition, corrosion involves the release of corrosion products in the coolant, which may deposit in the coldest parts of the system contributing to the plugging. In non-isothermal systems such as a nuclear reactor system, thermal mass transfers due to different solubility in hot and cold parts represent the driving force for corrosion processes (see Fig. 3.1). To the opposite, in isothermal systems corrosion process is governed by diffusion (rate determining step) and the dissolution decreases with time as dissolved metal concentrations decrease (saturation at steel/HLM interface).

The main corrosion mode of steels in HLMs are dissolution and oxidation. These degradation modes are influenced by parameters such as the oxygen concentration, temperature, HLM flow-rate and time [13]. Oxygen has influence on the capability of steels to form the Fe-Cr oxide layer on the surface, which acts as barrier against the HLM reducing the corrosion effect. The formation of the oxide layer is ensured when the oxygen concentration is high enough to form stable Fe₃O₄ in any

point of the nuclear system, requirement that has to be achieved by means of an adequate oxygen control system. If a sufficient oxygen concentration is not available in the HLM, severe corrosion is observed on steels. The temperature influences the dissolution and oxidation rate of steels so that, in principle, the higher is the temperature greater is the magnitude associated to dissolution and oxidation processes. Finally, the increase of HLM flow rate enhances corrosion process as shown in Fig. 3.13. For very high HLM flow-rate, the shear stress at steel/HLM interface is so high that HLM can strip the oxide layer on the surface and erosion/corrosion is likely to occur [12].

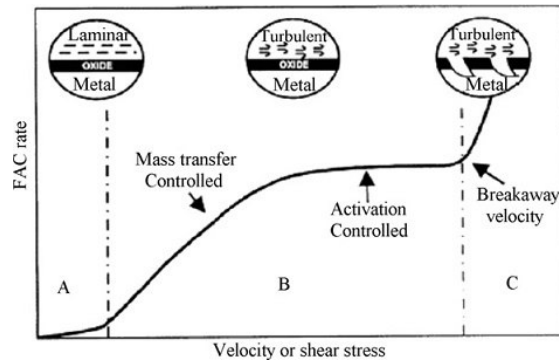


Fig. 3.13: Influence of HLM flow-rate on flow-accelerated corrosion (FAC). (A) low velocities (corrosion controlled by mass transfer), (B) high velocity (corrosion controlled by dissolution rate) and (C) very high velocity (cavities at steel/HLM interface and erosion) [12].

Oxide layers can form on austenitic and F/M steels in HLMs with a sufficient oxygen concentration. Such oxide layers can protect steels against rapid dissolution up to 450-480°C. The oxide layer on F/M steels is usually much thicker than the layer of austenitic steels ($\approx 30 \mu\text{m}$ versus 2-4 μm) and has a double-layer structure made of outer Fe_3O_4 (porous) and inner Fe-Cr spinel oxide (compact) [2,7,12]. Austenitic steels can have different structures according to the working temperature [12]:

- for $T \leq 450^\circ\text{C}$, the oxide layer is very thin and made of a single-layer of Fe-Cr oxide spinel or Cr-enriched oxide, which is protective and prevents strong dissolution;
- for $T > 450^\circ\text{C}$, the oxide layer may consist of a single or duplex layer structure (Fe-Cr oxide spinel or Fe-Cr oxide spinel plus Fe_3O_4), which is less protective and strong dissolution is usually observed.

For HLMs with oxygen control, oxygen is transported to steel surfaces by both diffusion and convection. At the beginning, oxidation and dissolution may occur simultaneously. If the oxidation process is favoured, protective oxide layers form on the steel surface. Once the oxide layer forms, the direct dissolution is reduced significantly. Here, iron diffuses through the oxide layer (see Fig. 3.14) and Fe_3O_4 formation and dissociation (assuming that Fe_3O_4 is the outer oxide) occurs at the oxide/HLM interface at the same time [12]. As time increases, the oxide layer becomes thicker and iron diffusion rate through the oxide layer becomes smaller because of the increasing thickness [12].

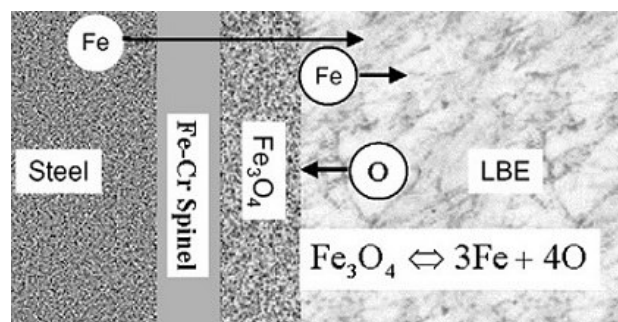


Fig. 3.14: Mechanism of oxide layer formation at steel/HLM interface under oxygen control [12].

Austenitic steels exposed to high-temperature Pb or LBE undergo preferential dissolution of Ni and Cr alloy elements from the bulk steel, which is responsible of the phase transformation from austenite to a porous ferrite-type structure on the outer surface of the steels [2,46]. The dissolution is often accompanied by penetrations of Pb and Bi through the corrosion layer [2,46]. An example of austenitic steel dissolution is given by Fig. 3.15, which shows the appearance of 316L steel after the exposure in flowing LBE at 550°C, with flow-rate 2 m/s and oxygen concentration 10^{-6} % wt. [2]. It is possible to see the porous depletion zone due to leaching of Ni and Cr from the bulk steel and the penetration of Pb and Bi through the corrosion layer. The dark spot in the middle is ascribable to a lower mass in the remaining steel (ferrite) with respect to that in the surrounding area.

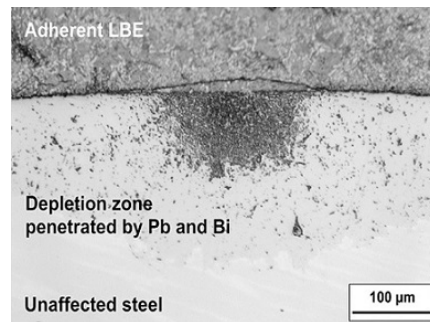


Fig. 3.15: AISI 316L after the exposure to flowing oxygen-containing LBE for 7518 hours at 550°C and 10^{-6} % wt. of dissolved oxygen, showing a localized zone affected by selective leaching of Ni and Cr [2].

Thus severe dissolution of an austenitic steel is occurring at 550°C even if in presence of a sufficient dissolved oxygen concentration in the HLM, demonstrating that the corrosion control via Fe-Cr oxide layer formation is not effective for high temperatures as a consequence of the loss of protectiveness of the oxide scale and the increase of the dissolution potential. The effect of the temperature on steel dissolution and oxide scale formation is explained in Fig. 3.16 [47], reporting cross-section images of 15-15Ti steel after the exposure in flowing LBE at 420°C, 550°C and 600°C, for 4000 hours and with oxygen concentration 10^{-6} % wt. The steel exposed to 420°C (left) does not show any evidence of dissolution attack and the surface is covered by a thin Cr_2O_3 -rich scale. To the opposite, a thick double scale consisting of Fe-Cr spinel oxide and Fe_3O_4 appears on the surface at 550°C (centre). Here, the fragile Fe_3O_4 layer is broken in two parts and penetrations of Pb and Bi are clearly visible below the spinel oxide (white areas). Then, at 600°C (right) severe dissolution attack occurred with strong leaching of Ni from the bulk material.

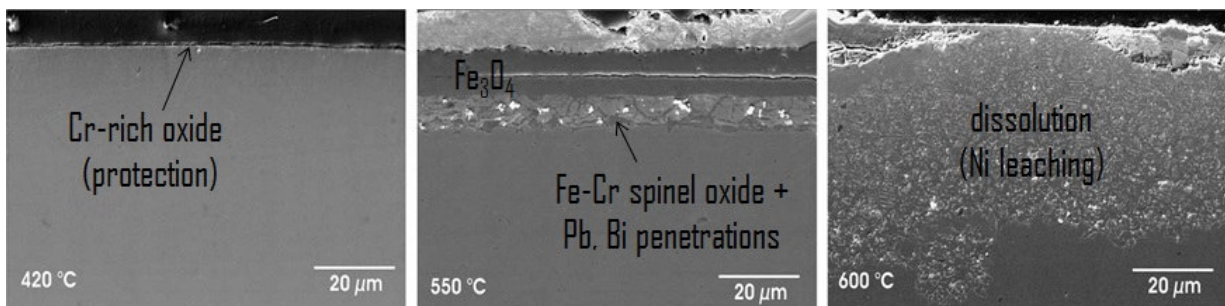


Fig. 3.16: 15-15Ti steel after exposure in flowing LBE at 420°C (left), 550°C (centre) and 600°C (right) for 4000 hours and with 10^{-6} % wt. of dissolved oxygen [47].

3.5.2 Materials protection

The high working temperatures expected for lead-cooled reactors will require the use of protection methods to prevent severe dissolution of steels. Components and structures exposed up to 450°C can be protected by controlling the oxygen concentration in the HLM at an optimum level to ensure

the self-oxidation of steels (but not the HLM oxidation). Nevertheless, for critical components such as fuel cladding tubes and heat exchanger tubes (expected to work at about 550°C and 480°C respectively in ALFRED), other strategies must be considered for a real and effective corrosion protection.

To date the most viable solution to protect critical components in the short-term is represented by surface modification with Al- based alloys or by the use of coatings. Indeed, these methods have the advantage to conserve the mechanical and irradiation properties of the coated steel substrate, making easier the procedures for the qualification of the nuclear material. In parallel, the investigation of new Al and Si-enriched steels with high-corrosion resistance performance is going on but longer qualification procedures are expected for such steels (especially from the point of view of neutron irradiation and thermal creep resistance). Fe-Cr steels with small amounts of Si ($\approx 2\%$ wt.) [48] or slightly larger amounts of Al (4-10 % wt.) [49,50] and also Alumina Forming Austenitic (AFA) steels with Al $\approx 2.5\%$ wt. [51] are capable of forming protective Al- or Si- containing oxide layers which exhibit high corrosion resistance performance even at very high temperatures.

Surface alloying

The techniques for the surface alloying of steels with Al consists in:

- a) melting a steel surface covered with an Al foil or with a deposited Al layer by pulsed electron beams;
- b) diffusion alloying with hot dipping aluminizing method or pack cementation technique.

The first method is referred to the German process called GESA (Gepulste Elektronenstrahl Anlage), which is considered for the protection of fuel cladding tubes. Al is alloyed to the steel surface in two steps: 1) covering the steel surface with an Al foil [52,53] or with an Al-based coating such as a FeCrAlY layer [54] and 2) GESA treatment, i.e. melting the coated surface with high-energy electron beam pulses [52-54]. The second treatment is required to have a final smooth and compact Al-enriched surface by eliminating pores and the surface roughness. In addition, the GESA melting process is fundamental to create a sort of welding between the steel substrate and coating via interdiffusion of the elements at the steel/coating interface. Fig. 3.17 shows an example of Al surface modification obtained with GESA process on a FeCrAlY-coated 15-15Ti steel. Good corrosion resistance was observed for FeCrAlY-alloyed 15-15Ti tubes exposed for 5000 hours to flowing LBE at 500, 550 and 600°C with oxygen concentration $10^{-6}\%$ wt. [54] and also for FeCrAlY-alloyed T91 tubes in flowing LBE for 2000 hours at 480, 550 and 600°C with $10^{-6}\%$ wt. of oxygen [55].

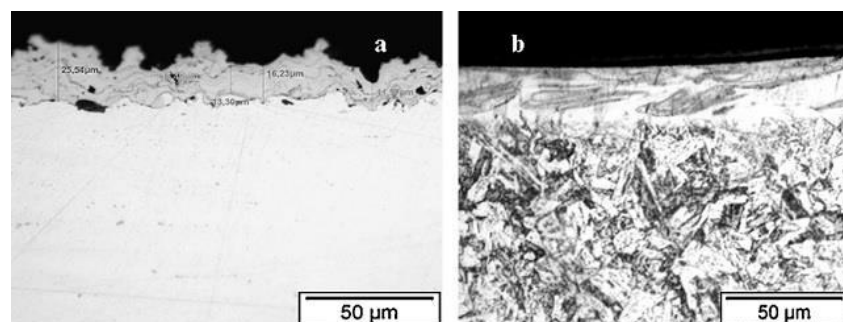


Fig. 3.17: Al surface alloying on 15-15Ti austenitic steel showing a) rough FeCrAlY coating obtained with LPPS (Low Pressure Plasma Spraying) and b) compact Al-modified surface after the GESA treatment [54].

Diffusion alloying methods such as Hot Dipping Aluminizing (HAD) and Pack Cementation are also considered. The methods involve the interdiffusion between the steel substrate and the Al (liquid or solid) on the steel surface. The hot dipping aluminizing is usually performed by dipping steel specimens into liquid Al at 700°C under a deoxidizing atmosphere [56]. The dipping time is about 30 seconds and subsequent heat treatments in the temperature range 700-1000°C are often performed

to restore the mechanical properties of the steel substrate. The formed Al-enriched layer is quite thick ($\approx 50\text{-}100\ \mu\text{m}$). The Al deposition via pack cementation is obtained by thermal decomposition at 750°C of powder mixtures containing Fe and Al (alloying elements) together with other powders such as NH_4Cl (activator) and Al_2O_3 (inert filler to reduce powders sintering) [57]. Pack cementation is industrially available for austenitic stainless steel but not for F/M steel. For the latter type, the process should be optimized at lower temperature ($\leq 750^\circ\text{C}$, tempering temperature) or eventually the process should include subsequent heat treatments optimized for the restore of the steel microstructure [57]. The thickness of the Al layer is usually $40\text{-}120\ \mu\text{m}$ depending on the process. The main issue with these methods concerns the control of the Al concentration in the outer layer, which is quite tricky. Indeed, brittle and highly-soluble Al-enriched phases (e.g. Al_5Fe_2) are prone to form when the Al concentration in the outer layer is high. In the case of hot dipping process, protective Al layers can be obtained by applying a suitable heat treatment after the deposition, which helps in completing the incorporation of Al into the steel matrix and transforming the Fe_2Al_5 phase into the more protective Fe-Al and $\alpha\text{-Fe(Al)}$ phases (see Fig. 3.18) [56]. Heat treatment is also important for the formation of an external thin Al_2O_3 scale with anti-corrosion properties. In the case of Pack cementation, the Al/Fe ratio in the powders has to be optimized to have a enough low Al activity in the final layer [57]. Experimental results about the exposure of Fe-Al pack cementation layer in LBE revealed that the layer provided a good protection of steels in static conditions for low oxygen concentrations ($10^{-7}\text{-}10^{-8}\ \%$ wt.) up to 500°C [57]. In dynamic conditions, localized corrosion attacks were found on aluminized steel both at moderate and high temperature (400 and 600°C) [57].

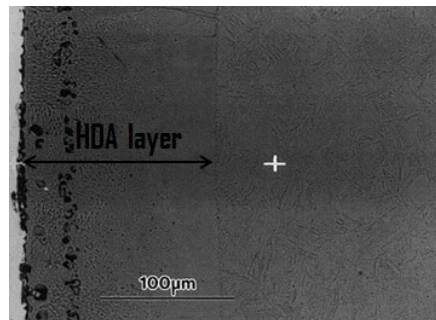


Fig. 3.18: Hot Dipping Aluminized F/M steel (MANET, Cr 11%, Mo 0.8%) after exposure in flowing HLM (Pb-16Li eutectic alloy) at 480°C for 10000h. The layer consists of external Fe-Al and internal $\alpha\text{-Fe(Al)}$ phases [56].

Coatings

Several types of coating were investigated as protective tools from HLM corrosion in recent years. Coatings have the main advantage to maintain the mechanical properties of the steel substrate. The major drawback is the lack of self-healing properties, meaning that the steel could be exposed to HLM attack if the coating is damaged or spalled off. Among the various coating produced with various techniques, some tested in HLMs are listed below:

- *Si- and Al- containing coatings* → Such coatings require a sufficient oxygen concentration in the HLM to promote the formation of a self-healing and stable Si- or Al- based oxide layer. An example of protective Si-containing coating is given by the Fe-12Cr-2Si coating, which demonstrated to have good corrosion protection when exposed in LBE with high and low oxygen concentration at 600 and 700°C [48];
- *Refractory Metal based coatings* → Refractory metals coatings such as Ta, W, Mo, Nb have very low solubility in liquid lead alloys [58-60] but they are very sensitive to high-temperature oxidation [11] and require an environment with very low oxygen activity to prevent the formation of the non-protective oxide scale. Exposure tests of Ta in static lead alloys at different temperatures between $400\text{-}900^\circ\text{C}$ and oxygen concentration ranging from the saturation to $10^{-6}\ \%$ wt. exhibited non-protective oxidation which becomes more severe with increasing temperature

(see Fig. 3.19) [61,62]. To the opposite, Ta exposed at very low oxygen concentration ($\leq 10^{-8}$ % wt.) showed no evidence of oxidation and dissolution [61,62].

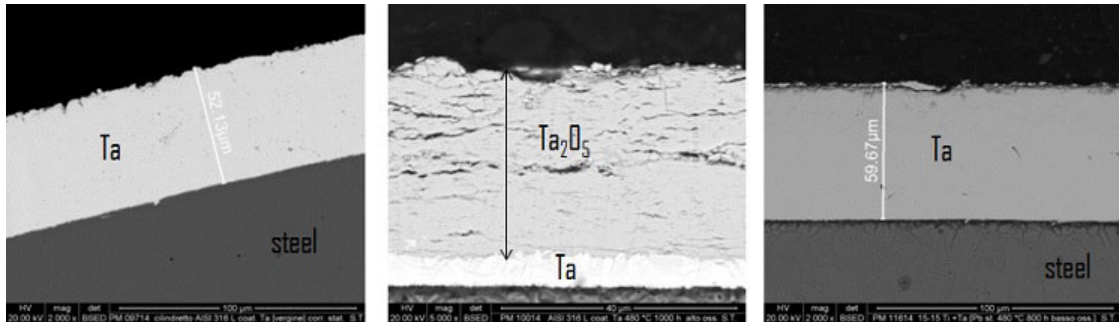


Fig. 3.19: Ta coating as deposited (left), exposed to static oxygen-saturated Pb at 480°C (10^{-4} % wt.) for 1000h (centre) and exposed in Pb at 480°C with low oxygen concentration (10^{-8} % wt.) for 700h [62].

- *Carbides and Nitrides based coatings* → Carbides and Nitrides such as SiC, Ti_3SiC_2 , TiN and CrN are very resistant to HLM corrosion [58,59,63] but they need an environment with low oxygen activity to prevent the degradation of the ceramic layer by oxidation. An example is given by TiN coating (Fig. 3.20), which tends to form TiO_2 when exposed to oxygen-saturated HLM [62].

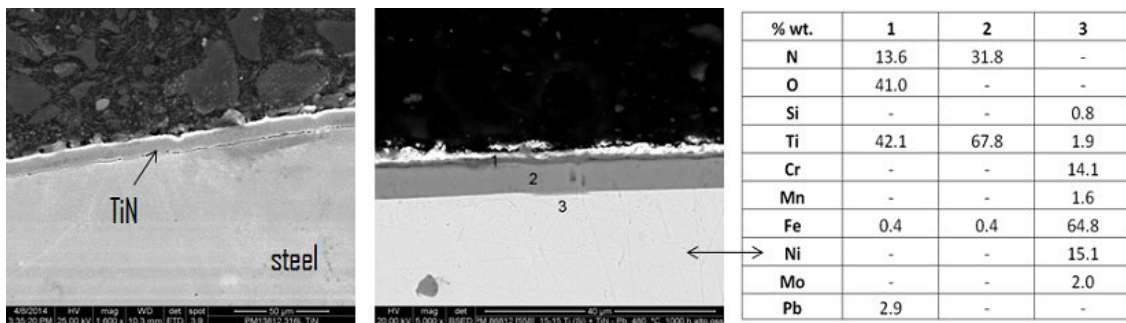


Fig. 3.20: TiN coating as deposited (left) and exposed to static oxygen-saturated Pb at 480°C (10^{-4} % wt.) for 1000h (centre) with indication of the local elemental composition obtained with EDS. The outer zone of the coating (1) underwent oxidation [62].

- *Oxide coatings* → Al_2O_3 coatings are very promising from the point of view of corrosion resistance. An example of such coating is the Al_2O_3 coating produced with Pulsed Laser Deposition (PLD) technique, which consists in an Al_2O_3 amorphous matrix with nano-crystalline inclusions [64-66]. The coating demonstrated high HLM corrosion resistance at 550°C even at low oxygen concentration (see Fig. 3.21) [66]. Since Al_2O_3 has high thermodynamic stability, the degradation of the coating is not expected in the oxygen concentration ranges in practice achievable in HLM.

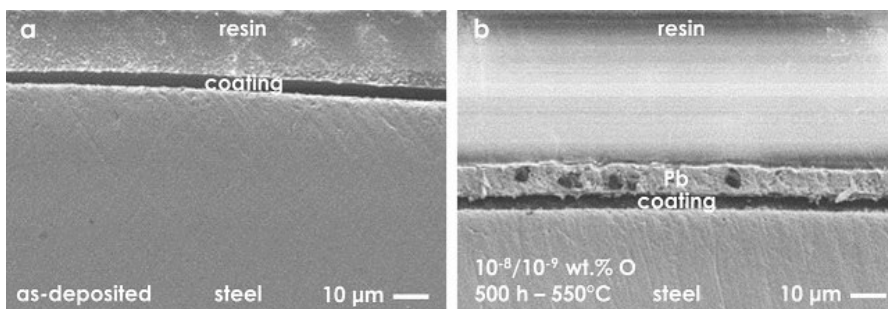


Fig. 3.21: Al_2O_3 coating before (a) and after (b) exposure in Pb at 550°C for 500 hours with low oxygen concentration 10^{-8} - 10^{-9} % wt. [66].

3.6 REFERENCES

- [1] OECD/NEA, "Handbook on lead-bismuth eutectic alloy and lead properties, materials compatibility, thermal-hydraulics and technologies", (2015).
- [2] C. Schroer, O. Wedemeyer, J. Novotny, A. Skrypnik, J. Konys, "Selective leaching of nickel and chromium from type 316 austenitic steel in oxygen-containing lead-bismuth eutectic (LBE)", *Corros. Sci.* 84 (2014) 113-124.
- [3] P.N. Martynov, A.V. Gulevich, Yu.I. Orlov, V.A. Gulevsky, "Water and hydrogen in heavy liquid metal coolant technology", 1st COE-INES International Symposium, October 31-November 4, 2004, Tokyo, Japan.
- [4] C. Schroer, O. Wedemeyer, J. Konys, "Aspects of minimizing steel corrosion in liquid Lead-alloys by addition of oxygen", *Nucl. Eng. Des.* 241 (2011) 4913-4923.
- [5] J-L. Courouau, S. Sellier, F. Balbaud, K. Woloshun, A. Gessi, P. Schuurmans, M. Ollivier, C. Chabert, "Initial start-up operations chemistry analysis for MEGAPIE", 5th MEGAPIE Technical Review Meeting, 2004, Nantes, France.
- [6] J.-L. Courouau, P. Agostini, P. Turrone, H. Glassbrenner, "Review of the oxygen control for the initial operations and integral tests of the MEGAPIE spallation target", 6th MEGAPIE Technical Review Meeting, 2005, Mol, Belgium.
- [7] C. Schroer, O. Wedemeyer, J. Novotny, A. Skrypnik, J. Konys, "Performance of 9% Cr steels in flowing lead-bismuth eutectic at 450 and 550°C, and 10⁻⁶ mass % dissolved oxygen", *Nucl. Eng. Des.* 280 (2014) 661-672.
- [8] M. Tarantino, S. Bassini, D. Rozzia, "ALFRED PROJECT. Research and Development Needs", ENEA Technical Report LR-P-R-126 (2015).
- [9] C. Schroer, J. Konys, "Physical chemistry of corrosion and oxygen control in liquid lead and lead-bismuth eutectic", Report FZKA 7364, Forschungszentrum Karlsruhe, Germany (2007).
- [10] P.R. Roberge, "Handbook of corrosion engineering", McGraw-Hill Education (1999).
- [11] "Uhlig's corrosion handbook", Third Ed., Edited by R. Winston Revie (2011).
- [12] J. Zhang, N. Li, "Review of the studies on fundamental issues in LBE corrosion", *J. Nucl. Mater.* 373 (2008) 351-377.
- [13] K. Lambrinou, S. Gavrillov, A. Heinzl, G. Schumacher, A. Weisenburger, L. Gomez-Briceño, "Liquid metal corrosion results", MATTER collaborative project G.A. 269706 (EURATOM FP7), Deliverable 3.6 Part A: Literature review (2015).
- [14] V. Beznosov, A.D. Zudin, A.V. Lvov, A.O. Soloviev, A.S. Chernysh, "Experimental research of the performance of devices used to regulate thermodynamic activity of oxygen and purify a lead coolant on high-temperature benches", Proceedings of Innovative Designs and Technologies of Nuclear Power Conference, October 7-10, 2014, "Nikiet" Moscow, Vol.2, 382-389.
- [15] C. Fazio, I. Ricipito, G. Scaddozzo, G. Benamati, "Corrosion behaviour of steels and refractory metals and tensile features of steels exposed to flowing PbBi in the LECOR loop", *J. Nucl. Mater.* 318 (2003) 325-332.
- [16] H.O. Nam, J. Lim, D.Y. Han, I.S. Hwang, "Dissolved oxygen control and monitoring implementation in the liquid lead-bismuth eutectic loop: HELIOS", *J. Nucl. Mater.* 376 (2008) 381-385.
- [17] C. Schroer, O. Wedemeyer, J. Konys, "Gas/liquid oxygen-transfer to flowing lead alloys", *Nucl. Eng. Des.* 241 (2011) 1310-1318.

- [18] I. Ricapito, C. Fazio, G. Benamati, "Preliminary studies on PbO reduction in liquid Pb-Bi eutectic by flowing hydrogen", *J. Nucl. Mater.* 301 (2002) 60-63.
- [19] V.M. Poplavsky, A.D. Efanov, F.A. Kozlov, Y.I. Orlov, A.P. Sorokin, "Liquid metal coolants technology for Fast Reactors", *Journal of Materials Science and Engineering B* 1 (2011) 913-928.
- [20] J. Zhang, N. Li, Y. Chen, "Oxygen control technique in molten lead and lead-bismuth eutectic systems", *Nucl. Sci. Eng.* 154 (2006) 223-232.
- [21] R.Sh. Askadullin, "Development of oxygen sensors, systems of control of oxygen content in lead coolants for test loops and facilities", Final Report ITSC Project #3020, Institute for Physics and Power Engineering (IPPE), Obninsk, Russia (2007).
- [22] N. Li, "Lead-alloy coolant technology and materials - Technology readiness level evaluation", *Progr. Nucl. Energ.* 50 (2008) 140-151.
- [23] J. Ejenstam, "Corrosion resistant alumina-forming alloys for lead-cooled fast reactors", Doctoral Thesis in Chemistry, Stockholm, Sweden, 2015.
- [24] C.H. Lefhalm, J.U. Knebel, K.J. Mack, "Kinetics of gas phase oxygen control system (OCS) for stagnant and flowing Pb-Bi systems", *J. Nucl. Mater.* 296 (2001) 301-304.
- [25] G. Muller, A. Heinzl, G. Schumacher, A. Weisenburger, "Control of oxygen concentration in liquid lead and lead-bismuth", *J. Nucl. Mater.* 321 (2003) 256-262.
- [26] L. Brissonneau, F. Beauchamp, O. Morier, C. Schroer, J. Konys, A. Kobzova, F. Di Gabriele, J.-L. Courouau, "Oxygen control systems and impurity purification in LBE: Learning from DEMETRA project", *J. Nucl. Mater.* 415 (2011) 348-360.
- [27] Y.I. Orlov, A.D. Efanov, P.N. Martynov, V.A. Gulevsky, A.K. Papovyants, Y.D. Levchenko, V.V. Ulyanov, "Hydrodynamic problems of heavy liquid metal coolants technology in loop-type and mono-block-type reactor installations", *Nucl. Eng. Des.* 237 (2007) 1829-1837.
- [28] V.M. Poplavsky, A.D. Efanov, F.A. Kozlov, Y.I. Orlov, A.P. Sorokin, "Liquid metal coolants technology for fast reactors", International Conference on Fast Reactors and Related Fuel Cycles (FR09): Challenges and opportunities, 2009, Kyoto, Japan.
- [29] M. Kondo, M. Takahashi, K. Miura, T. Onizawa, "Study on control of oxygen concentration in lead-bismuth flow using lead oxide particles", *J. Nucl. Mater.* 357 (2006) 97-104.
- [30] P.N. Martynov, R.Sh. Askhadullin, A.A. Simakov, A.Yu. Chaban', A.Yu. Legkikh, "Designing mass exchangers for control of oxygen content in Pb-Bi (Pb) coolants in various research facilities", in Proceedings of the 17th International Conference on Nuclear Engineering (ICONE17), n°75506, July 12-16, 2009, Brussels, Belgium.
- [31] A. Marino, J. Lim, S. Keijers, J. Van den Bosch, J. Deconinck, F. Rubio, K. Woloshun, M. Caro, S.A. Maloy, "Temperature dependence of dissolution rate of a lead oxide mass exchanger in lead-bismuth eutectic", *J. Nucl. Mater.* 450 (2014) 270-277.
- [32] J. Lim, A. Marino, G. Manfredi, J. Van den Bosch, "Lead bismuth eutectic (LBE) chemical process control loop: MEXICO", Proceedings of the SEARCH/MAXSIMA International Workshop, October 7-10, 2014, Karlsruhe, Germany.
- [33] K. Naito, T. Tsuji, T. Matsui, K. Une, "Purification of inert gas: removal of oxygen with a metallic getter", *J. Nucl. Sci. Technol.* 11(1) (1974) 22-28.
- [34] K. Kitahara, K. Ohtsuka, N. Takemasa, S. Kamiyama, "Process for purification of rare gas", US Patent US 5194233 A (1993).
- [35] J.T. Snow, W. Plante, R.S. Zeller, "High-efficiency metal membrane getter element and process for making", US Patent 5456740 A (1995)

- [36] T.C. Golden, C.H. Johnson III, "Adsorbent for removal of trace oxygen from inert gases", US Patent US5536302 A (1996).
- [37] A. Dobi, D.S. Leonard, C. Hall, L.J. Kaufman, T. Langford, S. Slutsky, Y.-R. Yen, "Study of a zirconium getter for purification of xenon gas", Nucl. Instrum. Meth. A 620 (2010) 594-598.
- [38] B.R. Grundy, "Getter trap for removing hydrogen and oxygen from a liquid metal", US Patent US4830816 (1989).
- [39] R.S. Reid, M.A. Merrigan, J.T. Sena, "Review of liquid metal heat pipe work at Los Alamos", Proceedings of 8th Symposium on Space Nuclear Power Systems, M.S. El-Genk and M.D. Hoover Ed., American Institute of Physics, New York, CONF-910116 (1991).
- [40] G. Ilinev, "Research results on the corrosion effects of liquid heavy metals Pb, Bi and Pb-Bi on structural materials with and without corrosion inhibitors", Nucl. Eng. Des. 217 (2002) 167-177.
- [41] J.R. Weeks, C. J. Klamut, "Reactions between steel surfaces and zirconium in liquid bismuth", Nucl. Sci. Eng. 8 (1960) 133-147.
- [42] C. Cristalli, A. Gessi, P. Agostini, S. Eremin, "Corrosion behaviour of reference materials exposed to Pb, after fast neutrons irradiation in the BOR60 reactor up to 16 DpA", NUMAT Conference, October 2014, Florida, USA.
- [43] P. Agostini, "Materials properties and selection", MATTER collaborative project G.A. 269706 (EURATOM FP7), Deliverable D9.2 (2011).
- [44] M. Caro, K. Woloshun, F. Rubio, S.A. Maloy, P. Hosemann, "Heavy liquid metal corrosion of structural materials in advanced nuclear systems", JOM, Vol. 65, No. 8 (2013), DOI: 10.1007/s11837-013-0663-7.
- [45] D. Gorse, T. Auger, J.-B. Vogt, I. Serre, A. Weisenburger, A. Gessi, P. Agostini, C. Fazio, A. Hojna, F. Di Gabriele, J. Van Den Bosch, G. Coen, A. Almazouzi, M. Serrano, "Influence of liquid lead and lead-bismuth eutectic on tensile, fatigue and creep properties of ferritic/martensitic and austenitic steels for transmutation systems", J. Nucl. Mater. 415 (2011) 284-292.
- [46] Y. Kurata, "Corrosion behavior of cold-worked austenitic stainless steels in liquid lead-bismuth eutectic", J. Nucl. Mater. 448 (2014) 239-249.
- [47] G. Muller, A. Heinzl, J. Konys, G. Schumacher, A. Weisenburger, F. Zimmermann, V. Engelko, A. Rusanov, V. Markov, "Behavior of steels in flowing liquid PbBi eutectic alloy at 420-600°C after 4000-7200h", J. Nucl. Mater. 335 (2004) 163-168.
- [48] M.P. Short, R.G. Ballinger, H.E. Hänninen, "Corrosion resistance of alloys F91 and Fe-12Cr-2Si in lead-bismuth eutectic up to 715°C", J. Nucl. Mater. 434 (2013) 259-281.
- [49] J. Ejenstam, M. Halvarsson, J. Weidow, B. Jönsson, P. Szakalos, "Oxidation studies of Fe₁₀CrAl-RE alloys exposed to Pb at 550°C for 10,000 h", J. Nucl. Mater. 443 (2013) 161-170.
- [50] A. Jianu, R. Fetzer, A. Weisenburger, S. Doyle, M. Bruns, A. Heinzl, P. Hosemann, G. Mueller, "Stability domain of alumina thermally grown on Fe-Cr-Al-based model alloys and modified surface layers exposed to oxygen containing molten Pb", J. Nucl. Mater. 470 (2016) 68-75.
- [51] J. Ejenstam, P. Szakalos, "Long term corrosion resistance of alumina forming austenitic stainless steels in liquid lead", J. Nucl. Mater. 461 (2015) 164-170.
- [52] G. Mueller, V. Engelko, A. Weisenburger, A. Heinzl, "Surface alloying by pulsed intense electron beams", Vacuum 77 (2005) 469-474.
- [53] A. Heinzl, M. Kondo, M. Takahashi, "Corrosion of steels with surface treatment and Al-alloying by GESA exposed in lead-bismuth", J. Nucl. Mater. 350 (2006) 264-270.

- [54] A. Weisenburger, G. Muller, A. Heinzl, A. Jianu, H. Muscher, M. Kieser, "Corrosion, Al containing corrosion barriers and mechanical properties of steels foreseen as structural materials in liquid lead alloy cooled nuclear systems", Nucl. Eng. Des. 241 (2011) 1329-1334.
- [55] A. Weisenburger, A. Heinzl, G. Muller, H. Muscher, A. Rousanov, "T91 cladding tubes with and without modified FeCrAlY coatings exposed in LBE at different flow, stress and temperature conditions", J. Nucl. Mater. 376 (2008) 274-281.
- [56] H. Glasbrenner, J. Konys, Z. Voss, O. Wedemeyer, "Corrosion behaviour of Al based tritium permeation barriers in flowing Pb-17Li", J. Nucl. Mater. 307-311 (2002) 1360-1363.
- [57] Ph. Deloffre, F. Balbaud-Célérier, A. Terlain, "Corrosion behaviour of aluminized martensitic and austenitic steels in liquid Pb-Bi", J. Nucl. Mater. 335 (2004) 180-184.
- [58] A. K. Rivai, M. Takahashi, "Compatibility of surface-coated steels, refractory metals and ceramics to high temperature lead-bismuth eutectic", Progr. Nucl. Energ. 50 (2008) 560-566.
- [59] A. K. Rivai, M. Takahashi, "Corrosion investigations of Al-Fe-coated steels, high Cr steels, refractory metals and ceramics in lead alloys at 700°C", J. Nucl. Mater. 398 (2010) 146-152.
- [60] E. Noah, V. Boutellier, R. Brüttsch, R. Catherall, D. Gavillet, J. Krbanjevic, H.P. Linder, M. Martin, J. Neuhausen, D. Schumann, T. Stora, L. Zanini, "Post-irradiation analysis of the tantalum container of an ISOLDE LBE target", J. Nucl. Mater. 431 (2012) 60-65.
- [61] A. Heinzl, G. Müller, A. Weisenburger, "Corrosion behaviour of welds and Ta in liquid lead", J. Nucl. Mater. 469 (2016) 62-71.
- [62] S. Bassini, "Prove di corrosione su materiali strutturali ricoperti in piombo stagnante in funzione del tenore di ossigeno", ADP ENEA-MiSE, Technical Report ADPFISS-LP2-098 (in italian) (2015).
- [63] H. Glasbrenner, F. Groschel, "Exposure of pre-stressed T91 coated with TiN, CrN and DLC to Pb-55.5Bi", J. Nucl. Mater. 356 (2006) 213-221.
- [64] F. García Ferré, E. Bertarelli, A. Chiodoni, D. Carnelli, D. Gastaldi, P. Vena, M.G. Beghi, F. Di Fonzo, "The mechanical properties of a nanocrystalline Al₂O₃/α-Al₂O₃ composite coating measured by nanoindentation and Brillouin spectroscopy", Acta Mater. 61 (2013) 2662-2670.
- [65] F. García Ferré, M. Ormellese, F. Di Fonzo, M.G. Beghi, "Advanced Al₂O₃ coatings for high temperature operation of steels in heavy liquid metals: a preliminary study", Corros. Sci. 77 (2013) 375-378.
- [66] F. García Ferré, A. Mairov, M. Vanazzi, S. Bassini, M. Utili, M. Tarantino, L. Ceseracciu, Y. Serruys, L. Beck, M.G. Beghi, K. Sridharan, F. Di Fonzo, "Ceramic coatings for innovative nuclear systems", Proceedings of NEA International Workshop on Structural Materials for Innovative Nuclear Systems, 11-14 July 2016, Manchester, UK.

4. OXYGEN SENSORS FOR HLM

4.1 GENERALITY

The accurate measure of the oxygen concentration in HLMs is fundamental to control the oxygen concentration in LFR and ADS. Consequently, reliable devices to monitor the oxygen concentration in the HLM are foreseen to be essential instruments in Pb-cooled nuclear systems.

In the last decade potentiometric ceramic-based sensors for the monitoring of the dissolved oxygen concentration in Pb and LBE have been developed and studied. These ceramic-based sensors have been proven to be highly accurate and reliable and they have been successfully employed in small scale experimental tests (e.g. small vessels and facility loops). However, concerning large scale experiments (e.g. large HLM pool facility), the main issue in the development of oxygen sensors is related to the ceramic fragility and the technological challenge is to guarantee an adequate protection of the ceramic inside the large HLM volume.

Up to now the most studied reference systems are the air system, such as the Pt-air system, and the liquid metal/metal-oxide system, in which the metal part is molten in the typical temperature range of HLM systems [1,2]. Among the latter, Bi/Bi₂O₃ and In/In₂O₃ systems (the melting point are 271°C and 157°C respectively) were widely investigated [2]. However, also solid metal/metal oxide reference systems can be employed and some have been recently studied in liquid Pb alloys and other molten metals (e.g. Cu/Cu₂O, Ni/NiO and Fe/Fe₃O₄) [3-5].

The ceramic used in the oxygen sensors is a “stabilized zirconia”, which is a zirconia doped with compounds such as Y₂O₃ and MgO. These compounds are required to stabilize up to room temperature the crystalline cubic form of zirconia, which is the conductive form of oxygen ions [6-9]. Chemical incompatibility of the stabilized zirconia with HLMs is not expected (and it has not been reported in studies about electrochemical sensors in these HLMs) because the oxygen concentration to be measured are much higher than the threshold for decomposition of the zirconia electrolyte. Furthermore, neutron irradiation on the zirconia does not involve damage or a change of the crystalline structure. According to the literature, the neutron flux on the zirconia affects only the electric potential of the sensor as a consequence of the arising of a new electric field in the electrolyte [10]. Anyhow, oxygen sensors in the nuclear reactor would be placed far away from the core and in positions where the neutron flux is low.

4.2 THE ELECTRIC POTENTIAL

Fig. 4.1 shows the conceptual scheme for the measurement of the oxygen concentration in HLM using a ceramic-based sensor. The ceramic acts as solid electrolyte and divides two media with different oxygen activity. In particular, the solid electrolyte divides the HLM, where the oxygen concentration has to be measured, from a reference system (gas or metal/metal-oxide), where the oxygen concentration is known and constant [11]. As a consequence of the different oxygen activity into the two media, an electromotive force (emf) arises across the ceramic element [11].

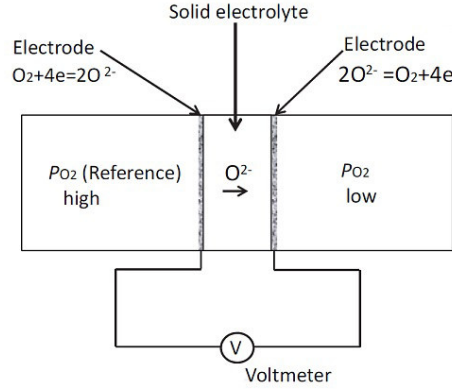


Fig. 4.1: Scheme of the oxygen measurement in HLMs using oxygen-conductive solid electrolyte [12].

The difference between the oxygen activities in the reference and in the working electrode promotes the rising of an electromotive force (emf) across the solid electrolyte, which is expressed by Nernst's law (assuming pure ionic conduction in the solid electrolyte):

$$E_{th} = \frac{RT}{4F} \cdot \ln \frac{p_{O_2(ref)}}{p_{O_2(Pb,LBE)}} \quad \text{Eq. 4.1}$$

where E_{th} is the theoretical emf (V), R is the gas constant (8.3145 J/mol·K), F is the Faraday constant (96484.6 C/mol), T is the temperature (K), $p_{O_2(ref)}$ and $p_{O_2(Pb,LBE)}$ are the oxygen partial pressures (bar) in the reference and in HLM respectively.

Considering oxygen sensors based on metal/metal-oxide and air reference systems, the electrochemical cell schemes are expressed as follows:

Mo (or SS), M/M_xO_y (reference) // solid electrolyte // Pb + PbO (lead alloy solution), SS

Pt, O₂ (reference) // solid electrolyte // Pb + PbO (lead alloy solution), SS

Mo is used as electrode wire in liquid metal/metal-oxide references and it is chosen for its insolubility in liquid Bi and In [13-17]. If the metal/metal-oxide reference is solid, a conventional stainless steel wire (SS) can be employed [3]. For air reference system, Pt wire acts as catalyst for the dissociation and reduction of the air O₂ molecules at the solid electrolyte surface according to the reaction reported in Fig. 4.1 [12].

The oxygen partial pressure $p_{O_2(Pb,LBE)}$ in HLMs is defined by Pb/PbO equilibrium according to Eq. 3.1 and the following equation:

$$p_{O_2(Pb)} = \frac{\Delta G_{PbO}^\circ}{RT} + 2 \ln \frac{a_O}{a_{Pb}} \quad \text{Eq. 4.2}$$

with $a_{Pb}=1$ if the working system is made of pure Pb and $a_{Pb}<1$ if the working system is made of LBE.

The oxygen partial pressure into the reference system $p_{O_2(ref)}$ is equal to 0.21 bar in the case of air reference (pressure in the air atmosphere), whereas in the case of metal/metal-oxide systems $p_{O_2(ref)}$ is defined by M/M_xO_y equilibrium according to Eq. 3.6 and the following equation:

$$p_{O_2(ref)} = \frac{\Delta G_{M_xO_y}^\circ}{RT} \quad \text{Eq. 4.3}$$

where the latter is true considering the activity of the metal and its oxide equal to 1.

By inserting into Eq. 4.1 the value of $p_{O_2(ref)}$ for air system (0.21 bar) and Eq. 4.2 defining $p_{O_2(Pb,LBE)}$ in the HLM working system, E_{th} for air sensors is defined as:

$$E_{th (air)} = -\frac{\Delta G_{PbO}^{\circ}}{4F} + \frac{RT}{4F} \cdot \ln 0.21 - \frac{RT}{2F} \ln \frac{a_{O}}{a_{Pb}} \quad \text{Eq. 4.4}$$

E_{th} for metal/metal-oxide sensors is defined by inserting Eq. 4.2 and Eq. 4.3 into Eq. 4.1:

$$E_{th (M/M_xO_y)} = \frac{\Delta G_{M_xO_y}^{\circ} - \Delta G_{PbO}^{\circ}}{4F} - \frac{RT}{2F} \ln \frac{a_{O}}{a_{Pb}} \quad \text{Eq. 4.5}$$

Tab. 4.1 reports standard Gibbs' free energies of formation ΔG° of some common oxides for the calculation of the theoretical electric potential of air and metal/metal-oxide based sensors. The data are referred to the consumption of one mole of O_2 .

Tab. 4.1: Standard Gibbs' free energy of formation of some oxides per mole of O_2 consumed.

Reaction	$\Delta G^{\circ}_{(J/mol)} = \Delta H^{\circ}_{(J/mol)} - T_{(K)} \cdot \Delta S^{\circ}_{(J/mol \cdot K)}$	T range ($^{\circ}C$)	Reference
$4Cu + O_2 \leftrightarrow 2 Cu_2O$	$-338528 + 148.1 \cdot T_{(K)}$	200-450	[3]
$4/3 Bi + O_2 \leftrightarrow 2/3 Bi_2O_3$	$-389140 + 192.6 T_{(K)}$	127-727	[11]
$2 Pb + O_2 \leftrightarrow 2 PbO$	$-437608 + 199.1 T_{(K)}$	127-727	[11]
$4/3 In + O_2 \leftrightarrow 2/3 In_2O_3$	$-618674 + 216.8 T_{(K)}$	127-727	[11]

Tab. 4.2 reports the final equations to determine the theoretical electric potential for oxygen-saturated ($E_{th,sat}$) and oxygen-unsaturated conditions ($E_{th,unsat}$) as a function of temperature (T) for some metal/metal-oxide and air sensors in Pb and LBE. Note that the electric potential in oxygen-saturated conditions only depends on the temperature, whereas the electric potential in oxygen-unsaturated conditions depends on temperature and oxygen concentration ($C_{O, \%wt.}$).

Tab. 4.2: Theoretical electric potential as a function of temperature and oxygen concentration for Bi/ Bi_2O_3 , In/ In_2O_3 , Cu/ Cu_2O metal/metal-oxide and air based sensors in Pb and LBE.

Reference	Pb	LBE
Bi/Bi_2O_3	$E_{th,sat} (V) = 0.1256 - 0.00001684 \cdot T_{(K)}$ $E_{th,unsat} (V) = -0.3743 + 0.0003033 \cdot T_{(K)} - 0.0000431 \cdot T_{(K)} \cdot \ln C_{O \%wt.}$	$E_{th,sat} (V) = 0.1198 - 0.00005390 \cdot T_{(K)}$ $E_{th,unsat} (V) = -0.2891 + 0.0001691 \cdot T_{(K)} - 0.0000431 \cdot T_{(K)} \cdot \ln C_{O \%wt.}$
In/In_2O_3	$E_{th,sat} (V) = -0.4693 + 0.00004586 \cdot T_{(K)}$ $E_{th,unsat} (V) = -0.9692 + 0.0003660 \cdot T_{(K)} - 0.0000431 \cdot T_{(K)} \cdot \ln C_{O \%wt.}$	$E_{th,sat} (V) = -0.4751 + 0.000008803 \cdot T_{(K)}$ $E_{th,unsat} (V) = -0.8840 + 0.0002318 \cdot T_{(K)} - 0.0000431 \cdot T_{(K)} \cdot \ln C_{O \%wt.}$
Cu/Cu_2O	$E_{th,sat} (V) = 0.2567 - 0.0001321 \cdot T_{(K)}$ $E_{th,unsat} (V) = -0.2432 + 0.0001881 \cdot T_{(K)} - 0.0000431 \cdot T_{(K)} \cdot \ln C_{O \%wt.}$	$E_{th,sat} (V) = 0.2509 - 0.0001691 \cdot T_{(K)}$ $E_{th,unsat} (V) = -0.1528 + 0.00005389 \cdot T_{(K)} - 0.0000431 \cdot T_{(K)} \cdot \ln C_{O \%wt.}$
Air	$E_{th,sat} (V) = 1.1339 - 0.0005495 \cdot T_{(K)}$ $E_{th,unsat} (V) = 0.6340 - 0.0002293 \cdot T_{(K)} - 0.0000431 \cdot T_{(K)} \cdot \ln C_{O \%wt.}$	$E_{th,sat} (V) = 1.1281 - 0.0005866 \cdot T_{(K)}$ $E_{th,unsat} (V) = 0.7244 - 0.0003635 \cdot T_{(K)} - 0.0000431 \cdot T_{(K)} \cdot \ln C_{O \%wt.}$

Equations in Tab. 4.2 enable to plot the E vs T diagram with $C_{O, \%wt.}$ depicted as iso-concentration line, allowing to easily check out the oxygen concentration in the HLM. The potential output can also be compared to the oxygen potential corresponding to the Pb/PbO equilibrium (oxygen saturation and PbO formation) and other oxides equilibria, e.g. the Fe/ Fe_3O_4 equilibrium useful to define the

minimum oxygen concentration required for the self-protection of steels. The E vs T diagrams of $\text{Bi}/\text{Bi}_2\text{O}_3$, $\text{Cu}/\text{Cu}_2\text{O}$ and air based sensor are reported in Fig. 4.2, Fig. 4.3 and Fig. 4.4 for Pb and LBE.

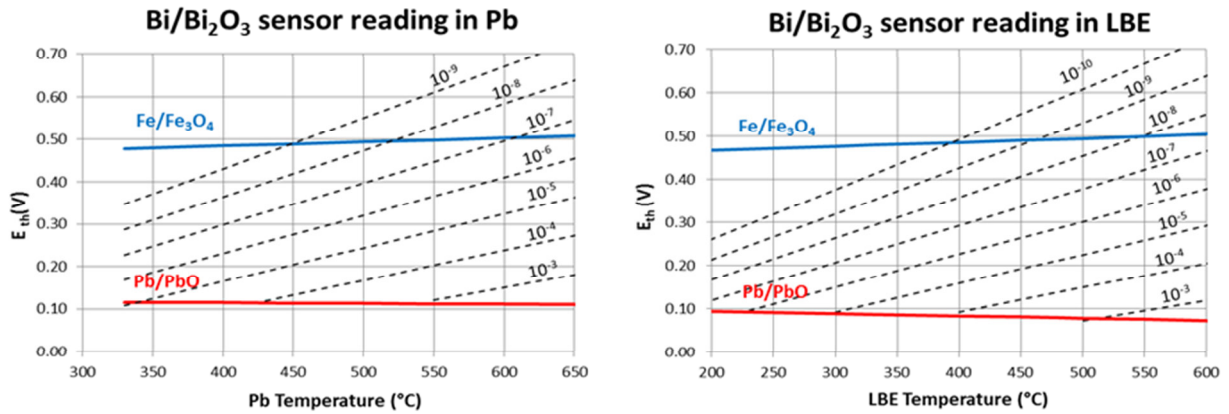


Fig. 4.2: E_{th} vs T diagram for $\text{Bi}/\text{Bi}_2\text{O}_3$ sensor in Pb (left) and LBE (right) showing the oxygen iso-concentration lines (% wt.) as well as the Pb/PbO and the Fe_3O_4 equilibria.

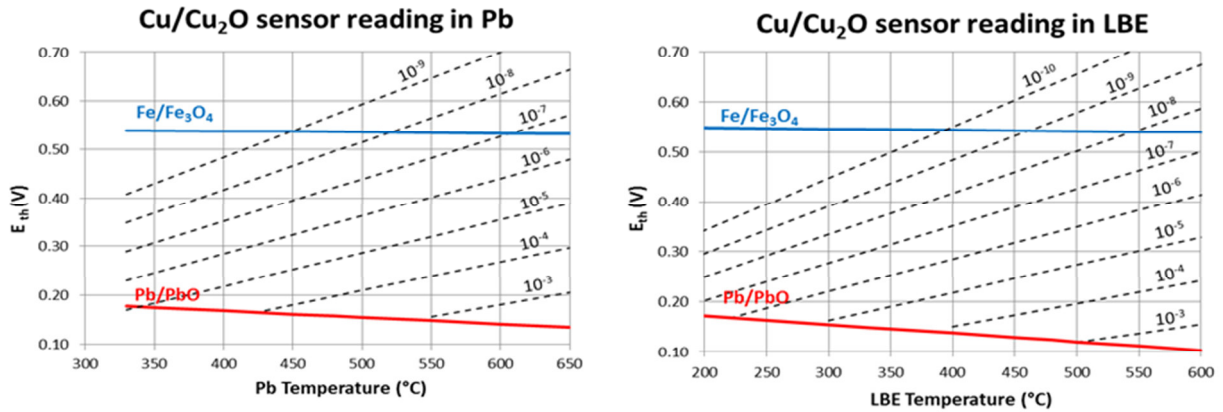


Fig. 4.3: E_{th} vs T diagram for $\text{Cu}/\text{Cu}_2\text{O}$ sensor in Pb (left) and LBE (right) showing the oxygen iso-concentration lines (% wt.) as well as the Pb/PbO and the Fe_3O_4 equilibria.

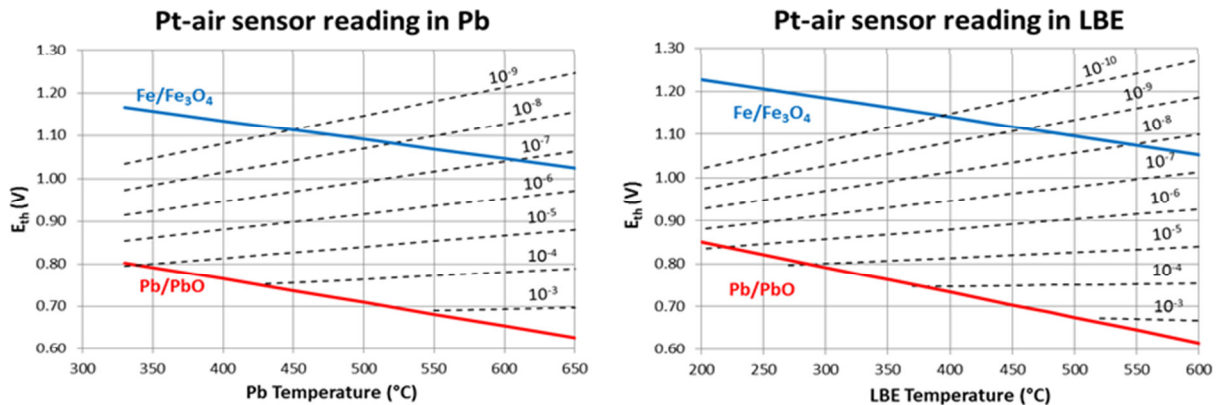


Fig. 4.4: E_{th} vs T diagram for air sensor in Pb (left) and LBE (right) showing the oxygen iso-concentration lines (% wt.) as well as the Pb/PbO and the Fe_3O_4 equilibria.

4.3 FEATURES

4.3.1 Manufacturing and Use

For tests in laboratory or in loop facility, the common oxygen sensor design is based on a one-end closed tube made of the oxygen-conductive ceramic (stabilized zirconia) and a reference electrode contained within the tube. The ceramic tube allows the separation of the reference from the HLM, as depicted in the scheme reported in Fig. 4.5. A metal housing at the end of the tube is normally used to accommodate the fittings for the electrode wire and other electrical connections.

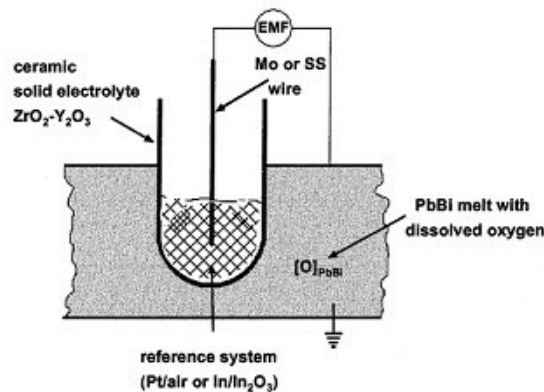


Fig. 4.5: Illustration of an oxygen sensor for HLM. The ceramic one-end closed tube contains the reference system, e.g. a Pt-air or a Mo-metal/metal-oxide electrode [1].

For air reference system, the housing provides also openings for gas inlet into the solid electrolyte tube. The air-tightness of the joint can easily be achieved by means of a pressed polymer O-ring with sufficient thermal stability [8]. The wire electrode is usually made of steel and it has a platinized tip in contact with the bottom of the electrolyte tube. Fig. 4.6 shows the image of a Pt-air oxygen sensor developed at KIT for the operation in static conditions in a small amount of melt [18].



Fig. 4.6: Pt-air oxygen sensor for the operation in static Pb and LBE (small amount of melt) [18].

Concerning the manufacturing of a metal/metal-oxide reference electrode (liquid and solid), metal and metal-oxide powders are mixed together and put at the bottom of the one-end closed tube [8,13-17]. The electric wire is made of Mo or SS, depending on whether a liquid or solid liquid metal/metal-oxide references is used. Particular attention must be paid to the tightness of the ceramic tube in order to prevent oxygen contamination inside the reference system and thus the entire consume of the metal phase. Methods to achieve the tightness consists in sealing the gap between the reference electric wire and the electrolyte tube walls with a ceramic sealant [8] or using pulsed electromagnetic force to compress the steel tube (housing) on the electrolyte tube [16,17]. In

alternative, the design of the sensor in Fig. 4.6 could be used also for metal/metal-oxide systems by omitting the openings for air.

Once the manufacturing is complete, the sensor in the HLM needs some time for its "activation". For Pt-air sensor, activation is required to start the oxygen ions catalysis by Pt wire. For metal/metal-oxide sensor, activation consists in consuming the excess of oxygen in the reference system and thus reaching the M/M_xO_y oxygen partial pressure equilibrium. Activation is usually achieved during calibration procedure in the temperature range 450-550°C. When the potential output is stable, the reference system is at the thermodynamic equilibrium and the sensor is considered activated and ready for the operation.

The emf is measured with a high impedance voltmeter (>10 Gohm), which is recommended in particular with air sensors to avoid deviations from the theoretical values at low temperatures [19].

4.3.2 Operating Temperature

One of the main drawbacks of ceramic sensors is the scarce conductivity of the ceramic element at low temperature (below 350-300°C). The resistance of ions movement through the solid electrolyte increases with decreasing temperature affecting the output at lower temperature. Concerning Pt-air system, the phenomenon is even more pronounced due to the higher resistance of the gas/solid electrolyte junction. To the opposite, liquid metal/metal oxide systems provide a better contact thanks to the HLM/solid electrolyte junction. As a results, the minimum operating temperature for a Pt-air based sensor is reported to be around 400°C [12,13] whereas for a liquid metal/metal-oxide sensor is around 300°C [16,17].

The scarce performances at low temperature of air based sensors depend also on the catalytic behaviour of the electrode material. For instance, perovskite oxides, already used for Solid-Oxide Fuel Cells (SOFCs), have been demonstrated better performance than Pt. In a study performed by Lim [19], the performance of air reference systems based on LSM/GDC (Strontium-doped Lanthanum Manganite/Gadolinium-Doped Ceria) were compared to standard Pt-air reference (and Bi/Bi₂O₃) at low temperature, using for both the same type of solid electrolyte (Yttria Stabilized Zirconia, YSZ). The results indicate that LSM/GDC electrode exhibits a good behaviour in HLMs even down to 200°C, demonstrating that the performances of air based sensors depends largely on the catalytic behaviour of the electrode material.

Another example of improvement of the performance at low temperature is given by Cu/Cu₂O reference system. A recent study carried out by Manfredi [3] reveals that oxygen sensors with such reference are able to measure oxygen correctly even down to 200°C.

4.3.3 Ceramic Failure and Protection

Oxygen sensors manufactured as shown in Fig. 4.6 are strongly subjected to thermal gradients and shear stresses when exposed to flowing HLM or large HLM volume. In such conditions, the ceramic electrolyte is prone to crack.

For liquid metal/metal-oxide sensors the chance of ceramic failure is even greater than in air sensors as a result of internal stresses during solidification and melting steps induced by the volume changes of the liquid metal inside the electrolyte tube [2]. As a consequence, internal stresses will lead to the failure of the ceramic tube if the electrolyte undergoes rapid thermal gradients. To the opposite, air based sensors are not subjected to internal stresses and exhibit higher service lifetime when compared to liquid metal/metal-oxide systems [8,13].

The limitation of liquid metal/metal-oxide reference systems could be circumvented by using solid metal/metal-oxide electrodes (e.g. Cu/Cu₂O and Fe/Fe₃O₄) in which the metal phase is solid throughout the entire working temperature range. Although the study of these reference systems has begun only recently, this positive feature makes these reference systems very promising [3,4].

The choice of a suitable ceramic helps in reducing the chance of failure of the solid electrolyte. For instance, Yttria Stabilized Zirconia (YSZ) exhibits higher mechanical and thermal shock resistance when compared with other stabilized zirconia [6]. Among YSZ ceramics, the partially stabilized zirconia (YPSZ with 3-5 % mol of Y_2O_3 , mixture of tetragonal and cubic crystalline phase) exhibits higher mechanical strength than the fully stabilized one (Y-FSZ with 8 % mol of Y_2O_3 , only cubic crystalline phase), which on the contrary exhibits higher ionic conductivity [6,8,9]. The addition of small amounts of Al_2O_3 ($\leq 2\%$ wt.) also enhances the mechanical strength of zirconia [8,9].

In addition, a proper sensor design can protect the solid electrolyte during the operation and thus reduce the chance of failure. Among the various options, one consists in protecting the ceramic tube with a metallic sheath able to reduce the mechanical and thermal shock along the electrolyte tube [8,20]. The steel sheath around the tube is in fact helpful in distributing the heat along the electrolyte, thus reducing thermal stresses. Fig. 4.7 (left) reports an example of oxygen sensor with perforated steel sheath for the protection of the solid electrolyte. The perforation of the sheath allows the close contact between the electrolyte and the HLM. Pieces resulting from accidental failure of the electrolyte during operation could be retained inside the sheath if the end is closed with either a grid or impermeable plate.

Another option to avoid the failure of the solid electrolyte consists in using a short ceramic thimble instead of the long one-end closed tube. The joint between the solid electrolyte and the steel body is obtained by using a glass ceramic cement (Fig. 4.7, center) as developed by IPPE [21] or a graphite seal for the tightness (Fig. 4.7, right) as developed at LANL (Los Alamos National Laboratory) [22].

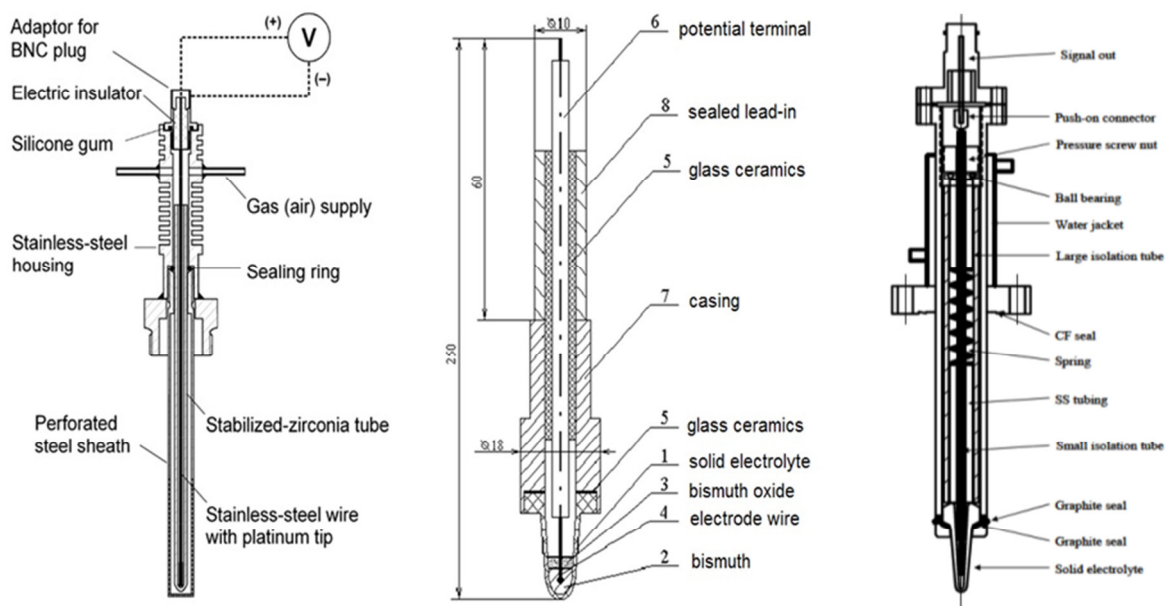


Fig. 4.7: Sensor designs for the protection of the solid electrolyte; Pt-air sensor with perforated steel sheath (left) [8], liquid metal/metal-oxide sensor with YSZ thimble and glass ceramic (center) [21] and liquid metal/metal-oxide sensor with YSZ thimble and graphite seal developed (right) [22].

4.3.4 Effect of Impurities

The sensor output is very sensitive to the presence of impurities in the HLMs (e.g. dissolved metallic impurities and metallic oxides). In long-term operation the signal can be affected by time drift due to the deposition of impurities at the solid electrolyte interface [20].

According to Courouau [20], impurities at the ceramic interface create an environment with different impurities and oxygen concentrations compared to the HLM bulk. In this environment, the oxygen may react with metallic impurities (e.g. forming metallic oxides), decreasing the local oxygen

concentration. The use of a metallic sheath or metallic mesh to protect the ceramic tube can even stimulate this tendency [8,20]. Indeed, sheaths or meshes do not encourage the renewal of HLM at the ceramic interface thus favouring the deposition of metallic impurities (also coming from the sheath itself).

The mechanism of the deposition of impurities on an oxygen sensor (fouling) protected by metallic sheath [20] is depicted in Fig. 4.8. During the correct operation, the sensor monitors an oxygen concentration at the solid electrolyte interface $[O]_i$ equal to the one in the HLM bulk $[O]_{bulk}$. The subsequent deposition of impurities gradually modified the oxygen concentration close to interface $[O]_i$, which keeps on evolving independently from that one in the HLM bulk $[O]_{bulk}$.

A sensor fouled by impurities can be easily recovered by applying a cleaning procedure. For instance, the aqueous solution made of hydrogen peroxide and acetic acid or also the nitric acid solution are effective in removing oxides and residual Pb and Bi [23]. Once cleaned, the sensor can be recalibrated and reused.

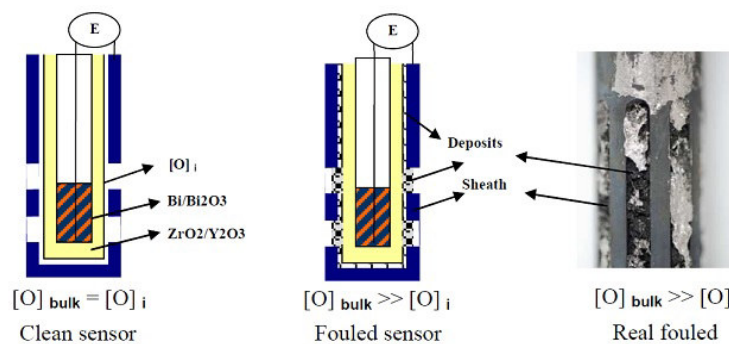


Fig. 4.8: Schematic illustration of the formation of deposits (fouling) at the solid electrolyte interface and qualitative effect on the oxygen concentration at the electrolyte surface $[O]_i$ compared to the concentration in the HLM bulk $[O]_{bulk}$ [20].

4.4 CALIBRATION

Calibration of oxygen sensors is based on the comparison of the potential output with the expected theoretical emf for well-defined oxygen concentrations. The main difficulty in the calibration procedure consists in defining exactly the oxygen concentration in the HLM since the oxygen is dissolved at ppm levels and its concentration in the HLM might be influenced by the presence of other impurities.

Several methods to assess the accuracy of the oxygen sensors in HLMs were developed in the last decade. All the methods rely on specific procedures to create a static environment with well-defined oxygen concentrations, e.g. by using the Pb/PbO equilibrium at different temperatures [1,2,16], by using a cover gas with a specific H_2/H_2O ratio [13] or by using electrochemical oxygen pump [24]. Among that, the first method is the simplest and the most frequently used since it is possible to know with good accuracy the oxygen concentration in the HLM from the solubility equations available in literature [1,2,15]. Another method used by Lim [16] is based on temperature variation in oxygen-saturated liquid Sn. Liquid Sn has a low melting point (232°C) and this allows to calibrate sensors easily. Furthermore, the Sn/SnO₂ equilibrium is close to the Fe/Fe₃O₄ one, which means performing a sensor calibration closed to the oxygen potential required for Fe₃O₄ formation.

During the calibration procedures, a slight scatter of few mV from the theoretical values is always observed, probably ascribable to the presence of impurities in HLM which may react at the solid electrolyte interface. However, a scatter of this magnitude can be considered negligible and, once assessed the sensor accuracy, the theoretical emf equations for the evaluation of the oxygen concentration can be used as well.

4.5 OXYGEN SENSORS FOR LARGE HLM POOL

The monitoring of the oxygen concentration in large HLM pool is one of the key work areas in the development of an effective oxygen control system in Pb-cooled nuclear reactors. The experimental work performed in recent years led to development of suitable sensor for HLM loops, allowing to start the study of the oxygen control devices. Now the technological challenge consists in transferring the acquired know-how to sensors for HLM pool type facilities, where technological and safety requirements are completely different.

In particular, an oxygen sensor for HLM pool should meet the following requirements [2,8,13,14,25]:

- high resistance to high HLM pressure, mechanical stresses and thermal gradients typical of a large HLM volume, with particular attention to the solid electrolyte (the weakest part);
- sensor electric connectors should provide non-trouble operation under the conditions of temperature, pressure and humidity of the HLM pool environment;
- long-term service capability;
- safety devices in case of failure of the solid electrolyte, to avoid drawbacks such ceramic pieces running into the pool and prevent leaks of activated gases or Pb alloys outside the vessel.

A first effort in the development and testing of oxygen sensors for HLM pools had been made in the LBE-cooled pool facility CIRCE in ENEA Brasimone [25]. The sensors consisted in a ceramic thimble made of YSZ containing a Bi-Bi₂O₃ reference system. The thimble was connected with a metallic casing by means of a high temperature sealant to ensure a good air-tightness and a reliable connection. The sensor design is depicted in Fig. 4.9. For the experimental test, three oxygen sensors were manufactured with three different lengths to monitor the oxygen concentration at different depths in the pool (900, 2900 and 4900 mm) [25]. During the experimental test only two of the three oxygen sensors worked, while the third was likely broken since it showed a negative potential output [25]. Anyhow, the latter two sensor demonstrated to have a very short service lifetime (< 1000 hours), demonstrating that further efforts were needed to get to reliable devices for large HLM pool.

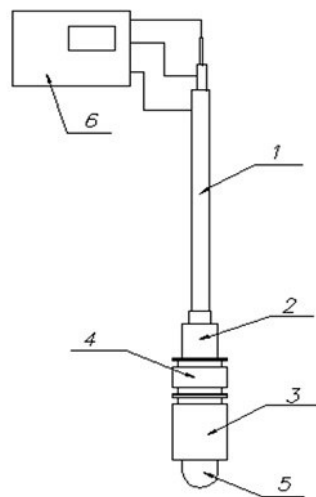


Fig. 4.9: Oxygen sensor tested in CIRCE pool showing 1) two-shell potential terminal lead, 2) sealed lead-in, 3) metallic casing of ceramic sensitive element, 4) adapter/sensor body, 5) YSZ element containing Bi/Bi₂O₃ reference and 6) measuring system with potential guarding [25].

4.6 REFERENCES

- [1] J. Konys, H. Muscher, Z. Voß, O. Wedemeyer, "Development of oxygen meters for the use in lead-bismuth", J. Nucl. Mater. 296 (2001) 289-294.

- [2] J.-L. Courouau, "Electrochemical oxygen sensors for on-line monitoring in lead-bismuth alloys: status of development", *J. Nucl. Mater.* 335 (2004) 254-259.
- [3] G. Manfredi, J. Lim, K. Rosseel, J. Van den Bosch, Th. Doneux, C. Buess-Herman, A. Aerts, "Comparison of solid metal-metal oxide reference electrodes for potentiometric oxygen sensors in liquid lead-bismuth eutectic operating at low temperature ranges", *Sensor. Actuat. B-Chem* 214 (2015) 20-28.
- [4] R. Van Nieuwenhove, J. Ejenstam, P. Szakalos, "Development of oxygen sensors for use in liquid metal", Abstract #19 - ANIMMA International Conference, 20-24 April 2015, Lisbon.
- [5] R. Kurchania, G. M. Kale, "Oxygen potential in molten Tin and Gibbs energy of formation of SnO₂ employing an oxygen sensor", *J. Mater. Res.*, Vol. 15, No. 7 (2000) 1576-1582.
- [6] P. N. Martynov, M. E. Chernov, V. A. Gulevskii, A. A. Provorov, "Development of a capsule-type electrochemical sensor for monitoring oxygen in heavy coolant", *Atom. Energy*, Vol. 98, No. 5, 2005.
- [7] A. K. Rivai, M. Takahashi, "Investigations of a zirconia solid electrolyte oxygen sensor in liquid lead", *J. Nucl. Mater.* 398 (2010) 160-164.
- [8] C. Schroer, J. Konys, A. Verdaguer, J. Abellà, A. Gessi, A. Kobzova, S. Babayan, J.-L. Courouau, "Design and testing of electrochemical oxygen sensors for service in liquid lead alloys", *J. Nucl. Mater.* 415 (2011) 338-347.
- [9] A. Mariën, J. Lim, K. Rosseel, W. Vandermeulen, J. Van den Bosch, "Solid electrolytes for use in lead-bismuth eutectic cooled nuclear reactors", *J. Nucl. Mater.* 427 (2012) 39-45.
- [10] N. Hiura, Y. Endo, T. Yamaura, T. Hoshiya, M. Niimi, J. Saito, "Electrical properties of neutron-irradiated oxygen potential sensors using stabilized zirconia solid electrolyte", *J. Nucl. Mater.* 258-263 (1998) 2041-2045.
- [11] OECD/NEA, "Handbook on lead-bismuth eutectic alloy and lead properties, materials compatibility, thermal-hydraulics and technologies", 2015.
- [12] Y. Kurata, "Application of electromotive force measurement in nuclear systems using lead alloys", *Electromotive Force and Measurement in Several Systems* (2011) Prof. Sadik Kara (Ed.), InTech, available at: <http://www.intechopen.com/books/electromotive-force-and-measurement-in-severalsystems/application-of-electromotive-force-measurement-in-nuclear-systems-using-lead-alloys>
- [13] J. Konys, H. Muscher, Z. Voß, O. Wedemeyer, "Oxygen measurements in stagnant lead-bismuth eutectic using electrochemical sensors", *J. Nucl. Mater.* 335 (2004) 249-253.
- [14] A. K. Rivai, T. Kumagai, M. Takahashi, "Performance of oxygen sensor in lead-bismuth at high temperature", *Prog. Nucl. Energ.* 50 (2008) 575-581.
- [15] S. Colominas, J. Abellà, "Evaluation of potentiometric oxygen sensors based on stabilized zirconia for molten 44.5% lead-55.5% bismuth alloy", *Sensor. Actuat. B-Chem* 145 (2010) 720-725.
- [16] J. Lim, A. Mariën, K. Rosseel, A. Aerts, J. Van den Bosch, "Accuracy of potentiometric oxygen sensors with Bi/Bi₂O₃ reference electrode for use in liquid LBE", *J. Nucl. Mater.* 429 (2012) 270-275.
- [17] G. Manfredi, J. Lim, K. Rosseel, J. Van den Bosch, A. Aerts, Th. Doneux, C. Buess-Herman, "Liquid metal/metal oxide reference electrodes for potentiometric oxygen sensor operating in liquid lead bismuth eutectic in a wide temperature range", *Eurosensors 2014, Procedia Eng.* 87 (2014) 264-267.

- [18] Corrosion Department of Institute for Applied Materials Material Process Technology, Karlsruhe Institute of Technology (KIT), "Experimental capsule for exposure of steels to oxygen-containing lead alloys: Technical documentation and user instructions", (2013).
- [19] J. Lim, G. Manfredi, A. Mariën, J. Van den Bosch, "Performance of potentiometric oxygen sensors with LSM-GDC composite electrode in liquid LBE at low temperatures", *Sensor Actuat. B-Chem* 188 (2013) 1048-1054.
- [20] J.-L. Courouau, C. Chabert, L. Pignoly, L. Gicquel, K. Ginestar, L. Brissonneau, "Demonstration of the effect of impurities on the long term behaviour of electrochemical oxygen sensor during the STELLA 2006 tests", *Proceeding of the 1st International Workshop on Technology and Components of Accelerator Driven Systems*, 2010, Karlsruhe, Germany.
- [21] R. Sh. Askadullin, "Development of oxygen sensors, systems of control of oxygen content in lead coolants for test loops and facilities", *Final Report ITSC Project #3020*, Institute for Physics and Power Engineering (IPPE), Obninsk, Russia (2007).
- [22] B. Fu, Y. Jiang, J. Ma, "Developing a sensing system for the measurement of oxygen concentration in liquid Pb-Bi eutectic", (2004) available at http://digitalscholarship.unlv.edu/me_fac_articles/10
- [23] S. Saito, T. Sasa, M. Umeno, Y. Kurata, K. Kikuchi, M. Futawaka, "Technology for cleaning of Pb-Bi adhering to steel. Basic Tests", *Technical Report JAERI-Tech2004-074* (2004).
- [24] V. Ghetta, J. Fouletier, M. Hénault, A. Le Moulec, "Control and monitoring of oxygen content in molten metals, application to lead and lead-bismuth melts", *J. Phys. IV* 12 (8) (2002) pp. 123-140.
- [25] IAEA, "Development of tools for on-line monitoring and control of HLM coolant chemistry", Chapter 8, *Report TECDOC-1696* (2013).

5. EXPERIMENTAL PART I: DEVELOPMENT OF OXYGEN SENSORS

5.1 ASSESSMENT OF THE PERFORMANCE OF OXYGEN SENSORS

5.1.1 Aim of the work

The performance of potentiometric oxygen sensors in HLMs is influenced by reference electrode as well as by the solid electrolyte used. Specifically, the type of reference electrode and solid electrolyte influences the minimum reading temperature, which is the last value of HLM temperature for which the sensor electric potential is still in agreement with the theoretical potential. The minimum reading temperature is a fundamental parameter for the application of oxygen sensors in HLMs and it determines the feasibility for a specific HLM environment.

In order to understand clearly the features influencing the performance in HLM, a baseline study about different oxygen sensors was performed. For the purpose, oxygen sensors with different reference electrodes and two solid electrolytes were manufactured, tested and compared one with each other. The reference electrodes chosen for the investigation were Pt-air, Bi/Bi₂O₃ and Cu/Cu₂O reference and the solid electrolyte used were Yttria Partially Stabilized Zirconia (YPSZ) and Yttria Totally Stabilized Zirconia (YTSZ). Pt-air (gas) and Bi/Bi₂O₃ (liquid) metal/metal-oxide references are among the most used in HLM but they both have a weak point: Pt-air sensor has a high minimum reading temperature around 400°C and Bi/Bi₂O₃ suffers from internal stresses induced by bismuth volume variations with temperature, which may lead to the sensor failure in the long-term. Cu/Cu₂O (solid) metal/metal-oxide reference has recently obtained some attention thanks to the low minimum reading temperature and the “solid” feature, which does not promote internal stresses inside the solid electrolyte compared to Bi/Bi₂O₃ one.

In the work below, oxygen sensors with Pt-air, Bi/Bi₂O₃ and Cu/Cu₂O references coupled with YPSZ solid electrolyte were investigated in HLM in the temperature range 160-550°C in order to evaluate their suitability in terms minimum reading temperature and accuracy. The investigation of Pt-air reference with YTSZ electrolyte were also performed to evaluate the influence of a different solid electrolyte on the minimum reading temperature. Finally, error analysis on the electric potential was preliminarily performed for some sensors (Pt-air and Cu/Cu₂O sensor with YPSZ) in order to estimate the intrinsic error of solid-electrolyte based sensors and the error on the oxygen concentration.

5.1.2 Experimental Setup

Sensor Fabrication and Description

Pt-air sensor was manufactured and supplied by KIT [1]. The sensor was composed of 250 mm long one-end closed tube of YPSZ with an external and internal diameter of 6 and 3 mm respectively. The electric lead of the reference electrode was a 316Ti stainless steel wire with a platinized tip in contact with the bottom of the YPSZ tube. A steel housing with openings for air ingress was in the upper part of the YPSZ tube. The same oxygen sensor was used for testing also YTSZ solid electrolyte. For this purpose, YPSZ tube was substituted with a one-end closed tube of YTSZ produced by FER Strumenti Srl (Seregno, Italy). The elemental composition of the YPSZ and YTSZ solid electrolytes determined by EDS is reported in Tab. 5.1.

Tab. 5.1: Elemental composition (% wt.) determined by EDS of YPSZ electrolyte from KIT sensor and YTSZ electrolyte produced by FER Strumenti.

Element (% wt.)	O	Al	Hf	Y	Zr
YPSZ	19.9	1.9	1.6	10.5	66.1
YTSZ	19.5	0.7	2.0	13.4	64.4

Sensors with Bi/Bi₂O₃ and Cu/Cu₂O references were manufactured in ENEA Brasimone. The solid electrolyte was a one-end closed tube of YPSZ supplied by Friatec AG (Y₂O₃ ≈ 5 mol. % ≈ 10 % wt.). The YPSZ tube was 400 mm long with external and internal diameter of 8 and 5 mm respectively. To create the metal/metal-oxide reference, metal and metal-oxide powders were mixed together with 9:1 ratio and loaded at the bottom of the YPSZ tube. The features of the powders were the following: Cu 99 %, 14-25 μm, (Sigma-Aldrich), Cu₂O 97 %, ≤ 7 μm (Sigma-Aldrich), Bi 99 %, 100 mesh (Sigma-Aldrich) and Bi₂O₃ 99.9 %, 10 μm (ReagentPlus). 316 stainless steel wire and Mo wire were used as electric lead for Cu/Cu₂O and Bi/Bi₂O₃ reference respectively. A refractory ceramic based on silicates (operative range up to 1200°C) was finally used to create the sealing in the upper part of YPSZ tube. Fig. 5.1 shows the pictures of the Pt-air sensor and metal/metal-oxide sensors tested in this study.

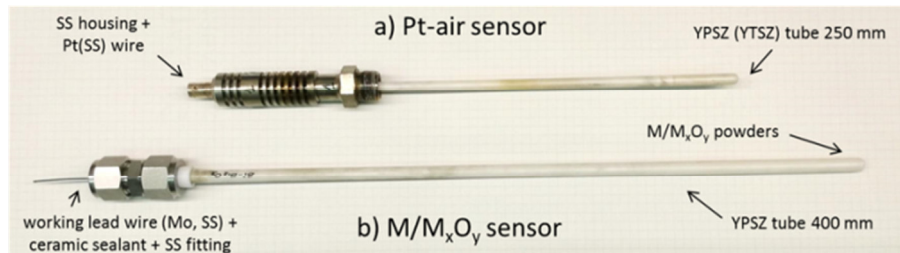


Fig. 5.1: Oxygen sensors with a) Pt-air reference (by KIT) and b) metal/metal-oxide reference.

Sensor Calibration

The sensor performance was assessed by calibration method in oxygen-saturated HLM in the range 160-550°C. The electric potential was compared to the theoretical one in different temperature conditions to define the accuracy of the measure and the minimum reading temperature.

Sensor calibrations were performed each one separately in experimental steel capsules (designed by KIT) containing oxygen-saturated HLM [1]. Pt-air sensors were tested in Pb in the temperature range 340-540°C whereas Bi/Bi₂O₃ and Cu/Cu₂O ones were tested in LBE in the ranges 260-550°C and 160-550°C respectively. The schematic set-up of the calibration in the steel capsules is shown in Fig. 5.2.

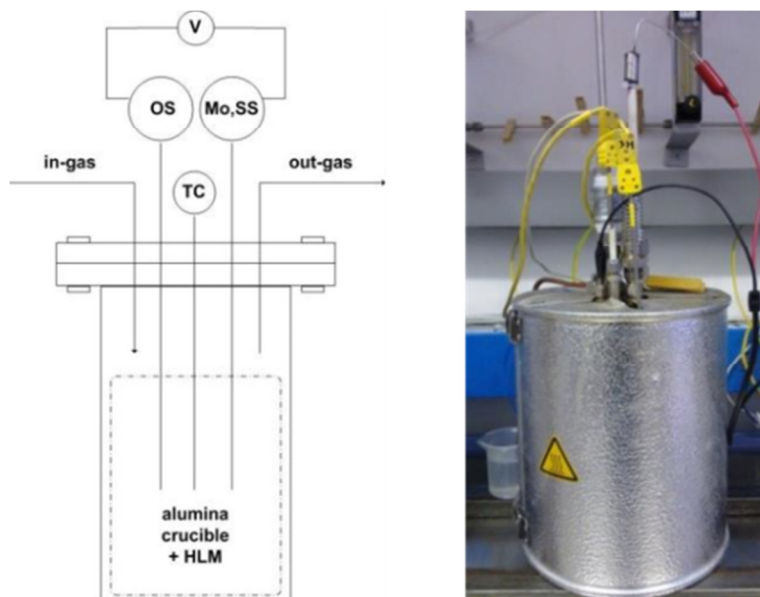


Fig. 5.2: Schematic set-up of sensor calibration in Pb and LBE (OS = oxygen sensor, TC = thermocouple, Mo, SS = working electric lead, V = multi-meter) and a picture of the calibration in steel capsule [1].

An alumina crucible placed at the bottom of the capsule was used as chemical inert container of about 750 g of HLM. The Pb had a nominal purity of 99.97% and it was provided by Ecobat Spa, whereas the LBE had a nominal composition of 44.6% Pb and 55.3 % Bi and it was provided by *Stachow-Metall* GmbH. Before the calibration, a steel tool was used to mechanically remove the free level of the fresh HLM at low temperature in order to reduce starting contaminations such as oxides and metal impurities. A K-type thermocouple (operative range 0-1100°C) inside a one-end close tube of alumina was used to monitor the temperature of the HLM. During the calibration, flowing argon cover gas (SAPIO S.r.l., purity 99.9999%, O₂=0.1 ppm mol, H₂O=0.5 ppm mol) was introduced above HLM surface to maintain the oxygen saturation. To close the electric circuit of the oxygen measurement, 316 stainless steel and Mo wires were used as working electric lead and dipped in the HLM. The potentiometric cells for the oxygen measurement are represented as follows:

Mo, Pb + PbO // YPSZ // Air, Pt(316Ti SS)

Mo, Pb + PbO // YTSZ // Air, Pt(316Ti SS)

316 SS, LBE + PbO // YPSZ // Bi + Bi₂O₃, Mo

316 SS, LBE + PbO // YPSZ // Cu + Cu₂O, 316 SS

The oxygen sensors were pre-heated inside the capsules and dipped in HLM immediately after the melting ($T_{m,Pb} = 327^{\circ}\text{C}$ and $T_{m,LBE} = 125^{\circ}\text{C}$) to prevent the failure of the zirconia tube due to thermal shocks. During the calibration, the HLM temperature was moved down from 550°C at a rate of 2°C/min setting the parameters on the Data Acquisition and Control System (DACS). Once each temperature step was reached, it was waited about 20 minutes before collecting the experimental electric potential values in order to reach the thermodynamic equilibrium at the HLM side and reference side. Four electric potential values were at least collected with a frequency of 30 minutes for each temperature step to assess the steady state condition, then a mean value was calculated for each calibration temperature. The measurements were performed with Hewlett Packard 34401A multi-meter setting an impedance $\geq 10\text{ G}\Omega$. The error of the multi-meter on the electric potential was assessed with an advanced modular calibrator (Druck DPI 620 Genii) and it was $\pm 0.2\text{ mV}$ in the potential range 0-150 mV and $\pm 0.1\text{ mV}$ in the range 150-1300 mV. Before the analysis of the experimental data, the electric potential points were corrected by subtracting a small thermoelectric potential arising from the coupling of different materials exposed at different temperatures. The experimental electric potential was then calculated according to the equation:

$$E_{exp} = U - U_{th} \quad \text{Eq. 5.1}$$

where U is the electric potential from the multi-meter and U_{th} the thermoelectric voltage.

Considering the potentiometric cell of the Cu/Cu₂O sensor calibration, no thermoelectric voltage was considered since both reference and working lead wires were made of the same material (i.e. 316).

For the calibration of the Pt-air sensor, a small thermoelectric voltage was instead considering due to the coupling between the 316Ti SS wire (side of the reference electrode) and the Mo wire (side of the working electrode). The 316Ti SS/Pt junction composing the reference electric lead was not considered as the two materials were exposed at the same temperature (determined by the HLM) and so no thermoelectric voltage should be resulted in theory. For the evaluation of the thermoelectric voltage the following relationship established by Schroer et al. [2] was used:

$$U_{th} = C \cdot (T_1^2 - T_2^2) \quad \text{Eq. 5.2}$$

where U_{th} is the thermoelectric voltage, T_1 is the temperature of the lead alloy melt (in K), T_2 is the temperature of the junction 316Ti SS/Mo (in K) and C is the Seebeck coefficient depending on the type of materials coupled. When Mo wire is connected to the negative polarity of the multi-meter,

$C = 1.251 \cdot 10^{-8} \text{ V/K}^2$ and U_{th} presents negative values. Thus, the overall effect was positive and about 3-6 mV were added to U values coming from the calibration of Pt-air sensor at 340-540°C.

Concerning the calibration of the Bi/Bi₂O₃ sensor, the coupling was between Mo wire (side of the reference electrode) with 316 SS wire (side of the working electrode). In this case, the thermoelectric voltage was calculated using $C = 1.251 \cdot 10^{-8} \text{ V/K}^2$. The reversal of the position of the SS wire with the Mo one generated in a positive thermoelectric voltage of 3-7 mV in the whole calibration temperature range that had the effect of lowering the experimental electric potential measured with the multi-meter.

To estimate the intrinsic error of potentiometric oxygen sensors in HLMs, trend over time of the electric potential in oxygen-saturated HLM at two temperatures was acquired for Pt-air and Cu/Cu₂O sensors with YPSZ solid electrolyte. Specifically, the electric potential of Pt-air sensor was acquired in liquid Pb at 543°C and 402°C whereas the potential of Cu/Cu₂O sensor in LBE at 498°C and 397°C. The electric potential was collected in stable conditions with the Hewlett Packard 34401A multi-meter for 3 hours with a frequency of 1 minute, so that 180 points were collected in total for each temperature. For the whole duration of the test, atmospheric air was provided inside the experimental capsule containing the HLM through a penetration on the cover flange in order to keep a stable oxygen saturation without fluctuations. Before starting the acquisition of the electric potential points, we waited about 30 minutes to reach the steady state condition. The points collected by the multi-meter were used to determine the standard deviation of the electric potential in stable condition. The calculated standard deviation was then compared with the error of the multi-meter to check if the intrinsic error of the oxygen sensor was higher than the error of the measure. Then the rules for error propagation were used for the estimation of the error on the oxygen concentration in the HLM.

The potentiometric cells describing the oxygen measurement during the test are the following:

Mo, Pb + PbO // YPSZ // Air, Pt(316Ti SS)

Mo, LBE + PbO // YPSZ // Cu + Cu₂O, 316 SS

Mo wire was used as electric lead of the working system and a small thermoelectric voltage should be considered for the determination of the oxygen concentration in the HLM according to Eq. 5.2. However, the error on the thermoelectric voltage (U_{th}) was here neglected and considered a constant for a given temperature, thus the only standard deviation on the electric potential acquired by the multi-meter (U) was used to assess the intrinsic error of the oxygen sensor.

5.1.3 Calibration Results

Pt-air reference + YPSZ electrolyte

Fig. 5.3 shows the results of the calibration of the Pt-air sensor with YPSZ tube in oxygen-saturated liquid Pb in the temperature range 340-540°C. The experimental points consist in mean values (blue points) with standard deviation of the various points collected at the different temperatures. The points are compared with the theoretical electric potential calculated from Eq. 4.4. Some theoretical electric potential lines (red lines) are plotted by using different equations available in literature for the calculation of the ΔG_{PbO}° as a function of temperature. The equations considered and the corresponding theoretical electric potential lines are reported in Tab. 5.2. Looking at Fig. 5.3, it is possible to see the theoretical lines are all mutually consistent and there is a very high agreement between the electric potential lines calculated using ΔG_{PbO}° proposed by Courouau, Konys and Ganesan [4-6].

Analysing the experimental points, Pt-air sensor with YPSZ provided an electric potential output generally in agreement (deviation within $\pm 1 \%$) with the theoretical lines between 400°C and 540°C. When the temperature was lowered more than 400°C, the sensor output shifted from the theoretical

electric potentials with negative deviation of about -2 % at 380°C and -4 % at 340°C. A more accurate observation of the experimental points revealed, however, two different trends in the range 400-540°C. Two experimental regression lines were so calculated for the experimental points: one for the points between 470-540°C and another one for the points between 400-470°C. The resulting equation corresponding to the first set of points is in very good agreement with the theoretical equation with ΔG_{PbO}° from Courouau, Konys and Ganesan [4-6]. Conversely, the equation corresponding to the second set of points exhibits slightly lower values of intersection and slope, which could be ascribable to a slight loss of sensitiveness when the temperature decreases.

Tab. 5.2: Standard free energy of formation of PbO according to the reaction $2Pb + O_2 \leftrightarrow 2PbO$ and corresponding theoretical electric potentials in oxygen-saturated Pb.

References	$\Delta G^\circ \text{ PbO (J/mol)}$	$E_{th} \text{ in Pb (V)}$
Courouau [3,4]	$-437608 + 199.1 \cdot T_{(K)}$	$0.9838 - 0.0005495 \cdot T_{(^\circ C)}$
Konys [5]	$-436850 + 198.0 \cdot T_{(K)}$	$0.9826 - 0.0005466 \cdot T_{(^\circ C)}$
Ganesan [6]	$-437960 + 199.3 \cdot T_{(K)}$	$0.9846 - 0.0005499 \cdot T_{(^\circ C)}$
Kishimoto [7]	$-435000 + 197.2 \cdot T_{(K)}$	$0.9783 - 0.0005446 \cdot T_{(^\circ C)}$

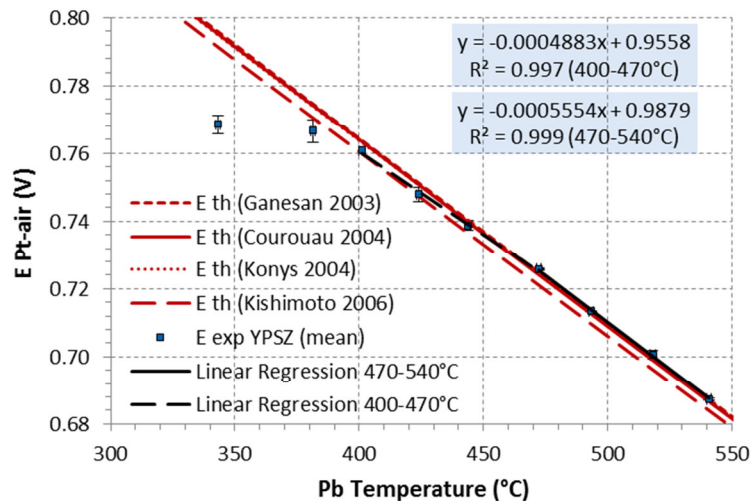


Fig. 5.3: Calibration of Pt-air sensor with YPSZ in oxygen-saturated Pb in the range 340-550°C showing the theoretical electric potential (red lines), the mean experimental electric potential with standard deviation (blue points) and the experimental regression line (black lines).

Pt-air reference + YTSZ electrolyte

The effect of a different solid electrolyte on the performance of potentiometric oxygen sensors was investigated by calibrating the Pt-air sensor with a YTSZ tube in Pb in the temperature range 350-440°C. The results obtained are described in Fig. 5.4. Unlike the Pt-air sensor with YPSZ tube (see Fig. 5.3), the Pt-air sensor with YTSZ tube provided an electric potential in good agreement with the theoretical lines even at 350°C, i.e. close to the melting point of Pb. For such sensor, the deviation of the experimental points (yellow points) from the theoretical lines is around $\pm 0.6\%$ for each temperature. The good agreement is also confirmed by the values of the experimental regression line (black line) of the electric potential as a function of temperature, which are very similar to the theoretical equations calculated with ΔG_{PbO}° from Courouau, Konys and Ganesan reported in Tab. 5.2 [4-6].

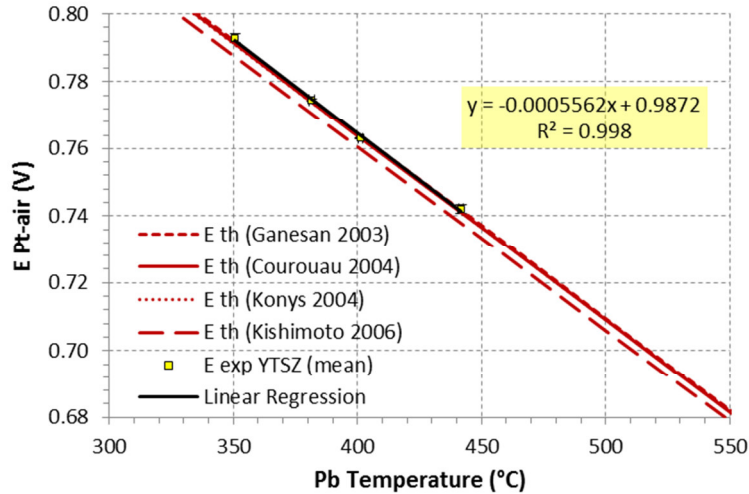


Fig. 5.4: Calibration of Pt-air sensor with YTSZ in oxygen-saturated Pb in the range 350-440°C showing the theoretical electric potential (red lines), the mean experimental electric potential with standard deviation (yellow points) and the experimental regression line (black lines).

Bi/Bi₂O₃ reference + YPSZ electrolyte

Bi/Bi₂O₃ oxygen sensor with YPSZ tube was calibrated in oxygen-saturated LBE in the range 260-550°C. When the Bi/Bi₂O₃ sensor was dipped in the LBE for the first time, it took some time before the sensor started to give electric potentials in agreement with the theoretical ones. Indeed, the sensor needed time to consume the atmospheric oxygen entrapped in the YPSZ tube during the manufacturing and reach the thermodynamic equilibrium between bismuth and its oxide. The same behaviour was detected for the Cu/Cu₂O sensor.

The results of the calibration are reported in Fig. 5.5. The theoretical electric potential of Bi/Bi₂O₃ sensor is calculated according to Eq. 4.5 considering ΔG_{PbO}° from Courouau (selected for the good agreement with experimental data of Fig. 5.3 and Fig. 5.4, see Tab. 5.2) and different equations for the calculation of $\Delta G_{Bi_2O_3}^\circ$. The equations for the $\Delta G_{Bi_2O_3}^\circ$ and the corresponding theoretical electric potentials are listed in Tab. 5.3. The various theoretical electric potential lines are quite consistent (see Fig. 5.5): two groups of lines are clearly distinguishable and each one differs from the other of about 6-8 mV.

The analysis of the experimental points (grey points) shows that Bi/Bi₂O₃ sensor gave consistent output in the range 290-550°C. When the temperature of the LBE was moved down beyond the melting point of Bi (i.e. beyond 271°C), the sensor stopped working as consequence, probably, of the block of the oxygen diffusion in the Bi solid phase. The experimental points and the calculated regression line are in fairly agreement with the theoretical electric potentials calculated with $\Delta G_{Bi_2O_3}^\circ$ by Courouau and Konys [4,5] in the range 290-550°C. The deviation from these theoretical potentials are within $\pm 2\%$ and $\pm 3\%$ respectively for each experimental points. Conversely, the deviation of the experimental points from the potentials obtained with $\Delta G_{Bi_2O_3}^\circ$ from Kishimoto and Ganesan [7,8] is much higher and ranged from -5% to -9% in the same temperature range.

Tab. 5.3: Standard free energy of formation of Bi_2O_3 according to the reaction $4/3\text{Bi} + \text{O}_2 \leftrightarrow 2/3\text{Bi}_2\text{O}_3$ and corresponding theoretical electric potentials in oxygen-saturated LBE.

References	$\Delta G^\circ \text{Bi}_2\text{O}_3$ (J/mol)	E_{th} in LBE (V)
Courouau [4]	$-389140 + 192.6 \cdot T_{(\text{K})}$	$0.1051 - 0.0000539 \cdot T_{(\text{C})}$
Konys [5]	$-386790 + 189.0 \cdot T_{(\text{K})}$	$0.1074 - 0.0000605 \cdot T_{(\text{C})}$
Kishimoto [7]	$-384333 + 190.9 \cdot T_{(\text{K})}$	$0.1109 - 0.0000535 \cdot T_{(\text{C})}$
Ganesan [8]	$-388933 + 195.9 \cdot T_{(\text{K})}$	$0.1087 - 0.0000458 \cdot T_{(\text{C})}$

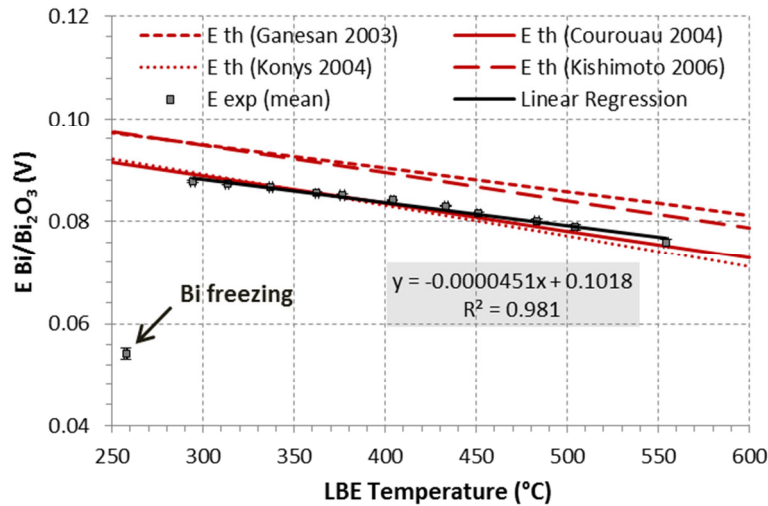


Fig. 5.5: Calibration of $\text{Bi}/\text{Bi}_2\text{O}_3$ sensor with YPSZ tube in oxygen-saturated LBE in the range 260-550°C showing the theoretical electric potential (red lines), the mean electric experimental potential with standard deviation (grey points) and the experimental regression line (black lines).

Cu/Cu₂O reference + YPSZ electrolyte

Fig. 5.6 shows the results of the calibration of $\text{Cu}/\text{Cu}_2\text{O}$ sensor in oxygen-saturated LBE in the range 160-550°C. The theoretical electric potential lines are calculated using the equations for the calculation of $\Delta G_{\text{Cu}_2\text{O}}^\circ$ listed in Tab. 5.4. It is possible to see that the theoretical electric potential lines are all mutually consistent and they differed one with each other within about 2 mV in the range 160-550°C.

Concerning the experimental points (green points), they are all in agreement with the theoretical lines in the range 200-550°C with a slight deviation of $\pm 2\%$. When the temperature of LBE was lowered more than 200°C, a significant deviation of the output from the theoretical lines was observed (about -6% at 160°C). The calculated regression line in the range 200-550°C is in good agreement with the theoretical equations calculated with $\Delta G_{\text{Cu}_2\text{O}}^\circ$ reported by Manfredi, Holmes and O'Neill [9-11].

Tab. 5.4: Standard free energy of formation of Cu_2O according to the reaction $4\text{Cu} + \text{O}_2 \leftrightarrow 2\text{Cu}_2\text{O}$ and corresponding theoretical electric potentials in oxygen-saturated LBE.

References	$\Delta G^\circ \text{Cu}_2\text{O}$ (J/mol)	E_{th} in LBE (V)
Manfredi [9]	$-338528 + 148.1 \cdot T_{(\text{K})}$	$0.2047 - 0.0001692 \cdot T_{(\text{C})}$
Holmes [10]	$-348086 + 247.082 \cdot T_{(\text{K})} - 13.0 \cdot T_{(\text{K})} \cdot \ln T_{(\text{K})}$	$0.2027 - 0.0001654 \cdot T_{(\text{C})}$
O'Neill [11]	$-347705 + 246.096 \cdot T_{(\text{K})} - 12.9 \cdot T_{(\text{K})} \cdot \ln T_{(\text{K})}$	$0.2015 - 0.0001628 \cdot T_{(\text{C})}$

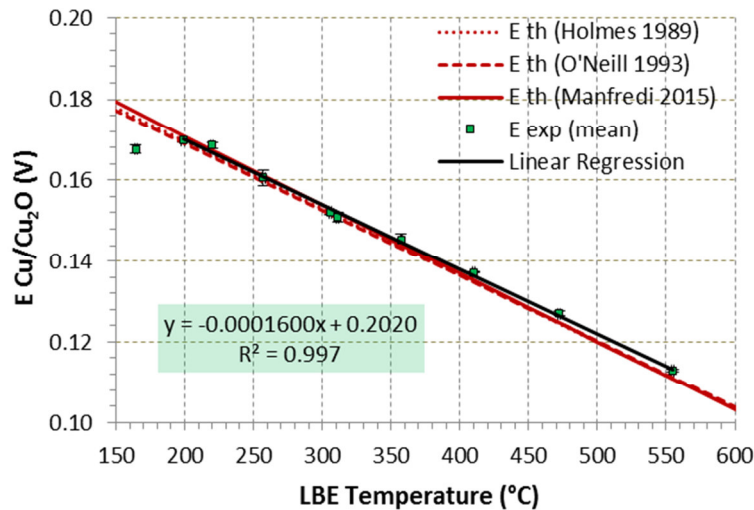


Fig. 5.6: Calibration of Cu/Cu₂O sensor with YPSZ in oxygen-saturated LBE in the range 160-550°C showing the theoretical electric potential (red lines), the mean experimental electric potential with standard deviation (green points) and the experimental regression line (black lines).

5.1.4 Error analysis

The intrinsic error of Pt-air and Cu/Cu₂O sensors with YPSZ electrolyte was evaluated from the standard deviation of the electric potential calculated on the trend over 3 hours (180 experimental points) in stable conditions of temperature and oxygen concentration (oxygen saturation). Fig. 5.7 shows the trend of the electric potential for Cu/Cu₂O sensor in oxygen-saturated LBE at 397°C acquired by the multi-meter with indication of the mean value and the calculated standard deviation. Similar graphs were obtained for Cu/Cu₂O sensor also at 498°C and for Pt-air sensor at 543°C and 402°C. The results obtained for Cu/Cu₂O and Pt-air sensor in terms of mean electric potential and standard deviation are summarized in Tab. 5.5. In general, the calculated standard deviations of the electric potential σ_U are all of the same order of magnitude and slightly higher for Cu/Cu₂O sensor. In addition, the standard deviations are of the same order of magnitude of the error of multi-meter (± 0.2 mV in the potential range 0-150 mV and ± 0.1 mV in the range 150-1300 mV), making difficult to discriminate with sureness if the trend of the electric potential depends on the intrinsic error of the sensor or the error of the multi-meter. More points and longer acquisition of the electric potential in stable conditions could be required in future to assess this issue.

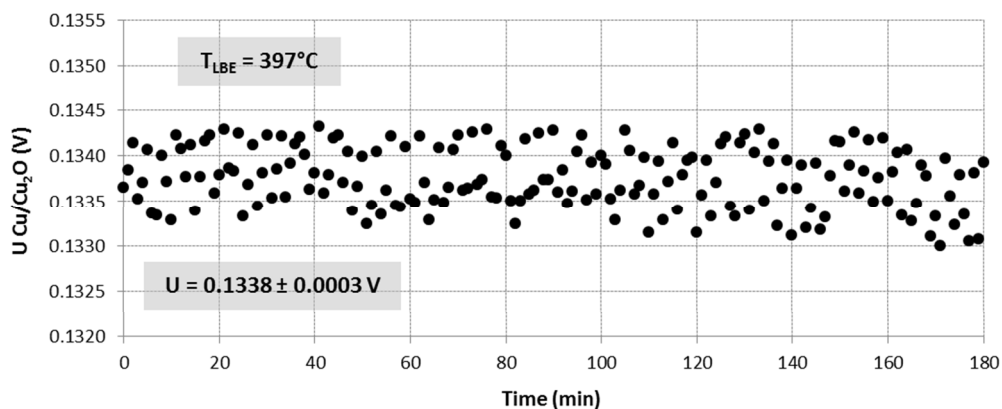


Fig. 5.7: Electric potential trend acquired by the multi-meter of Cu/Cu₂O oxygen sensor with YPSZ electrolyte in oxygen-saturated LBE at 397°C for 180 minutes, with indication of the mean value and standard deviation.

Tab. 5.5: Mean electric potential U and standard deviation σ_U of Pt-air and Cu/Cu₂O sensor in Pb and LBE respectively.

$T_{Pb} \pm \sigma_T$ (°C)	$U \pm \sigma_U$ Pt-air (V)	$T_{LBE} \pm \sigma_T$ (°C)	$U \pm \sigma_U$ Cu/Cu ₂ O (V)
402 ± 1	0.7599 ± 0.0002	397 ± 1	0.1338 ± 0.0003
543 ± 1	0.6809 ± 0.0001	498 ± 1	0.1171 ± 0.0003

However, since the estimated standard deviations σ_U were always equal or higher than the error of the multi-meter, σ_U standard deviations were considered to estimate the error on the oxygen concentration in the HLM in a conservative mode.

The standard deviation of the oxygen concentration σ_{C_O} was estimated from standard deviation of the electric potential σ_E by applying the rules for error propagation on Eq. 4.4 and Eq. 4.5. The error of thermodynamic data ΔG°_{PbO} and $\Delta G^\circ_{Cu_2O}$ as well as experimental data describing a_{Pb} (when LBE is used) and $C_{O,sat}$ were not included in the estimation in order to discriminate the only effect of the standard deviation of the electric potential measurement on the oxygen concentration. Thus, the standard deviation of the oxygen concentration σ_{C_O} was calculated from the standard deviation of the electric potential σ_E according to the equation:

$$\frac{\sigma_{C_O}}{C_O} = \frac{2F}{RT} \cdot \sigma_E = \frac{23208.76}{T} \cdot \sigma_E \quad \text{Eq. 5.3}$$

where $\frac{\sigma_{C_O}}{C_O}$ is the relative standard deviation of the oxygen concentration.

Considering also the thermoelectric voltage U_{th} for the electric coupling Mo-SS as a constant for a given temperature, Eq. 5.3 can be written as:

$$\frac{\sigma_{C_O}}{C_O} = \frac{2F}{RT} \cdot \sigma_U = \frac{23208.76}{T} \cdot \sigma_U \quad \text{Eq. 5.4}$$

where σ_U is the standard deviation of the electric potential measured with the multi-meter.

According to Eq. 5.4, the relative standard deviation on the oxygen concentration was ±0.4 % and ±0.7 % at 543°C and 402°C for Pt-air sensor and it was ±0.9 % and ±1.0 % at 498°C and 397°C for Cu/Cu₂O sensor. Assuming that the standard deviation of the electric potential σ_U is conserved also at lower temperatures for Cu/Cu₂O sensor (±0.3 mV, see Tab. 5.5), the relative standard deviation on the oxygen concentration is estimated ±1.2 % and ±1.5 % at 300°C and 200°C respectively.

In general, it is possible to state that an error of ±1% for the electric potential measurement is low and absolutely acceptable. However, for the estimation of the total error on the oxygen concentration it is necessary to consider the error associated with the HLM temperature measurement and thermodynamic and experimental data. Among that, the error on thermodynamic data (ΔG°) and experimental data (a_{Pb} , $C_{O,sat}$) should play the major roles in the estimation of the total error and further study is needed to evaluate the effect of these contributions.

5.1.5 Discussion

The calibration of the Pt-air sensor with YPSZ electrolyte in liquid Pb in the range 340-550°C showed that the sensor was able to provide a fairly accurate electric potential for temperatures higher than 400°C (Fig. 5.3). When the HLM temperature was moved down beyond 400°C, the sensor exhibited negative deviations from the expected electric potential with a magnitude increasing with the HLM temperature decrease. The significant deviation detected even at 380°C confirmed, as a first approximation, that the minimum reading temperature of a Pt-air sensor with YPSZ electrolyte is placed around 400°C, in agreement with past experiences on Pt-air sensors in HLMs. The preliminary error analysis associated with the electric potential measurement of Pt-air sensor with YPSZ

electrolyte revealed that the intrinsic error of the sensor is mostly equal to the error of the multi-meter and it is equal 0.1 or 0.2 mV (see Tab. 5.5).

When the YPSZ electrolyte was substituted with a YTSZ one, an improvement in the minimum reading temperature of the Pt-air sensor was observed (see Fig. 5.4). The Pt-air sensor with YTSZ electrolyte provided an electric potential very consistent with the theoretical one even down to 350°C. However, 350°C cannot be considered the ultimate limiting temperature for Pt-air sensor with YTSZ electrolyte since it was not possible to check the electric potential at lower temperature due to the near melting point of Pb. The improvement of 50°C in the minimum reading temperature is ascribable to the higher ionic conductivity of the YTSZ compared to the YPSZ [12,13]. Indeed, the ionic conductivity of a “stabilized zirconia” is maximized when the amount of dopant (in this case Y₂O₃) is added to the zirconia at the exact level required to achieve the full stabilization of the cubic phase, which is the O²⁻ conductive crystalline form of the zirconia. A lower amount of dopant provides a partial stabilization of the zirconia resulting in a mixture of cubic and tetragonal phase with a lower ionic conductivity but better thermo-mechanical strength. YTSZ had about 14 % wt. of Y₂O₃ (8 % mol., minimum level of dopant required for the full stabilization) and so higher ionic conductivity and better performance at low temperature compared to the YPSZ with about 10 % wt. of Y₂O₃ (5 % mol.).

Besides the ionic conductivity property of the solid electrolyte, it is worth reminding that the performance of an air sensor strongly depends also on the electrode material. Considering the case of a Pt-air sensor, Pt is in charge to catalyse the dissociation and reduction of the atmospheric O₂ at the side of the reference electrode according the following reaction:



Eq. 5.5 occurring above the Pt surface is characterized by high cathodic overpotential at low temperature and so the reaction kinetics is strongly slow down [12,14,15]. As a matter of fact, the performance of air-based sensors can be enhanced by using materials with better catalytic behaviour, such as perovskite-type oxides [14,15]. For instance, the performance of air oxygen sensor with a mixture of LSM (Lanthanum Strontium Manganite) and GDC (Gadolinium-Doped Ceria) perovskite oxides as catalytic electrode was recently tested in LBE down to 200°C with success [15].

The calibration of Bi/Bi₂O₃ sensor with YPSZ electrolyte performed in LBE showed that the sensor was able to detect oxygen down to 290°C (see Fig. 5.5), in agreement with past experiences. A strong deviation was detected when the LBE temperature was moved down to 260°C, making presume that the minimum reading temperature is connected with the freezing point of bismuth. The employment of a Bi/Bi₂O₃ sensor with YPSZ electrolyte provided an improvement of the minimum reading temperature compared to the Pt-air sensor with the same electrolyte. As a matter of fact, Bi/Bi₂O₃ internal reference should provide a major contact area between the internal electrode and the solid electrolyte, which should involve a fairly low ionic and electrical resistance at the reference/electrolyte side and allow a more correct measure at lower temperature [12]. Conversely, Pt-air reference has a higher resistance at the gas/electrolyte junction [12] and a low catalytic behaviour for the oxygen reduction, which both affect the electric potential output at low temperatures [14,15].

Cu/Cu₂O oxygen sensor provides even more an improvement in the oxygen measure at low temperature. The calibration in LBE of the sensor with YPSZ electrolyte showed that the sensor gave electric potentials in agreement with the theoretical expected even down to 200°C and with high accuracy (deviation from the theoretical of about ± 2%) whereas a substantial deviation was observed at lower temperature (see Fig. 5.6). Thus, the minimum reading temperature of a Cu/Cu₂O sensor in HLMs can be considered at around 200°C, taking into account that a similar result was recently obtained during the calibration of the Cu/Cu₂O sensor in the same HLM [9]. The preliminary

error analysis of the Cu/Cu₂O sensor measurement revealed that the intrinsic error of the sensor is slightly higher than the error of the multi-meter and it is equal 0.3 mV (see Tab. 5.5).

According to these results, the Cu/Cu₂O oxygen sensor can be fruitfully used in LBE-cooled systems where the working temperature ranges are low. The possibility of using a solid metal/metal-oxide (powder) reference such as the Cu/Cu₂O is also a great advantage which prevents the establishment of internal stresses and the chance of failure of the solid electrolyte. A problem encountered with Cu/Cu₂O reference is the sintering of Cu and Cu₂O powders inside the zirconia tube during sensor operation in HLMs (see Fig. 5.8), which seems to affect the service lifetime of the sensor. In addition, the black compound is probably CuO, which should form at high-temperature due to the interaction of Cu with oxygen and humidity inside the zirconia tube. The problem of sintering could be easily solved in future by mixing Cu and Cu₂O powders with ceramic oxide powders, e.g. YPSZ or GDC powders. Also, the problem of the formation of CuO could be solved by sealing the zirconia tube in a controlled atmosphere (e.g. in glove box filled with argon gas) to avoid the entrapment of oxygen and humidity traces in the ceramic tube.



Fig. 5.8: Sintering of the Cu/Cu₂O reference inside a YPSZ tube after 1000 hours of operation in HLM.

5.2 OXYGEN SENSORS FOR LARGE HLM POOL FACILITY

5.2.1 Aim of the work

The development of oxygen sensors for large HLM pools is considered a great technological challenge for the technical requirements that the oxygen sensors have to fulfill to provide reliable and long service capability. Among the various requirements needed, high mechanical and thermal strength is fundamental in large HLM volumes. Indeed, the pressure exercised by the HLM head in large pools is very huge and the HLM flow velocities in such systems are significant (1-2 m/s), which require high mechanical resistance to compression and shear stresses to provide long-term reliability. Moreover, for a reliable operation also in HLM storage tanks, oxygen sensors have to be resistant to several bars of gas pressure, which are usually provided in HLM storage tanks to move the HLM from the storage tank to the experimental facility (“filling” procedure). As introduced in section 4.5, oxygen sensors for large HLM pools were developed and tested some years ago for the first time in CIRCE pool-type facility in ENEA Brasimone but the reliability and the service lifetime demonstrated by the sensors were clearly insufficient.

In the framework of SEARCH (Safe ExploitAtion Related CHemistry for HLM reactors) and MAXSIMA (Methodology, Analysis and eXperiments for the Safety In MYRRHA Assessment) collaborative projects (7th Framework Program EU), an oxygen sensor prototype for large HLM pool system was designed, improved and tested. The aim of the study was to equip the large HLM pool facility CIRCE in Brasimone with oxygen sensors able to monitor the oxygen concentration with reliability and long service lifetime capability. The development of sensors for CIRCE pool facility is of primary relevance to get to define an adequate oxygen control system for large HLM pool, which is the typical configuration of nuclear reactors.

CIRCE basically consists of a cylindrical main vessel filled with about 70 tons of LBE [16,17]. It is internally equipped with a thermal-hydraulic test section (hung from the cover flange of the main vessel) which provides the LBE recirculation and the LBE heating and cooling. The vessels and the test

section are made of AISI 316L stainless steel. The facility also includes a storage tank for the LBE, a small transfer tank and DACS. The main vessel is 8500 mm height and 1200 mm large and it is connected by gates to the other vessels. It is externally equipped with heating cables installed at the bottom and on the lateral surface. The CIRCE test section is designed to reproduce the thermal-hydraulic behavior of the ADS concept [16,17]. The schematic illustration of CIRCE test section and the LBE flow path inside the main vessel is shown in Fig. 5.9.

Concerning the coolant chemistry control, the CIRCE test section includes gas injection with Ar-H₂ mixture in the riser column (oxygen removal), PbO MX (PbO Mass eXchanger, oxygen supply) anchored to the test section at the FPS (Fuel Pin Simulator) and installed in the pool, and two filtering sections, one at the outlet of the riser (to collect floating solid products) and another one at the outlet of HX (Heat eXchanger, to entrap impurities deposited after cooling). For the study of the oxygen control system, the installation of three oxygen sensors at different levels in the pool (600 mm, 4500 mm, 7500 mm) is foreseen.

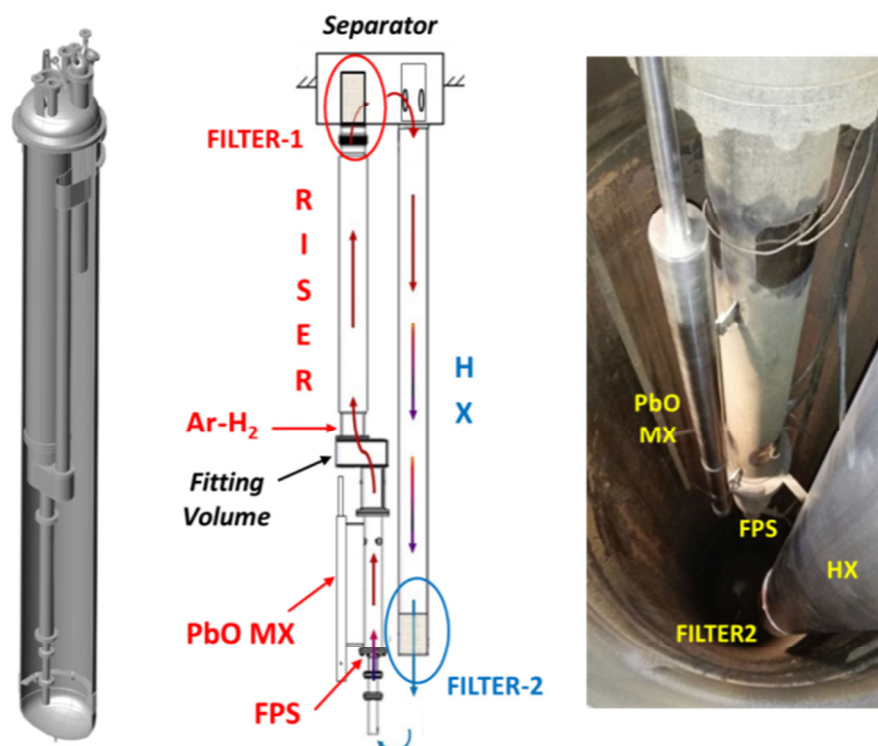


Fig. 5.9: Layout of the CIRCE pool facility (left) showing a schematic illustration of the main LBE flow path in the test section (center) and a picture of the components assembly inside the main vessel (right).

5.2.2 Experimental Setup

Sensor Development and Description

The development oxygen sensor for CIRCE pool facility was carried out in collaboration with FER Strumenti S.r.l., which has expertise in the development and fabrication of oxygen gas analysers.

The sensor design involves the use of a small zirconia thimble connected to a long and thick steel body. The steel body is required to ensure sufficient mechanical resistance in the large pool facility, being able to withstand the large pressures, the shear stresses and the thermal gradients inside the large HLM volume. During the development, the main difficulty encountered was to ensure a good tightness at the zirconia thimble level without affecting the sensor electric potential. For this purpose several sensor designs have been tested before achieving a good technological solution. Compared to the old configurations where the zirconia thimble was sheltered from the HLM by a tightness

flange provided with some holes (see Fig. 5.10), the current design ensures a more extended contact between the zirconia and the HLM, being the thimble completely exposed to the HLM.

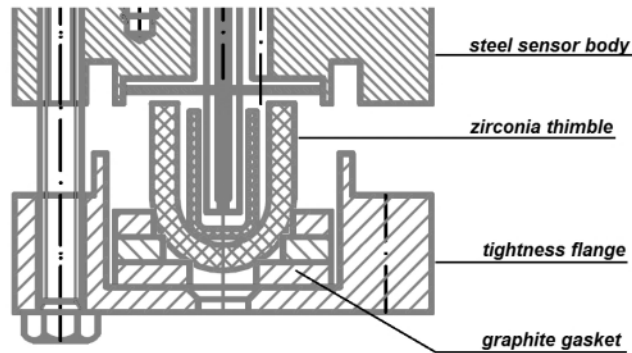


Fig. 5.10: Previous configuration of the sensitive part of the oxygen sensor for large HLM pool. The zirconia thimble was sheltered by the tightness flange, which prevented a good wetting with the HLM.

The schematic design and a picture of the current oxygen sensor design (lower part) are shown in Fig. 5.11. The oxygen sensor is 1 m long, it has a Pt-air reference electrode and YTSZ as solid electrolyte. The length of the sensor can be adapted according to the position in the HLM pool. The Pt-air reference electrode was chosen preliminarily for its simplicity of implementation and YTSZ for the higher ionic conductivity compared to the YPSZ.

The sensor body is a 2" tube made of AISI 316, which is in charge to ensure mechanical strength when the sensor is dipped in the large HLM volume. The YTSZ thimble ($d_{ext} = 20$ mm) is placed in the lower part of the sensor body. The zirconia thimble is machined to create a lateral step and is pressed against the sensor body by a perforated flange (made of AISI 316) which pushes on the step. The tightness is given by a graphite gasket placed between the thimble and the sensor body. To guarantee continuous atmospheric oxygen for the reference system in the lower part of the oxygen sensor, air is blown towards the zirconia thimble into an internal thinner tube (made of AISI 316 as well) placed inside the 2" steel tube. The Pt wire electrode is located inside the same internal tube and it is electrically insulated by alumina tubes. In the upper part of the sensor a terminal box collects the Pt lead, the pressure reducer and a flowmeter for dosing the air towards the YTSZ thimble.

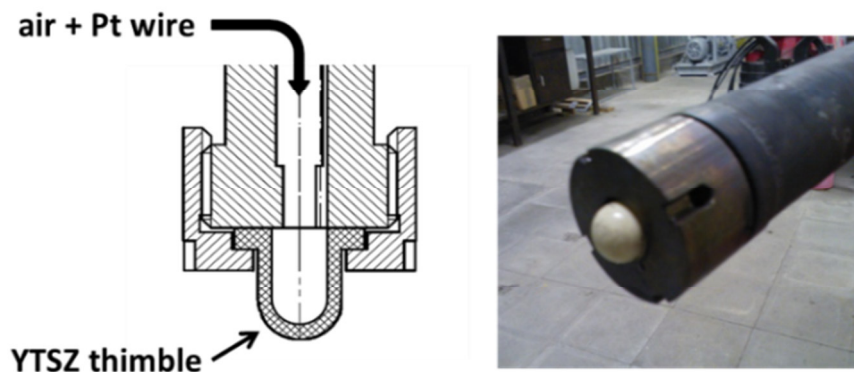


Fig. 5.11: Current configuration of the oxygen sensor for large HLM pool facility showing the lower part of the sensor with the YTSZ thimble and the steel perforated cap.

Sensor Calibration

The oxygen sensor prototype was calibrated in large HLM volume to assess the quality of the tightness and the accuracy of the measurement. The calibration was performed by varying the temperature in the range 350-550°C in oxygen-saturated Pb contained the storage tank of HELENA loop facility in Brasimone. The total Pb inventory inside the tank was about 285 L (3008 Kg). A picture of the oxygen sensor prototype in the storage tank is reported in Fig. 5.12.



Fig. 5.12: Oxygen sensor prototype in HELENA facility storage tank during the calibration in Pb.

The electric lead of the reference system of the sensor was composed of a stainless steel wire (AISI 316, $d_{\text{wire}} = 1 \text{ mm}$) with platinized tip obtained by electric point welding of a Pt foil anchored to the steel wire. The electric circuit of the oxygen measurement was closed by connecting the Pt(316 SS) lead of the sensor with the steel wall of the storage tank (made of AISI 316). No correction of the electric output was then needed due to the absence of a thermoelectric voltage. Finally, a continuous air flow ($\approx 0.2 \text{ NL/min}$) was provided inside the oxygen sensor to ensure a good level of atmospheric oxygen in the zirconia thimble. The potentiometric cell of the oxygen measurement is described as follows:

316 SS, Pb + PbO // YTSZ // Air, Pt(316 SS)

The oxygen-saturated condition for the calibration was ensured by a slight overpressure (0.3 bar) of argon gas (SAPIO S.r.l., purity 99.9999 %, $\text{O}_2=0.1 \text{ ppm mol}$, $\text{H}_2\text{O}=0.5 \text{ ppm mol}$) into the storage tank. The Pb temperature, monitored with a K-type thermocouple, was kept constant for several hours for each temperature step in order to give to the sensor enough time to reach the equilibrium with the Pb melt. The sensor electric potential was acquired by means of a PC software and collected with a frequency of 10 minutes for the data analysis.

5.2.3 Calibration Results

For the whole duration of the calibration test, no HLM penetration was observed in the zirconia thimble, indicating that the tightness of the sensor was globally good.

Concerning the electric potential, the trend over time of the electric output in the temperature range 350-480°C is shown in Fig. 5.13 with indication of the theoretical electric potential, which was plotted considering $\Delta G_{\text{PbO}}^\circ$ proposed by Courouau (see Tab. 5.2). The electric potential followed with good

agreement the expected electric potential in the range 400-480°C. Noisier output were initially observed at 380°C and 350°C but then the electric potential stabilized over time. It was not possible to define the reason of the noisy output at such temperatures. However, the subsequent stabilization of the output over time suggests that the noise was likely due to an electric disturb in the data acquisition rather than a problem with the oxygen sensor. In addition, some inertia in the response was observed during temperature variations, which is reasonable and ascribable to the stagnant condition of the large Pb volume inside the tank. However, a high stability of the electric output was observed over time (up to 10 days or more for each temperature).

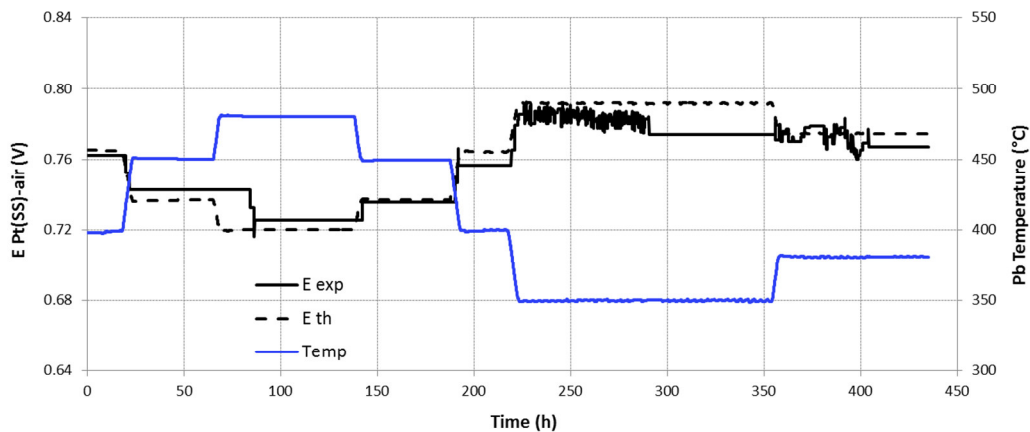


Fig. 5.13: Electric potential of Pt(316 SS)-air sensor prototype in oxygen-saturated Pb in the range 350-480°C in HELENA storage tank.

Mean values of the electric potential for each temperature step are plotted as a function of Pb temperature in Fig. 5.14. No hysteresis of the electric potential was observed during the temperature variation cycles from 400°C to 480°C, then from 480°C to 350°C and finally to 380°C.

Slight potential deviations towards higher potentials are clearly visible for measurements at 450°C and 480°C. These deviations are likely due to a non-complete oxygen-saturation of Pb when the temperature increased. However, the total deviation of the electric potential from the theoretical in the range 400-480°C is less than $\pm 1\%$, which is absolutely a good result considering that the calibration was not performed in controlled conditions such as in a chemical laboratory. The most significant deviation was observed when the temperature was moved down to 350°C: here the total deviations of the experimental electric potential from the theoretical one and is equal -1.6% (considering a mean value including the noise). Such higher deviation may indicate that the minimum reading temperature for the measure is placed above 350°C, even if a deviation of -1.6% (equal to 4 mV) could be considered still good and ascribable to the presence of impurities in HLM. For the measure at 380°C, the observed deviation in presence of noise is equal to -1.1% and is in agreement with the deviation in the range 400-480°C.

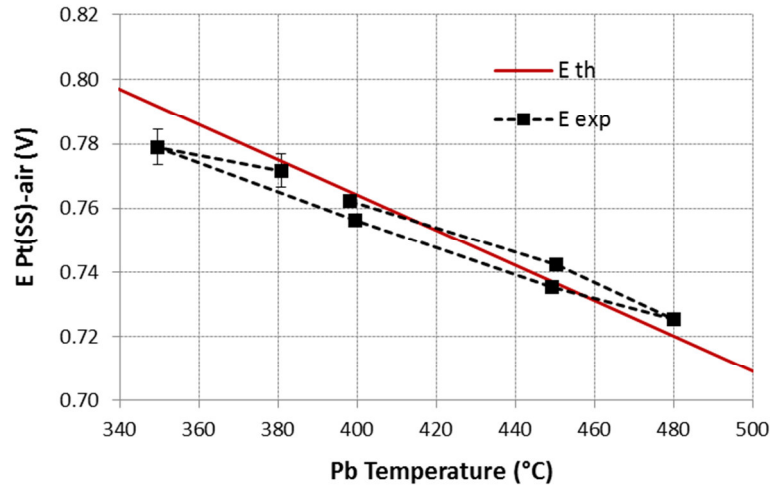


Fig. 5.14: Calibration of Pt(316 SS)-air sensor prototype in oxygen-saturated Pb in the range 350-480°C.

According to these results, the minimum reading temperature of the oxygen sensor prototype for large HLM pool can be set at about 380°C, in agreement with data obtained for small Pt-air sensors (Fig. 5.3 and Fig. 5.4). The intrinsic error of the sensor was approximately estimated from the trend over 30 minutes of the electric potential in oxygen saturation at 421°C, according to the method described in sections 5.1.2 and 5.1.4. The deviation observed was ± 0.0001 V, which is equal to the error of the multi-meter for high electric potential measurements. However, since the amount of data acquired is too poor for a statistical investigation, longer tests will be performed in future to confirm this result.

As the present configuration is able to measure oxygen only down to 380°C, the upgrade of the oxygen sensor with another reference system (such as Cu/Cu₂O) will be performed to have a detection capability down to 200°C. This implementation will allow to perform oxygen monitoring with good accuracy in the coldest zones of CIRCE large pool (which works at about 280°C). In addition, the use of YPSZ electrolyte should be preferred in place of the YTSZ to ensure higher service lifetime in CIRCE pool facility. Indeed, even if YTSZ has better ionic conductivity, it is more prone to crack than YPSZ and more than one failure of the YTSZ thimble occurred during various experimental tests. For that reason, the use of YPSZ thimble will be adopted in future and with a new geometry where sharp edges are reduced (see Fig. 5.15).

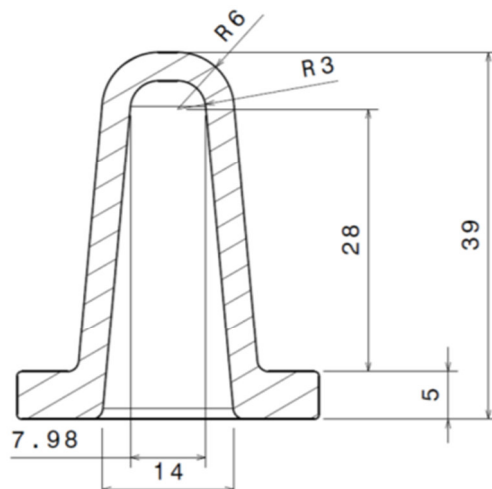


Fig. 5.15: New geometry of the ceramic thimble in YPSZ for oxygen sensors for large HLM pools.

5.3 EFFECT OF METALLIC IMPURITIES ON SENSOR OUTPUT

5.3.1 Experimental Setup

Dissolved metals and metal-oxides in HLMs may have strong influence on the oxygen concentration and thus on the sensor output. Indeed, even high-purity Pb and LBE contain some ppmw of metal impurities which are able to interact with the dissolved oxygen.

During a comparison test between two different oxygen sensor in liquid LBE, the influence of a metallic impurity dissolved in the HLM (specifically Fe) was analysed. Pt-air and Cu/Cu₂O sensors with YPSZ tube described in section 5.1.2 were used to monitor the oxygen concentration in the same LBE according to the experimental setup of Fig. 5.2. About 800 g of LBE provided by *Stachow-Metall GmbH* were contained in a chemically inert alumina crucible. Before the test, a steel tool was used to mechanically remove the free level of the fresh HLM at low temperature in order to reduce starting contaminations such as oxides and metal impurities. A little thermoelectric voltage was considered for both sensors for the presence of the Mo working electric lead in the LBE and calculated according to Eq. 5.2. The temperature of the HLM was first set at 400°C and the deoxygenation of the LBE was performed with bubbling Ar-7%H₂ gas mixture to achieve an oxygen concentration in the melt of about 10⁻⁷ % wt. The oxygen concentration was then stabilized under argon overpressure (SAPIO S.r.l., purity 99.9999%, 0.7 bar) and the LBE temperature moved fast at 3°C/min between 200 and 450°C to investigate sensors response in different temperature conditions. The experimental parameters and data were set and collected on a dedicated PC software in communication with DACS. The electrochemical cell schemes of the test are the following:

Mo, LBE + PbO // YPSZ // Air, Pt(316Ti SS)

Mo, LBE + PbO // YPSZ // Cu + Cu₂O, 316 SS

5.3.2 Results

The oxygen concentration monitored over time by Pt-air and Cu/Cu₂O sensors is plotted in Fig. 5.16. The oxygen concentration was determined from the sensor electric potential. ΔG_{PbO}° and $\Delta G_{Cu_2O}^{\circ}$ by Courouau and Manfredi reported in Tab. 5.2 and Tab. 5.4 were used for the calculation of the theoretical electric potential according to Eq. 4.4 and Eq. 4.5. Eq. 3.3 describing the oxygen solubility in LBE in the temperature range 400-740°C was used to extrapolate the oxygen solubility down to 200°C, being in good agreement with the oxygen solubility determined by Manfredi in the range 200-450°C [9]:

$$\ln C_{O,sat}^{LBE} (\text{wt.}\%) = 7.332 - \frac{11153}{T} \quad \text{Eq. 5.6}$$

Observing the figure, Pt-air and Cu/Cu₂O sensor detected the same oxygen concentration when the temperature is above 400°C whereas completely different concentrations are detected by the two sensors below 400°C. In addition, Pt-air sensor tried at first to follow the same trend of Cu/Cu₂O sensor during temperature decrease but then the output deviated when the temperature became more and more low. The deviation is easily explained considering the result of the calibration of Pt-air sensor in oxygen-saturated Pb reported in Fig. 5.3: significant deviations from the expected electric potential were observed when the temperature was moved below 400°C.

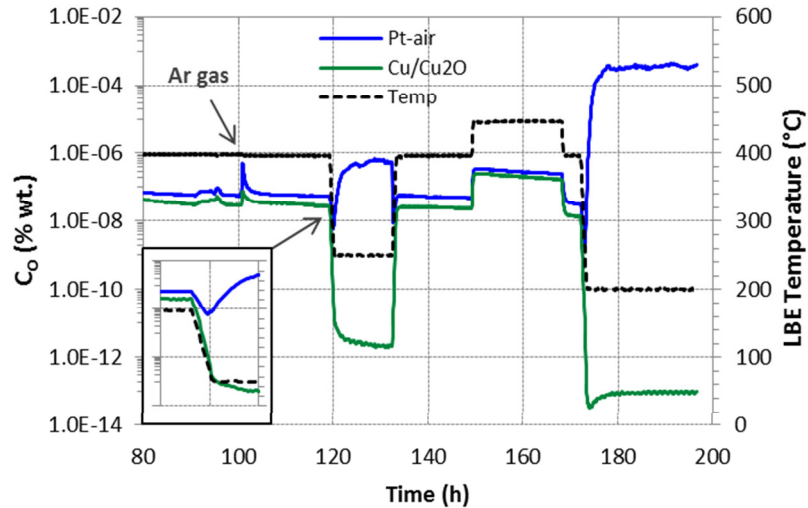


Fig. 5.16: Oxygen concentration in LBE monitored by Pt-air and Cu/Cu₂O sensors with YPSZ during temperature variations between 200-450°C under argon overpressure.

Analysing Fig. 5.16 in detail, it is to note that the oxygen concentration of 10^{-7} % wt. was not maintained during the temperature variation and strong deviations from the starting concentration were detected in particular at low temperature. This behaviour was explained by the likely establishment of an equilibrium with a metal impurity dissolved in the fresh LBE, which tends to subtract oxygen from the melt to form the corresponding oxide. About that, the formation of magnetite Fe_3O_4 was considered as the most likely equilibrium which could be established in the LBE melt, also taking into account the recent study about Fe-O interaction in the LBE performed by Aerts [18]. Indeed, the nominal composition of the LBE declared by the producer has a starting Fe concentration < 1 ppmw, which is sufficient to have stable Fe_3O_4 in the LBE melt since Fe solubility in the LBE at 450°C is around 0.8 ppmw according to Eq. 3.15 from Gossè [3,19].

To understand the possible influence of Fe impurity dissolved in the LBE, the experimental data in Fig. 5.16 were plotted in a graph “ C_{O} versus LBE temperature”, which includes also the Fe_3O_4 equilibrium plotted considering different Fe activity in the LBE. The equilibrium reaction concerning the formation of Fe_3O_4 in LBE is described by Eq. 3.8 and the oxygen concentration for the formation of Fe_3O_4 is described by Eq. 3.16 and Eq. 3.18 when $a_{\text{Fe}} = 1$ and $a_{\text{Fe}} < 1$ respectively. Fe solubility in LBE was calculated according to Eq. 3.15 valid in the temperature range 126-900°C [19].

The C_{O} versus LBE temperature is reported in Fig. 5.17. As supposed, the formation equilibrium of Fe_3O_4 have influenced the electric potential of Pt-air and Cu/Cu₂O sensors. In particular, in the range 400-450°C both the sensors monitored an oxygen concentration which is approximatively included between the Fe iso-concentration lines corresponding to $C_{\text{Fe}} = C_{\text{Fe,sat}}$ at 150°C and 200°C, which can be considered reasonable since the LBE surface free level was mechanically removed in this temperature range. Such behaviour was already detected by Courouau during the operation of LBE-cooled STELLA loop, where the oxygen sensors in the LBE were more prone to follow metal/metal-oxide equilibria such as the Fe/ Fe_3O_4 one instead of the oxygen iso-concentration lines [20]. According to this, the Cu/Cu₂O sensor kept on monitoring an oxygen concentration which followed the iron iso-concentration lines when the LBE temperature was below 400°C whereas Pt-air sensor strongly deviated from this behaviour (Fig. 5.17). The same oxygen concentration was monitored again by the two sensors when the LBE temperature was moved up to 400°C.

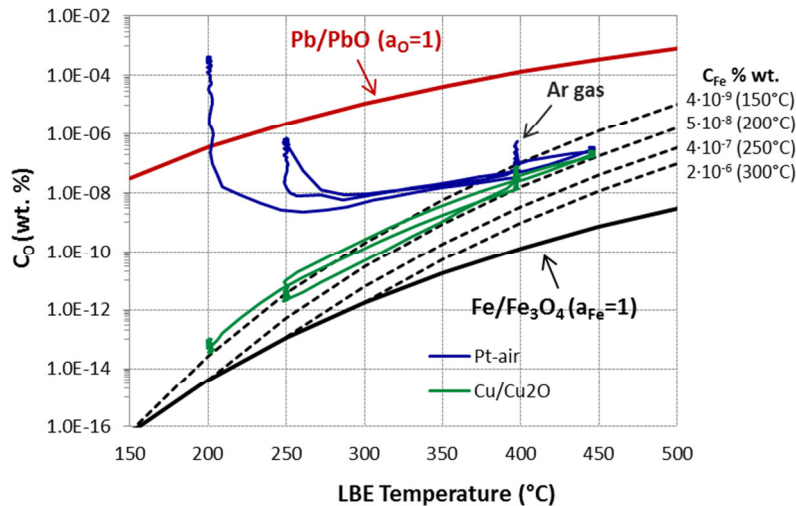


Fig. 5.17: Oxygen concentration as a function of LBE temperature monitored by Pt-air and Cu/Cu₂O sensors in the range 200-450°C. Pb/PbO, Fe/Fe₃O₄ equilibria and Fe iso-concentration lines are plotted.

5.4 CONCLUSIVE REMARKS

This chapter described the research activity performed in ENEA Brasimone about fabrication, study and development of oxygen sensors based on solid electrolytes for different applications in HLMs.

First, a baseline study on small oxygen sensors with different reference systems (Pt-air, Bi/Bi₂O₃ and Cu/Cu₂O) and solid electrolytes (YPSZ and YTSZ) was performed with the purpose to understand the chemical, physical and mechanical features influencing the oxygen sensor performance. This study was fundamental to get to select the proper requirements in terms of reference system and solid electrolyte for the various HLM conditions and applications (HLM fluid-dynamic, HLM temperature, HLM pressure). Sensors calibration in oxygen-saturated HLM showed that the best performance at low temperature are exhibited by Cu/Cu₂O sensor with YPSZ electrolyte with a minimum reading temperature at about 200°C. Bi/Bi₂O₃ oxygen sensor follows with a minimum reading temperature of 290°C and then Pt-air sensor with a minimum reading temperature of 400°C, both with YPSZ electrolyte. The use of Cu/Cu₂O reference is promising for the employment in LBE-cooled systems where the working temperature range is usually low. Moreover, the use of a solid reference such as the Cu/Cu₂O one is a great improvement compared to liquid Bi/Bi₂O₃ reference since solid powders do not generate internal stresses in the zirconia tube. However, solid powders may be affected by sintering and further improvement of the Cu/Cu₂O oxygen sensor has to be performed to reduce Cu powders sintering at high temperature. Concerning the solid electrolyte, the use of YTSZ electrolyte in place of YPSZ allows a gain of about 50°C in the minimum reading of Pt-air sensor thanks to the higher ionic conductivity of the YTSZ. However, YTSZ is characterized by lower mechanical strength compared to YPSZ electrolyte and shorter life-service capability is expected for sensors with this solid electrolyte, especially when exposed to HLM characterized by high pressure (large HLM pools and HLM storage tanks) or shear stresses (HLM loops). Finally, a preliminary error analysis was performed on the electric potential output of Pt-air and Cu/Cu₂O sensors to estimate the intrinsic error of solid electrolyte based sensors in HLMs. The analysis revealed that the standard deviation associated to the electric potential measurement is small and comparable to the error of the multi-meter (the maximum standard deviation observed was ±0.3 mV for Cu/Cu₂O sensor).

An oxygen sensor prototype with Pt-air reference system and YTSZ electrolyte and 1 m long was developed in parallel for the application in large HLM pool facility and, specifically, for CIRCE pool facility located at ENEA Brasimone. Different configurations were considered and tested during the last three years before obtaining the current configuration. The calibration test performed in HLM storage tank with 285 L of Pb showed good accuracy (deviation ± 1% from the expected electric

potential), no hysteresis in the range 380-450°C as well as satisfying tightness of the configuration at pressure near the atmospheric one. Tests at high-pressure conditions (up to 10 bar) are needed to assess if the tightness is sufficient also for the future application in HLM storage tanks during filling procedure. The baseline investigation on different oxygen sensors and the results obtained for the sensor for large pool helped in defining the next steps for the final development and the application in CIRCE. In order to have an accurate measure also at low temperature, the Cu/Cu₂O reference system will be used in place of the Pt-air one and YPSZ electrolyte will be employed to guarantee a long service lifetime of the sensor when installed in CIRCE. In addition, a new design of the solid electrolyte thimble has been identified, to reduce even more the change of failure of the ceramic.

Finally, the developed oxygen sensors allowed to investigate the influence of dissolved metals and metal-oxides in the HLM. The test performed in fresh LBE with low dissolved oxygen revealed that the electric potential of oxygen sensors is prone to follow Fe/Fe₃O₄ equilibrium rather than to follow oxygen iso-concentration lines. Dissolved metal impurities seem to enter in equilibrium with their corresponding oxides, influencing the oxygen behaviour and modifying the oxygen concentration in the HLM. Oxygen sensors in HLMs can give useful information about the impurities present in the melt. The results of this experiment are particularly interesting and demonstrate that oxygen-metal interactions may play fundamental role in the control of oxygen concentration in HLM-cooled systems, since the formation of a given oxide involves the consumption of dissolved oxygen. Moreover, this experiment validates the behaviour of oxygen sensors in low oxygen HLM, being the oxygen sensors able to work predictably also in this regime.

5.5 REFERENCES

- [1] Corrosion Department of Institute for Applied Materials Material Process Technology, Karlsruhe Institute of Technology (KIT), "Experimental capsule for exposure of steels to oxygen-containing lead alloys. Technical documentation and user instructions", 2013.
- [2] C. Schroer, J. Konys, A. Verdaguer, J. Abellà, A. Gessi, A. Kobzova, S. Babayan, J.-L. Courouau, "Design and testing of electrochemical oxygen sensors for service in liquid lead alloys", *J. Nucl. Mater.* 415 (2011) 338-347.
- [3] OECD/NEA, "Handbook on Lead-bismuth Eutectic Alloy and Lead Properties, Materials Compatibility, Thermal-hydraulics and Technologies", 2015.
- [4] J.-L. Courouau, "Electrochemical oxygen sensors for on-line monitoring in lead-bismuth alloys: status of development", *J. Nucl. Mater.* 335 (2004) 254-259.
- [5] J. Konys, H. Muscher, Z. Voß, O. Wedemeyer, "Oxygen measurements in stagnant lead-bismuth eutectic using electrochemical sensors", *J. Nucl. Mater.* 335 (2004) 249-253.
- [6] R. Ganesan, T. Gnanasekaran, R.S. Srinivasa, "Standard molar Gibbs free energy of formation of PbO(s) over a wide temperature range from EMF measurements", *J. Nucl. Mater.* 320 (2003) 258-264.
- [7] A. Kishimoto, A. Wada, T. Michimoto, T. Furukawa, K. Aoto, T. Oishi, "Solubility and activity of oxygen in Pb-Bi melts", *Mater. Trans.* 47 (2006) 122-128.
- [8] R. Ganesan, T. Gnanasekaran, R.S. Srinivasa, "Determination of standard molar Gibbs free energy of formation of Bi₂O₃ over a wide temperature range by EMF method", *J. Chem. Thermodyn.* 35 (2003) 1703-1716.
- [9] G. Manfredi, J. Lim, K. Rosseel, J. Van den Bosch, Th. Doneux, C. Buess-Herman, A. Aerts, "Comparison of solid metal-metal oxide reference electrodes for potentiometric oxygen sensors in liquid lead-bismuth eutectic operating at low temperature ranges", *Sensor. Actuat. B-Chem.* 214 (2015) 20-28.

- [10] R.D. Holmes, A.B. Kersting, R.J. Arculus, "Standard molar Gibbs free energy of formation for Cu_2O : high-resolution electrochemical measurements from 900 to 1300 K", *J. Chem. Thermodyn.* 21 (1989) 351-361.
- [11] H.St.C. O'Neill, M.I. Pownceby, "Thermodynamic data from redox reactions at high temperatures. I. An experimental and theoretical assessment of the electrochemical method using stabilized zirconia electrolytes, with revised values for the Fe-"FeO", Co-CoO, Ni-NiO and Cu-Cu₂O oxygen buffers, and new data for the W-WO₂ buffer", *Contrib. Mineral. Petr.* 114 (1993) 296-314.
- [12] S.P.S. Badwal, "Zirconia-based solid electrolytes: microstructure, stability and ionic conductivity", *Solid State Ionics* 52 (1992) 23-32.
- [13] A. Mariën, J. Lim, K. Rosseel, W. Vandermeulen, J. Van den Bosch, "Solid electrolytes for use in lead-bismuth eutectic cooled nuclear reactors", *J. Nucl. Mater.* 427 (2012) 39-45.
- [14] T. Inoue, N. Seki, K. Eguchi, H. Arai, "Low-temperature operation of solid electrolyte oxygen sensors using perovskite-type oxide electrodes and cathodic reaction kinetics", *J. Electrochem. Soc.* 137 (1990) 2523-2527.
- [15] J. Lim, G. Manfredi, A. Mariën, J. Van den Bosch, "Performance of potentiometric oxygen sensors with LSM-GDC composite electrode in liquid LBE at low temperatures", *Sensor. Actuat. B-Chem.* 188 (2013) 1048-1054.
- [16] M. Tarantino, P. Agostini, G. Benamati, G. Coccoluto, P. Gaggini, V. Labanti, G. Venturi, A. Class, K. Liftin, N. Forgione, V. Moreau, "Integral Circulation Experiment: Thermal-hydraulic simulator of a heavy liquid metal reactor", *J Nucl. Mater.* 415 (2011) 433-448.
- [17] M. Tarantino, D. Martelli, G. Barone, I. Di Piazza, N. Forgione, "Mixed convection and stratification phenomena in a heavy liquid metal pool", *Nucl. Eng. Des.* 286 (2015) 261-277.
- [18] A. Aerts, S. Gavrilov, G. Manfredi, A. Marino, K. Rosseel, J. Lim, "Oxygen-iron interaction in liquid lead-bismuth eutectic alloy", *Phys. Chem. Chem. Phys.* 18 (2016), 19526-19530.
- [19] S. Gossé, "Thermodynamic assessment of solubility and activity of iron, chromium, and nickel in lead bismuth eutectic", *J. Nucl. Mater.* 449 (2014) 122-131.
- [20] J-L. Courouau, C. Chabert, L. Pignoly, L. Gicquel, K. Ginestar, L. Brissonneau, "Demonstration of the effect of impurities on the long term behaviour of electrochemical oxygen sensor during the STELLA 2006 tests", *Proceeding of the 1st International Workshop on Technology and Components of Accelerator Driven Systems, 2010, Karlsruhe, Germany.*

6. EXPERIMENTAL PART II: EXPERIENCES IN OXYGEN CONTROL WITH GAS MIXTURES

6.1 OXYGEN CONTROL IN SMALL EXPERIMENTAL CAPSULES (RACHEL LAB)

6.1.1 Introduction

RACHEL laboratory (Reaction and Advanced CHEmistry of Lead) is an experimental laboratory at ENEA Brasimone, in operation from January 2014. The laboratory is devoted to the research activity on HLM chemistry, oxygen monitoring and control in HLMs and corrosion tests of steel specimens (bare and coated) in HLMs and it supports the technological development of Pb-cooled nuclear reactors. To this purpose, the laboratory is equipped with several experimental steel capsules (small and large) for the containment of small amounts of HLM (from 750 to 10000 g) heated up to 550°C. Fig. 6.1 shows the pictures of small and large capsules in RACHEL laboratory.



Fig. 6.1: Pictures from RACHEL laboratory showing small (left) and large (right) experimental capsules for HLM chemistry control tests and corrosion tests of specimens.

Since the beginning of the operation of RACHEL laboratory, several tests on HLMs were performed with deoxygenating Ar-H₂ gas mixtures with the goal to reach low oxygen conditions in the melt ($\approx 10^{-8}$ % wt.) in reasonable times. The deoxygenation occurs according to the chemical reaction reported in Eq. 3.20. The HLM conditioning to low oxygen has the scope to prepare the melt for corrosion tests of candidate materials in oxygen-controlled condition, which is the typical working condition foreseen in Pb-cooled reactors. Some examples of conditioning tests performed at 550°C are reported below. These tests acted as preliminary oxygen control tests and provided qualitative information about the management of the oxygen concentration with H₂ containing gas mixtures. The implementation of a flexible gas control system was put in place in the laboratory to achieve the HLM deoxygenation in reasonable times according to various operative conditions (HLM amount and HLM temperature).

6.1.2 Experimental Setup

Deoxygenation tests of HLM were performed in small and large experimental capsules designed to perform corrosion tests of candidate materials as well as oxygen sensors calibration in oxygen-controlled and oxygen-saturated conditions. Small capsules were manufactured by KIT and a brief description was already provided in section 5.1.2. Large capsules were instead designed and manufactured in ENEA. A detailed description of both is given below.

Small capsules consist in a stainless steel cylinder (AISI 316, total H= 180 mm) heated on the outer surface by a band heater (power 1kW) and are designed for a maximum operating temperature of 550°C. An alumina crucible (d=50 mm, H=75 mm) placed at the bottom of the steel cylinder acts as a

container of 750-800 g of HLM and prevents the contact between the HLM and the steel cylinder wall. Solid pieces of Pb alloy are introduced inside the alumina crucible, then melted and heated up to the working temperature (heating rate 2°C/min). The cover lid of the capsules is equipped with penetrations for the insertion of components inside the Pb melt: K-type thermocouple inside an alumina one-end closed tube, alumina open tube for gas bubbling in the HLM, fitting for the outgas, oxygen sensor, Mo wire electrode and one specimen hung up to a holder bar (when a corrosion test is performed). The monitoring of oxygen concentration in the melt is usually performed with Pt-air oxygen sensors manufactured by KIT, whose calibration and operation was described in section 5.1.3. A sealing ring made of Inconel 600 is placed between the steel cylinder and the cover lid to ensure the tightness. The thermal insulation is ensured by two aluminum sheets and mineral wool wrapped around the steel cylinder.

Large capsules are very similar to the small ones from the point of view of design. The steel cylinder is made of AISI 304 (H= 500 mm), which is heated on the outer surface by a spiral element (power 3kW). The maximum design temperature is 550°C. A large alumina crucible (d=110 mm, H=220 mm) is placed at the bottom of the steel cylinder and can contain up to 10 Kg of HLM. The cover flange is equipped with penetrations for the insertion of the components in the HLM. A polymeric O-ring (polytetrafluoroethylene) is used to ensure the tightness between the steel cylinder and the cover flange. Pt-air oxygen sensors with YTSZ or YPSZ tube (L=700 mm) and with a steel sheath (AISI 316, ½”) are used to monitor the oxygen concentration in the HLM. The steel sheath is necessary to distribute the heat along the ceramic tube and prevents strong thermal gradients which may lead to the failure of the ceramic.

The gas injection is provided to small and large capsules by means of a gas line fed with Ar-H₂ mixture (or also pure argon). A rotameter is placed before each capsules for dosing the gas independently. The gas flow-rate to small capsules is kept at around 3-5 cc/min to avoid violent bubbling and spread of HLM on the inner wall of the cylinder. The gas flow-rate to large capsules is kept at around 10-12 cc/min.

PLC (Programmable Logic Controller) by National Instruments is used to set and acquire the parameters of the test (HLM temperature, HLM heating and cooling rate, exposure time, electric potential of the oxygen sensor). PLC is in charge to manage the power on the band heater wrapped around the steel cylinder. The power control is obtained by PID (Proportional Integral Derivative) system setting the temperature on the thermocouple of the band heater. Parameters such as HLM temperature and heating rate, exposure time, sensor electric potential are set, monitored and acquired by a software created with Lab-view by ENEA (see Fig. 6.2) in communication with the PLC.

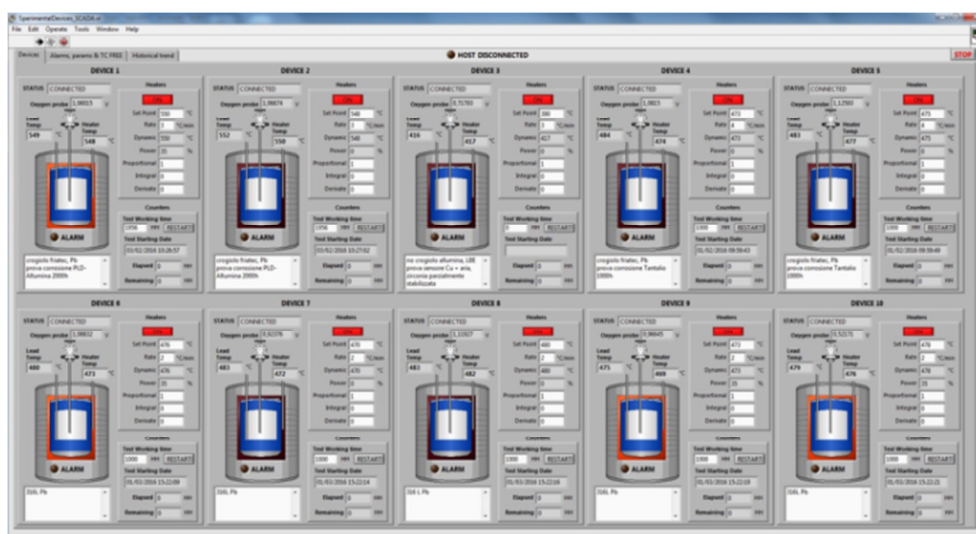


Fig. 6.2: Software for the management and acquisition of test parameters for small experimental capsules.

The deoxygenation tests described below were all performed in Pb with nominal purity of 99.97% provided by ECOBAT S.p.a. Before starting the tests, Pb pieces cut from ingots were mechanical polished using a grit paper (100P) to remove the typical oxide crust of ingots. Alternatively, solid slugs floating on liquid Pb free surface were removed with a steel tools when the temperature was close to melting point. These procedures were useful to minimize the starting impurities of the Pb alloy. At first some tests were performed by using commercial Ar-3% H_2 (% vol.) gas mixture provided by SAPIO S.r.l. (purity 99.9999 %, $O_2=0.1$ ppm mol, $H_2O=0.5$ ppm mol). Then other tests were carried out by using Ar- H_2 gas mixtures with higher H_2 concentration. Since gas mixtures with $H_2 > 3$ % are not commercially available, the mixture was directly produced in laboratory exploiting a gas control system implemented to feed all the capsules of the laboratory. Specifically, the mixture was created by mixing pure argon from cylinder (SAPIO S.r.l., purity 99.9999%, $O_2=0.1$ ppm mol, $H_2O=0.5$ ppm mol) with pure H_2 (purity 99.9999%) produced by H_2 electrolytic generator with PEM (Proton Exchange Membrane) technology (mod. H2PEM-100, Parker-Balston, 100 cc/min, 6.9 bar). Each gas was dosed and controlled with a digital mass-flow controller calibrated for the specific gas (mod. Bronkhorst) and sent together to a mixing chamber. Then, a digital pressure transducer (mod. Bronkhorst) with set-point at 1.7 bar was placed after the mixing chamber to keep the gas under pressure and to overcome any pressure drop in the feed line. Fig. 6.3 reports a picture of the gas panel with indication of the instrumentation for the control.

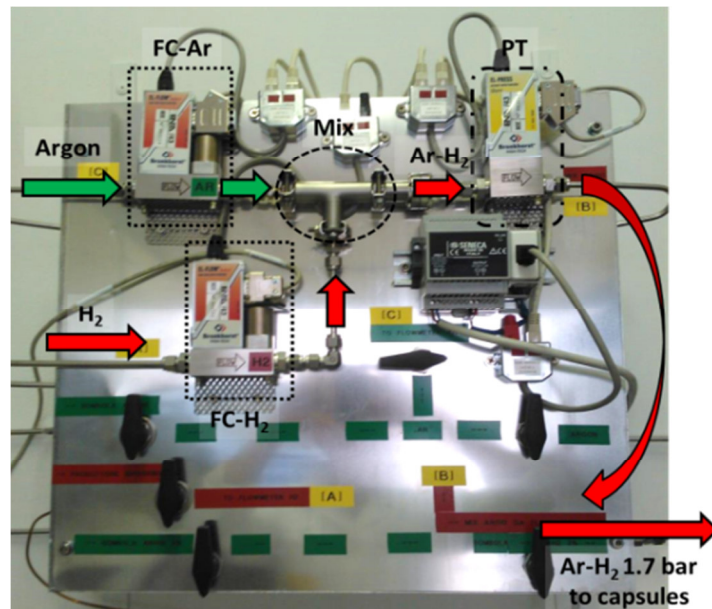


Fig. 6.3: Picture of the gas panel with indication of the instrumentation for the gas control (FC= Flow Controller, Mix= Mixing Chamber, PT =Pressure Transducer).

The implemented gas control system has two important advantage. The first is connected with flexibility of the H_2 concentration in the gas mixture. Indeed, H_2 concentration is freely set and varied through a pc software (by Bronkhorst) in communication with the pressure transducer and the mass-flow controllers. The second one is connected with the safe operation with H_2 . The generator produces H_2 at low pressure (1.7 bar, the pressure of the gas line) so that the potential risk of fire and explosion is considerably lower compared to use of H_2 from cylinder at hundreds of bar. In addition, the H_2 generator is equipped with safety blocks on the H_2 production in case of leakage or malfunctioning, which make the H_2 generator an instrument with intrinsic safety. Finally, the adequate ventilation of the laboratory through extractor fans located above the gas control panel and above the experimental capsules prevents the formation of H_2 gas pockets in the room, excluding the possibility of reaching the lower flammable limit of H_2 in air (4 % vol.).

6.1.3 Results

Deoxygenation tests with commercial Ar-3% H_2 gas mixture and gas flow rate 3-5 cc/min were performed at first on small amount of Pb (750-800 g) at 550°C. Before the test, solid impurities floating on the Pb free surface were removed at around 350°C. Pt-air sensor was used to monitor the oxygen concentration over time in the melt. Some results obtained are reported in Fig. 6.4. Global deoxygenation of the melt occurred when Ar-3% H_2 was bubbled in the small static. Some differences (mainly in terms of the reached oxygen concentration over time) were observed between the two tests, likely ascribable to different starting conditions of the Pb melt (floating oxides were manually removed with a steel tool) and also gas fluctuations supplied to the melt (some pressure drops were expected in the supply line in different positions as well as some deviations due to the use of rotameters for dosing the gas flow rate). Anyhow, a sufficiently low oxygen concentration was not achieved in reasonable times (within 300 hours), even if the trend of the sensor electric potential seemed to indicate that further deoxygenation may have occurred giving more time. Indeed, to have a concentration around 10^{-8} % wt. at 550°C, the sensor electric potential should fall at about 1.10 V, whereas the electric potential reached in 300 hours is included between 0.76 and 0.80 V, corresponding to an oxygen concentration around 10^{-5} % wt.

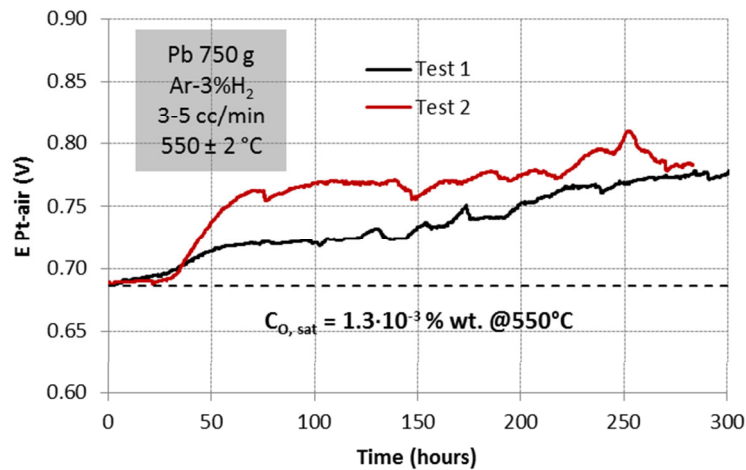


Fig. 6.4: Sensor electric potential during deoxygenation tests of Pb (750 g) at 550°C with 3-5 cc/min of Ar-3% H_2 with indication of the starting oxygen concentration.

The difficulty in reaching the low oxygen condition in static HLM can be explained assuming that the deoxygenation reaction occurs at the gas/liquid interface or in a reaction plane in the HLM very close to the interface. Indeed, oxygen has a significant solubility in Pb and LBE whereas H_2 gas is practically insoluble in such melts (the solubility in LBE is five orders lower than the oxygen one in the range 400-800°C) [1]. Considering also that oxygen and hydrogen diffusivities in Pb and LBE melts are comparable [1,2], the chemical absorption model characterized by fast reaction near the gas/liquid interface was assumed. Furthermore, Gonzalez Prieto et al. suggested that the scarce deoxygenation efficiency of small amounts of static HLM with Ar- H_2 gas mixtures depends on oxygen diffusive transport limitations [3], making presume that the main resistance to the deoxygenation process is the oxygen diffusion towards the reaction plane (resistance in the HLM phase).

According to this hypothesis, some options were considered to increase the process efficiency in the experimental capsules:

- 1) increasing the H_2 concentration in the inert gas (to promote the reaction rate);
- 2) increasing the HLM temperature (to promote the reaction rate and the diffusivity);
- 3) increasing the gas/liquid interface (to promote the exchange process at the interface, e.g. by reducing the gas bubble size);

- 4) increasing the HLM turbulence or mixing (to promote oxygen diffusion in the HLM phase, e.g. increasing the gas flow rate).

Unfortunately, the variation of parameters according to points 2, 3 and 4 has few margins of implementation in small experimental capsules and the variation according to point 1 was first considered. For the purpose, the gas system described by Fig. 6.3 was implemented and used to create gas mixtures with high H_2 concentration.

The result of the deoxygenation test performed in Pb (750 g) at 550°C with high H_2 concentration in the gas mixture is described in Fig. 6.5. In this case, the solid Pb pieces were polished with abrasive paper to remove the external oxide layer but dissolved metal impurities were not mechanically removed after melting. Using argon with 15 % vol. of H_2 , a low oxygen concentration was achieved in about 24 hours and stabilized slightly below to 10^{-8} % wt. over 150 hours. Specifically, the sensor output seems to follow the electric potential associated to Fe/Fe_3O_4 equilibrium at 550°C , which is reasonable considering that Pb 99.97 % contains several ppmw of Fe whereas Fe solubility in Pb is only 0.6 ppmw at 550°C [4]. In this phase, it is possible that the Fe_3O_4 formation equilibrium helped in keeping the oxygen concentration constant in the melt. Subsequently, when air was supplied to the melt, the electric potential of the sensor fell down to the potential corresponding to the oxygen saturation. The gas injection with 20 % H_2 rapidly restored the low oxygen condition and pushed the concentration down at about 10^{-9} % wt. (corresponding to 1.18 V).

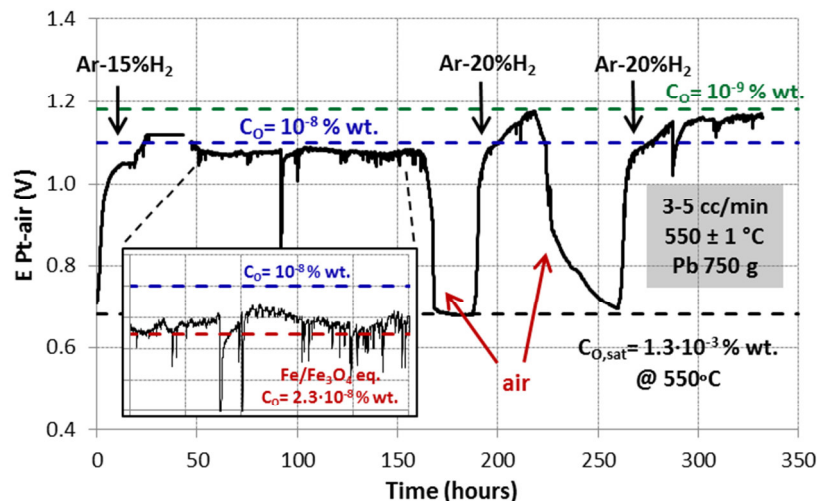


Fig. 6.5: Sensor electric potential during deoxygenation test of Pb (750g) at 550°C with 3-5 cc/min of argon with 15 % and 20 % of H_2 with indication of the reached oxygen concentration.

Deoxygenation tests with high H_2 level in the gas mixture was also performed in large capsules with 5-6 Kg of Pb. Before the tests, solid oxides and dissolved metal impurities were removed from the Pb free surface at 350°C . Fig. 6.6 reports the results of the deoxygenation of liquid Pb at 550°C with 10 % of H_2 . The deoxygenation process was globally rapid and easily repeatable after air injections in the capsule and the sensor output stabilized near the Fe_3O_4 formation equilibrium in the time range 150-220 hours. In this case the saturation of Pb with dissolved Fe could have occurred as a result of the concomitant corrosion of the steel sheath of the sensor during the test.

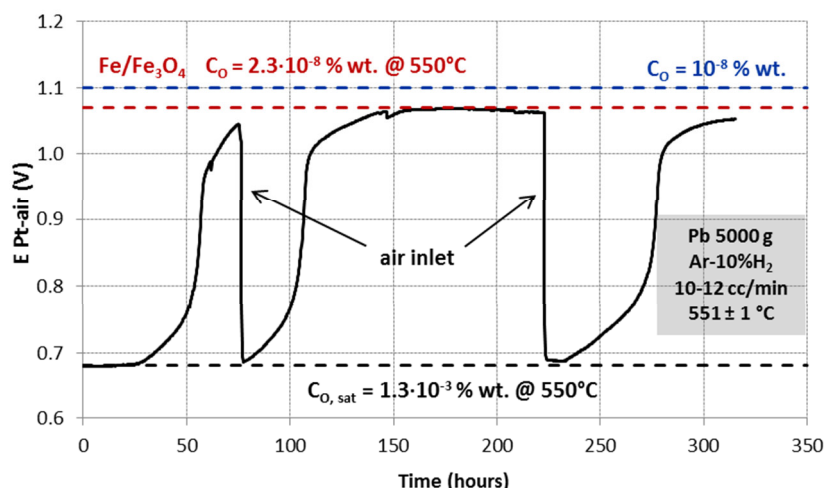


Fig. 6.6: Electric potential of the sensor during deoxygenation test in Pb (5000 g) at 551°C with 10-12 cc/min of argon with 10 % of H₂ with indication of the reached oxygen concentration.

These tests demonstrated that the deoxygenation process in small static HLM is promoted by increasing H₂ concentration in the gas mixture. Using H₂ concentration ranging from 10 to 20 %, it is possible to obtain low oxygen concentration. If Fe is dissolved up to the solubility, Fe/Fe₃O₄ equilibrium could be established in the HLM and have a role in stabilizing over time the low oxygen concentration. An example is given by Fig. 6.7, where long-term stabilization of the oxygen concentration was obtained near Fe/Fe₃O₄ equilibrium during a corrosion test of specimens in Pb at 550°C with Ar-10%H₂ bubbling gas.

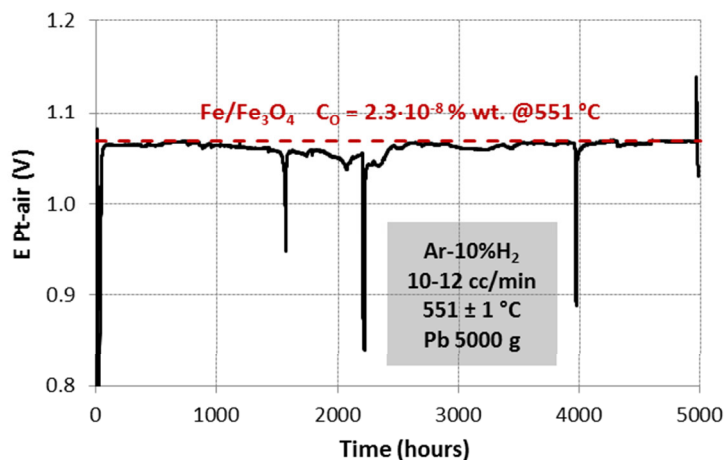


Fig. 6.7: Long-term stabilization of the oxygen concentration in Pb during a corrosion test at 550°C with Ar-10%H₂ bubbling gas.

6.2 OXYGEN CONTROL IN HLM STORAGE TANK (HELENA LOOP)

6.2.1 Goal of the work

Deoxygenation tests were performed in static HLM in larger scale experiment. Specifically, deoxygenation tests were performed in HLM storage tank with the purpose to reach a good level of HLM purification. The deoxygenation of the HLM in the storage tank of an experimental facility is a fundamental step in the oxygen control technology. Indeed, before loading the HLM into the experimental facility, the HLM should be purified in the storage tank from the excess of oxygen in order to simplify the oxygen control procedures during the operation of the facility.

The storage tank of HELENA facility in Brasimone was used for the purpose. Deoxygenation tests were performed with various bubbling Ar-H₂ gas mixtures at two temperatures. A test in cover gas was also performed to evaluate the effect of the HLM mixing on the process efficiency. A gas control system similar to that one employed for the deoxygenation in experimental capsules (see Fig. 6.3) was implemented for the scope and tested with success also in this application. Finally, the effect of the injection of pure argon and air on the deoxygenated Pb was analyzed.

6.2.2 Experimental Setup

HELENA storage tank is made of AISI 316 stainless steel and contains about 285 L of Pb (about 3008 Kg). The Pb volume was determined from the Pb level in the storage tank at 420°C. The design of the storage tank is shown in Fig. 6.8.

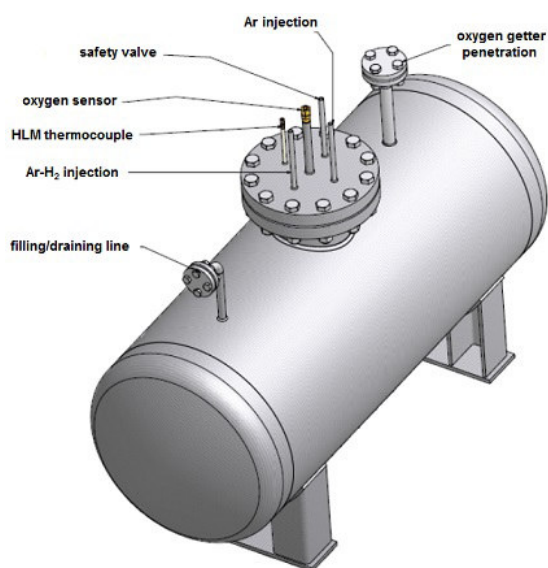


Fig. 6.8: Design of HELENA storage tank with description of the penetrations for components.

The power control for the HLM heating was obtained by PID (Proportional-Integral-Derivative) with temperature set point on the control thermocouple of the external heating cables. The Pb temperature was monitored over time with a K-type thermocouple (range 0-1100°C) dipped in the melt. The Ar-H₂ mixtures were prepared by using a similar setup of that described in section 6.1.2. Specifically, the mixture was created by mixing pure argon from cylinders (SAPIO S.r.l., BIP purity, O₂ < 10 ppb mol, H₂O < 20 ppb mol) with pure H₂ (purity 99.9999 %) produced by H₂ generator (mod. AD-1000, Cinel, 1000 cc/min, 10 bar). The two gases were dosed and controlled with digital mass-flow controllers calibrated for the specific gas (mod. Bronkhorst) and sent to the mixing chamber. No pressure transducer was used in this case. The H₂ concentration in the gas was set by means of a software developed in ENEA in communication with mass-flow controllers. The gas flow rate sent to the storage tank was kept at 1 NL/min to ensure a good level of HLM mixing. The gas mixture was bubbled in Pb (or injected as cover gas on the Pb free surface) through a ¼" one-end closed tube in AISI 316 provided with small holes (d= 1mm) in the terminal part. A slight gas overpressure of 0.3 bar was maintained in the storage tank and adjusted by a pressure safety valve. The oxygen concentration in Pb was monitored over time with the Pt-air oxygen sensor prototype developed for large HLM pools, whose description and calibration were reported in sections 5.2.2 and 5.2.3. The outgas line was provided by a ¼" steel tube. Each test was carried out starting from an oxygen-saturated condition without PbO floating on the Pb free surface. At the end of the tests, air was supplied to the HLM to ensure again the oxygen saturation. Before air injection, three-four cycles involving depressurization and pressurization with argon gas were performed in the tank to dilute H₂ and prevent hazardous contact with air. A scheme of the experimental setup is given in Fig. 6.9.

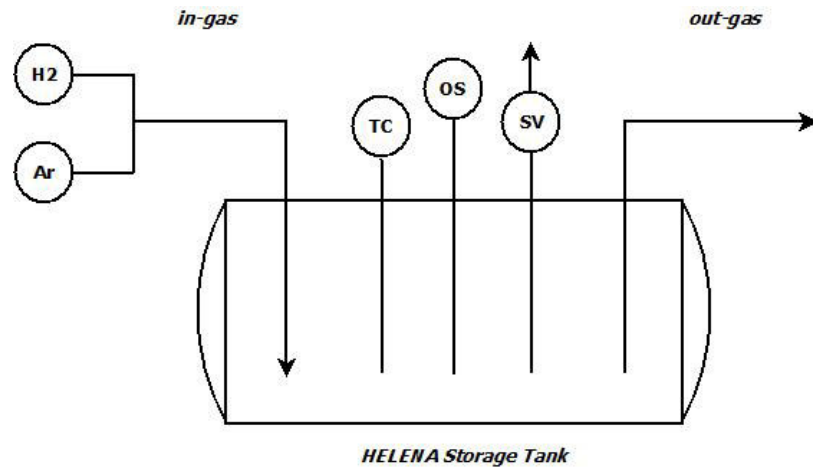


Fig. 6.9: Scheme of the experimental setup in HELENA storage tank for deoxygenation tests (Ar+H₂= gas mixture, TC= thermocouple, OS= oxygen sensor, SV= pressure safety valve).

The deoxygenation tests were performed with Ar-H₂ gas mixtures with different H₂ concentrations at two temperatures (420 and 480°C) in bubbling mode. A further test in cover gas mode was performed in order to discriminate the effect of the HLM mixing. The tests are summarized in Tab. 6.1. The H₂ concentration in the gas mixture is reported with the standard deviation evaluated on the gas flow rate data given by Bronkhorst mass-flow controllers.

Tab. 6.1: Test matrix for deoxygenation tests in HELENA storage tank.

Mode	T _{pb} (°C)	H ₂ (% vol.)	Gas flow rate (NL/min)	Cover gas pressure (bar)
Bubbling	480	26.7 ± 0.3	1	0.3
Bubbling	480	4.8 ± 0.3	1	0.3
Bubbling	420	17.8 ± 0.3	1	0.3
Bubbling	420	4.8 ± 0.3	1	0.3
Cover	420	20.0 ± 0.3	1	0.3

6.2.3 Results

The results of the deoxygenation tests in bubbling mode are reported in Fig. 6.10 and Fig. 6.11 at 480°C and 420°C respectively. Some useful results have been reported in Tab. 6.2 to have a better usability of the data. The starting oxygen concentration C_{O,sat} (oxygen saturation) and the final oxygen concentration C_{O,f} are reported together with the corresponding sensor electric potentials. The final time of the experiment was set at the time where the electric potential seemed almost stabilized over time (a slight and continuous increase of the electric potential was observed even at the end of the test). To have homogeneity between data, the final time for all the trends was considered after 17 hours from the last change of slope of trends reported in Fig. 6.10 and Fig. 6.11. The final oxygen concentration C_{O,f} was considered at this point calculating a mean value over the last 5 hours to minimize the noise in the electric potential acquisition. Finally, the total amount of oxygen removed during the tests was calculated from the total amount of Pb contained inside the storage tank (285 L, 3008 Kg) considering the equation for the calculation of the density recommended in [2].

As for the tests performed in experimental capsules (see section 6.1.3), one can immediately observe that the deoxygenation process proceeded faster when H₂ concentration was increased in the gas for a given temperature. This result confirms that the deoxygenation reaction rate is promoted by increasing H₂ concentration in the argon gas. In addition, the deoxygenation performed at 480°C was faster than that one performed at 420°C for the given H₂ concentration of 4.8 %. The increase of the reaction rate with the temperature is ascribable to the exponential dependence of the kinetic

constant with the temperature (according to Arrhenius equation) but also to the different oxygen concentration gradient (higher at 480°C than 420°C for the higher oxygen saturation concentration). Finally, slightly lower final oxygen concentrations were observed when higher H₂ concentrations in the gas mixture were used. Anyhow, the final oxygen concentration did not change significantly between the various tests at a given temperature, making presume that the final concentration reached the equilibrium independently from the H₂ concentration used.

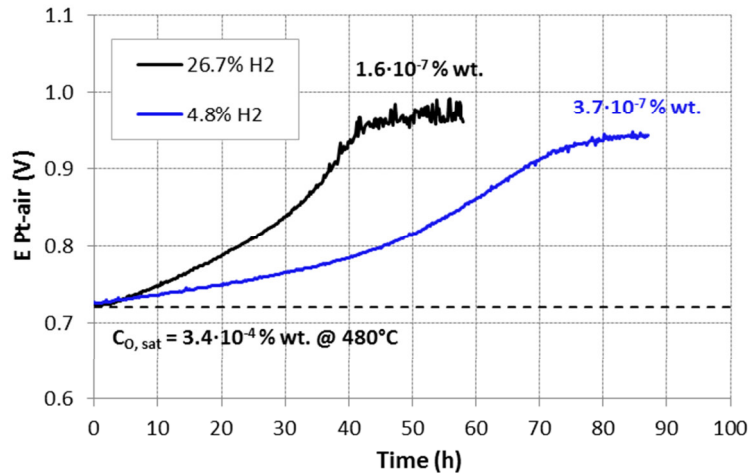


Fig. 6.10: Deoxygenation of Pb (bubbling mode) at 480°C with 26.7 and 4.8 % vol. of H₂ in argon (1 NL/min) in HELENA storage tank with indication of the starting oxygen concentration (oxygen saturation) and the final concentration.

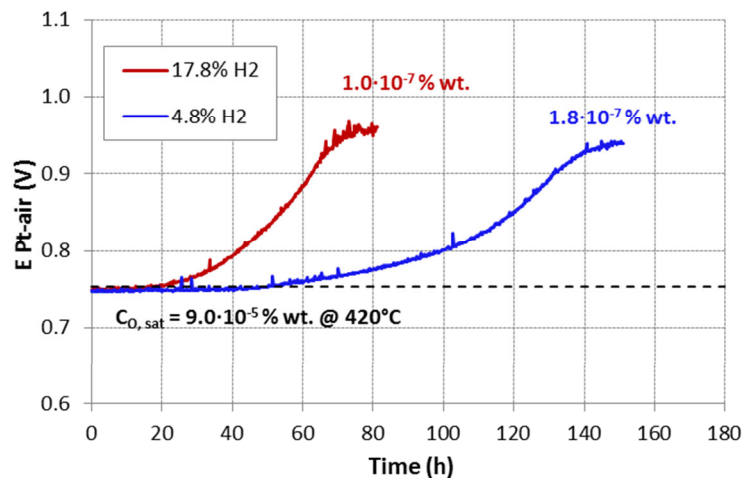


Fig. 6.11: Deoxygenation of Pb (bubbling mode) at 420°C with 17.8 and 4.8 % vol. of H₂ in argon (1 NL/min) in HELENA storage tank with indication of the starting oxygen concentration (oxygen saturation) and the final concentration.

Tab. 6.2: Summary of deoxygenation tests in Pb (385 L, 3008 Kg) at 480°C and 420°C (bubbling mode) with different H₂ % vol. in argon (flow rate 1NL/min).

T _{Pb} (°C)	H ₂ (% vol.)	E _i (V)	C _{O,sat} (% wt.)	Final Time (h)	E _f (V)	C _{O,f} (% wt.)	Total O removed (g)
480	26.7	0.725	$3.0 \cdot 10^{-4}$	58	0.970	$1.6 \cdot 10^{-7}$	9.019
480	4.8	0.725	$3.0 \cdot 10^{-4}$	87	0.942	$3.7 \cdot 10^{-7}$	9.013
420	17.8	0.749	$9.0 \cdot 10^{-5}$	81	0.956	$1.0 \cdot 10^{-7}$	2.706
420	4.8	0.749	$9.0 \cdot 10^{-5}$	151	0.938	$1.8 \cdot 10^{-7}$	2.705

From the comparison of data here described with data concerning tests in experimental capsules (section 6.1.3), it is possible to state that the increase of H₂ concentration in the gas promoted the deoxygenation rate for a given temperature both in small capsules and in storage tank. However, experiments performed in small capsules and storage tank involves different largeness of the gas/liquid interface surface as well as different magnitude of HLM mixing. HLM mixing in experimental capsules is expected to be very poor as a consequence of the low gas flow velocity and single bubble injection whereas higher HLM mixing is expected in the storage tank where the gas flow rate was set at 1 NL/min.

The test performed in cover gas mode was useful to discriminate the effect of the HLM mixing on the process efficiency. Fig. 6.12 shows the sensor electric potential during the deoxygenation test in cover gas mode at 420°C, with H₂ concentration of 20 % vol. and gas flow rate 1 NL/min. Comparing the oxygen trend in cover gas mode with the oxygen trend in bubbling mode at the same temperature and almost the same H₂ concentration in the gas (see Fig. 6.11), it is possible to observe a significant decrease of the process efficiency when HLM mixing is not provided in the storage tank. This result confirms the hypothesis of the resistance in the HLM phase, ascribable to the oxygen diffusion process towards the reaction plane.

The effect of the HLM mixing can now be sensed also from the comparison of the oxygen trends in bubbling mode in the storage tank (see Fig. 6.11) with the oxygen trends in experimental capsules (Fig. 6.4): a good HLM deoxygenation in the storage tank occurred in reasonable times even at 420°C with low H₂ concentration (4.8 % vol.) whereas poor deoxygenation was obtained in small capsules with lower amount of HLM and at higher temperature (550°C). About that, deoxygenation experiments performed in HLM loops (where the mixing is even more enhanced) could give more information to support this interpretation.

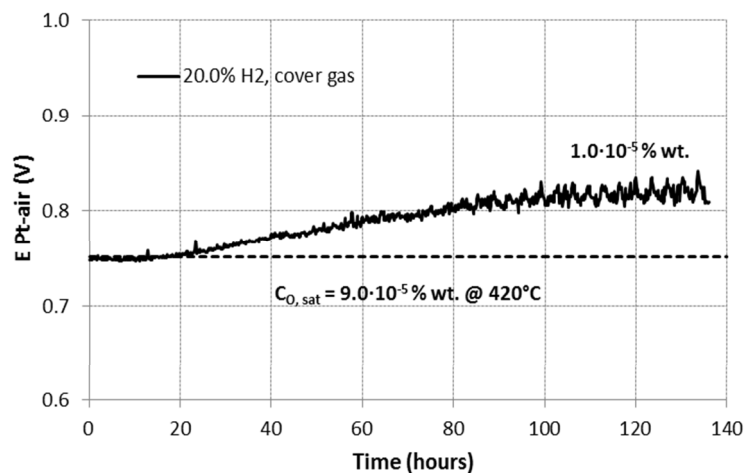


Fig. 6.12: Deoxygenation of Pb (cover gas mode) at 420°C with 20.0 % vol. of H₂ in argon (1 NL/min) in HELENA storage tank with indication of the starting oxygen concentration (oxygen saturation) and the final concentration.

Finally, the effect of pure argon gas and air on Pb was evaluated after a deoxygenation test performed at 480°C. Fig. 6.13 reports the trend of the electric potential of Pt-air sensor during the injection of pure argon (1 NL/min) and air (1NL/min) after the deoxygenation test with 4.8 % of H₂. When pure argon was supplied to the melt, the electric potential of the sensor decreased from about 0.950 V to 0.884 V over 340 hours, which means an increase of oxygen concentration from $2.9 \cdot 10^{-7}$ to $2.2 \cdot 10^{-6}$ (one order of magnitude). To the opposite, when air was injected in Pb the oxygen concentration increased from $2.2 \cdot 10^{-6}$ up to the saturation concentration (two orders of magnitude) in 15 hours. This simple test demonstrated that high-purity argon can be fruitful used as cover gas to maintain the low oxygen condition in the melt but it cannot be used as source of oxygen if needed.

To increase efficiently the oxygen concentration in the melt (e.g. to ensure an adequate protection of steels), air can be used more fruitfully. However, air injection needs some attention in dosing the flow rate in order to prevent uncontrollable oxidation of the HLM. To the purpose, the use of diluted air in argon gas seems to be a better solution for control the oxygen injection to the melt.

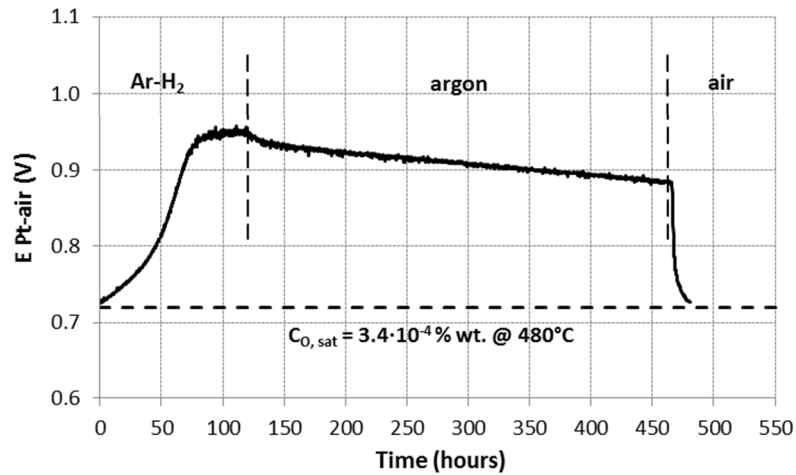


Fig. 6.13: Effect of argon and air injection on sensor electric potential after deoxygenation test with Ar-4.8%H₂ gas mixture in Pb at 480°C in HELENA storage tank.

6.3 OXYGEN CONTROL IN HLM LOOP FACILITY (NACIE-UP)

6.3.1 Goal of the work

NACIE-UP loop is an experimental thermal-hydraulic facility located in ENEA Brasimone. The facility works with LBE fluid and is characterized by very low working temperature range (between 200°C and 400°C) and narrow sections for LBE circulation in the primary loop. The combination of low temperatures and narrow sections makes necessary a deep deoxygenation of the circulating LBE to prevent the formation of coolant oxides, whose deposition in the narrow sections and above piping and components may strongly affect the LBE circulation or even cause total plugging.

The work described below illustrates the results of a deoxygenation test performed in the NACIE-UP loop facility. The goal of the experimental activity was primarily to achieve a low oxygen concentration in the HLM circulating in the primary loop of the facility in order to prevent HLM contamination with PbO and thus the plugging during experimental campaigns carried out at low temperature. To the purpose, oxygen sensor with Cu/Cu₂O internal reference was manufactured and installed in the expansion vessel of NACIE-UP loop to monitor the oxygen concentration in LBE down to 200°C according to results of Fig. 5.6. A proper LBE filling procedure in the primary loop was put in place to minimize the starting oxygen contamination due to coolant oxides and O₂ traces as recommended by Courouau [5]. Then injection of commercial Ar-3%H₂ gas mixture was carried out in the hot leg of the loop for 650 hours in the temperature range 230-400°C to reach a low oxygen concentration in the circulating LBE. Finally, the oxygen concentration monitored over time by Cu/Cu₂O sensor was analyzed to evaluate the magnitude of the deoxygenation and identify possible metal-oxygen interactions in the expansion vessel of the loop.

Since the working temperature conditions of NACIE-UP loop are usually between 200-400°C (excluding the hot spots on the electrical pins), the optimal oxygen concentration for NACIE-UP operation has been set to 10⁻⁸ % wt. as illustrated in Fig. 6.14. The blue line corresponds to the PbO formation equilibrium and represents $C_{O,sat}$ values. The red lines corresponds to Fe₃O₄ formation equilibrium (C_{O,Fe_3O_4} values) when Fe activity is equal to 1 (full line, no mass transfer considered) and when Fe activity is less than 1 and equal to Fe saturation point at 200°C (dashed line, Fe mass

transfer at the coldest point of NACIE-UP). The target concentration for NACIE-UP (black line) is then included between Fe/Fe₃O₄ and Pb/PbO equilibria to have, in principle, the formation of partially protective Fe₃O₄ above the steel surface but no formation of PbO.

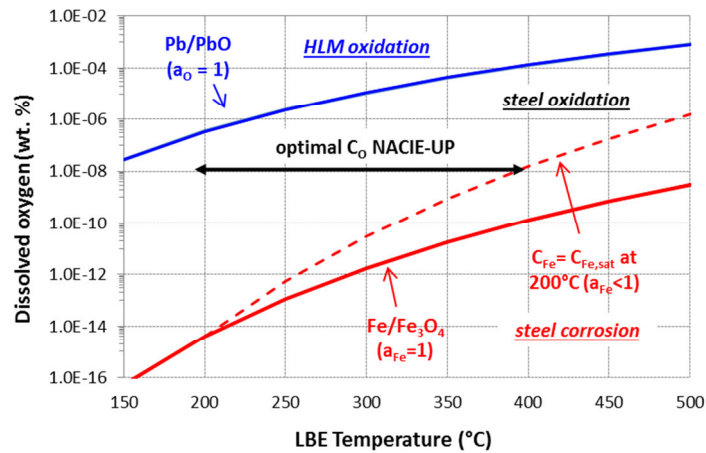


Fig. 6.14: Optimal oxygen concentration for NACIE-UP operation.

6.3.2 Description of NACIE-UP facility

NACIE-UP is a LBE-cooled experimental facility mainly devoted to thermal-hydraulics, fluid-dynamics and heat transfer studies [6]. The primary system of the facility mainly consists in a rectangular loop made of two vertical pipes acting as riser and downcomer (length 8 m, O.D. 2.5”) and two horizontal pipes (length 2.4 m, O.D. 2.5”). A sketch of the layout of the primary circuit is reported in Fig. 6.15. The pipes are made of AISI 304 stainless steel and the LBE inventory of the facility is about 200 L.

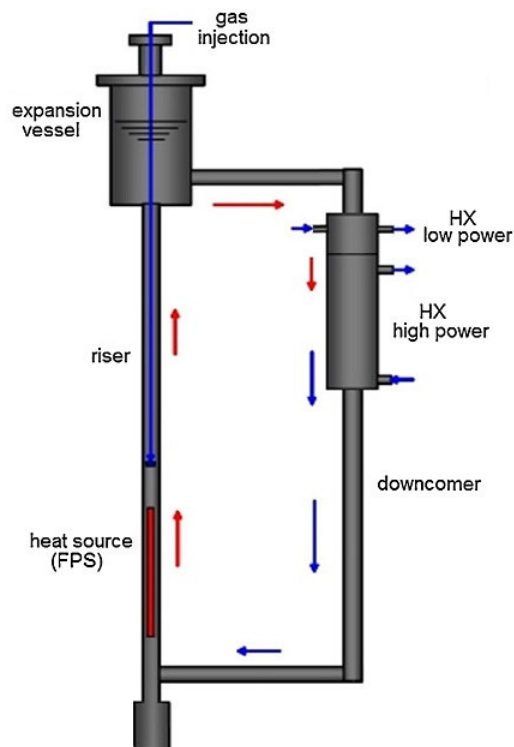


Fig. 6.15: Conceptual sketch of NACIE-UP facility [6].

In the current configuration, a prototypical wire-spaced FPS is installed at the bottom of the riser with a maximum power of 235 kW. A shell-double wall tube HX is placed in the upper part of the downcomer. A gas injection device is placed inside the riser and, once operating, provides the driving force to sustain the force circulation in the loop. An expansion tank is located at the end of the riser and it is partially filled by the cover gas to accommodate the thermal expansion of the LBE. The facility includes a secondary system filled with water at 16 bar for the cooling of the LBE. The system includes the shell side of the heat exchanger, a pump, a pre-heater, an air-cooler, by-pass and isolation valves, and a pressurizer with argon cover gas. Finally, an ancillary gas system ensures the cover gas in the expansion tank, provides the gas-lift injection in the riser, and allows the fill and drain system operation. The fill and drain system is composed by ½" pipes, isolation valves and a storage tank.

The primary loop of NACIE-UP is equipped with 3 bubble tubes to measure the LBE pressure inside the loop [7] and other pressure transducers to monitor the cover gas pressure. Differential pressure transducers are installed across the FPS, which is the component with major pressure drops in the loop. The 3 bubble tubes are placed in the riser column between FPS and the expansion vessel.

A prototypical thermal mass flow meter is installed in the lower horizontal pipe of the loop and it is reliable in the range of low and intermediate mass flow rates. Several bulk thermocouples monitor the temperature along the flow path in the loop. In particular, three TCs are installed in the cold leg (between the HX outlet and the FPS inlet), four TCs in the hot leg (between the FPS outlet and the HX inlet) and one TC measures LBE temperature inside the expansion vessel.

The device for the gas injection is inserted in the upper part of the expansion tank and it is composed of a AISI 304 pipe with length 6135 mm and O.D. ½". Technical details concerning the ending part of the device are reported in Fig. 6.16. The gas flows out through some 1 mm diameter holes aligned on a generatrix of four short pipes. The gas injection system was designed in such way to provide small diameter bubbles instead of single large bubbles released from a single hole tube. This should increase the exchange area at the gas/liquid interface and enhance the deoxygenation process when Ar-H₂ is injected. Furthermore, the bubbles rise about 5 m along the riser column before reaching the expansion tank and this long path should enhance the residence time of the gas in the HLM.

In addition, the 3 bubble tubes provides additional gas injection in the riser during the operation. The total amount of gas provided by these devices is 0.3 NL/min. This amount should be always added to the amount provided by the main injection system, which can be varied during the operation.

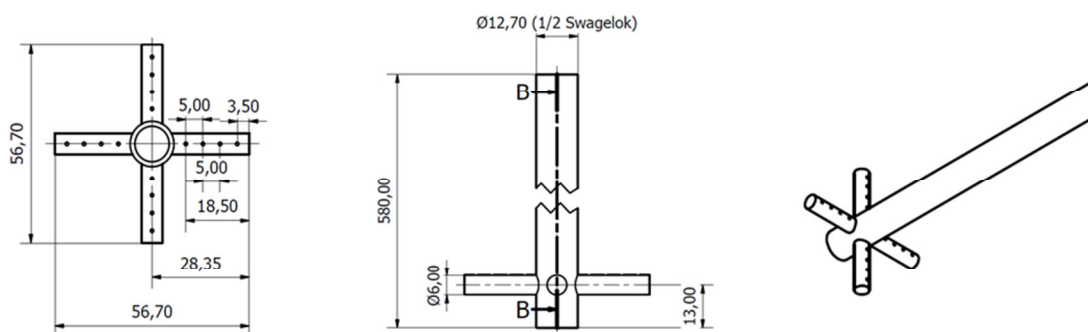


Fig. 6.16: Technical drawings of the gas injection device (Ar or Ar-H₂) in NACIE-UP loop.

6.3.3 Experimental Setup

Fabrication of the oxygen sensor for NACIE-UP

Cu/Cu₂O sensor for NACIE-UP loop was manufactured using a one-end closed tube of YPSZ (600 mm long) supplied by Friatec AG. The reference electrode was created by mixing together metal and

metal-oxide powders and loaded them at the bottom of the YPSZ tube. AISI 316 stainless steel wire was used as electric lead of the reference electrode. A high-temperature ceramic was used to create the sealing in the upper part of the YPSZ tube. Finally, AISI 316 steel tube (½") was used as protective sheath for the YPSZ tube to minimize thermal and mechanical stresses during the operation in flowing LBE. A picture of the oxygen sensor for NACIE-UP is reported in Fig. 6.17.

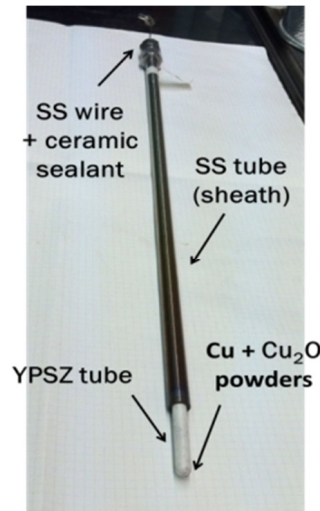


Fig. 6.17: Picture of Cu/Cu₂O oxygen sensor for NACIE-UP loop.

After the construction, the Cu/Cu₂O sensor was calibrated in oxygen-saturated LBE to assess the quality of the manufacturing. The calibration was performed in the temperature range 200-550°C according to the experimental procedure described in section 5.1.2. The LBE used for the calibration was the same contained in NACIE-UP loop. The result of the calibration (in Fig. 6.18) shows that the sensor electric potential (black points) was in good agreement with the theoretical potential (red line) expected in oxygen-saturated LBE in the range 200-550°C. The obtained fitting equation (black) was consistent with the theoretical one (red).

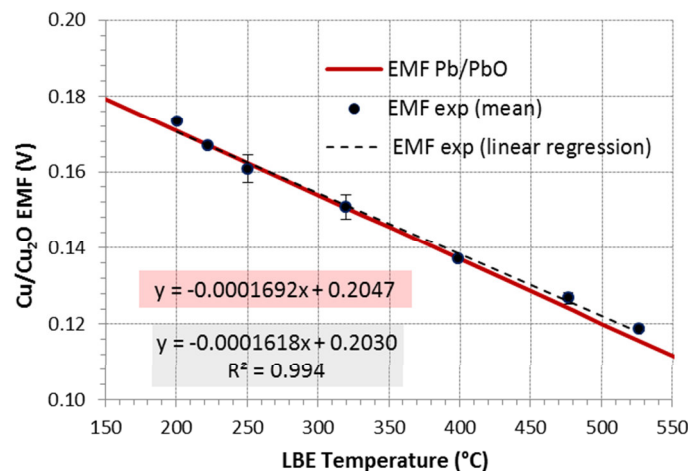


Fig. 6.18: Cu/Cu₂O sensor calibration in oxygen-saturated LBE in the range 200-550°C according to the potentiometric cell scheme 316 SS, LBE + PbO // YPSZ // Cu + Cu₂O, 316 SS.

The variation of the oxygen concentration during the experiment can be determined quickly by reading the graph of Fig. 6.19, which shows the electrical potential of the Cu/Cu₂O sensor versus the LBE temperature and the oxygen concentration (expressed as iso-concentration lines). The graph

shows also the electric potential lines associated to the Pb/PbO (oxygen saturation) and Fe/Fe₃O₄ formation equilibria.

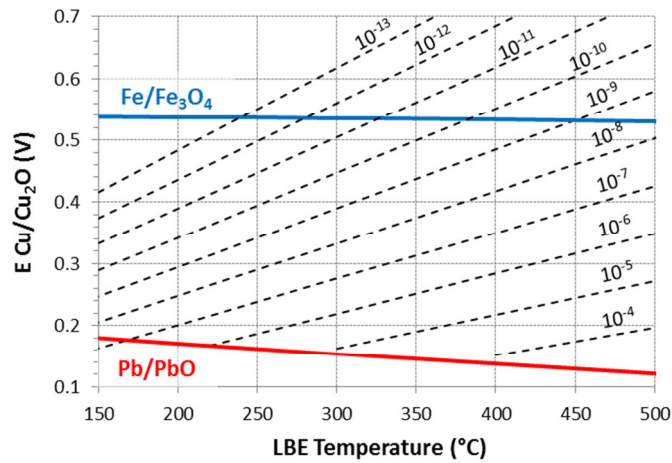


Fig. 6.19: Electric potential as a function of temperature and oxygen concentration (expressed in % wt. as iso-concentration lines) for Cu/Cu₂O sensor in LBE.

Operative procedure

The deoxygenation experiment in NACIE-UP loop was put in place by following some steps aiming at minimizing the oxygen content inside the loop and speed up the conditioning of the LBE to a low oxygen condition. The operative steps consist in: 1) cleaning cycles, 2) filling operation and 3) in-loop deoxygenation.

The cleaning cycles were performed to minimize the presence of traces of air and oxygen inside the loop before the filling with LBE. The cleaning consisted in the following steps: a) pressurization of the loop with argon at 450 mbarg, b) argon circulation (about 1 NL/min) inside the primary loop and gas system for some minutes and c) depressurization of the loop at 200 mbarg and new pressurization. The cleaning process was repeated several times at different temperatures (from 20°C to 250°C).

The filling of the primary loop was performed with the secondary system empty. The LBE temperature in the storage tank was previously set at 150°C in order to lower as much as possible the amount of dissolved oxygen in the LBE. The LBE in the storage tank was then pushed inside the loop through the filling lines and it was forced to pass through a mechanical filter in charge to prevent the entry of oxides and other impurities inside the loop. During the latter operation the temperature of the primary loop was kept to 250°C and Ar-3%H₂ gas mixture provided by SAPIO S.r.l. (purity 99.9999%, 0.1 ppmv of O₂) was injected through the gas-injection system. The pressure in the primary loop was fixed to 200 mbarg.

Once the LBE was loaded, Ar-3%H₂ gas mixture was continuously injected at a variable flow rate between 0.3 NL/min (only bubble tubes) and 1 NL/min (direct injection) for 650 hours. The trend over time of the gas flow rate supplied in the riser column through the only injection system is reported in Fig. 6.20 (the gas amount provided by the bubble tubes must be added to the amount shown in the graph). The temperature of the LBE inside the loop was changed several times between 230°C and 400°C using the heating cables wrapped around the piping. Indeed, the secondary system was empty during the test and the loop could be considered isothermal for a given temperature set point. The oxygen concentration was monitored by the Cu/Cu₂O oxygen sensor installed in the expansion vessel of the loop and dipped in the LBE volume for about 100 mm. Unfortunately, it was not possible to install other oxygen sensors in different position of the primary loop due to the lack of penetration in the piping.

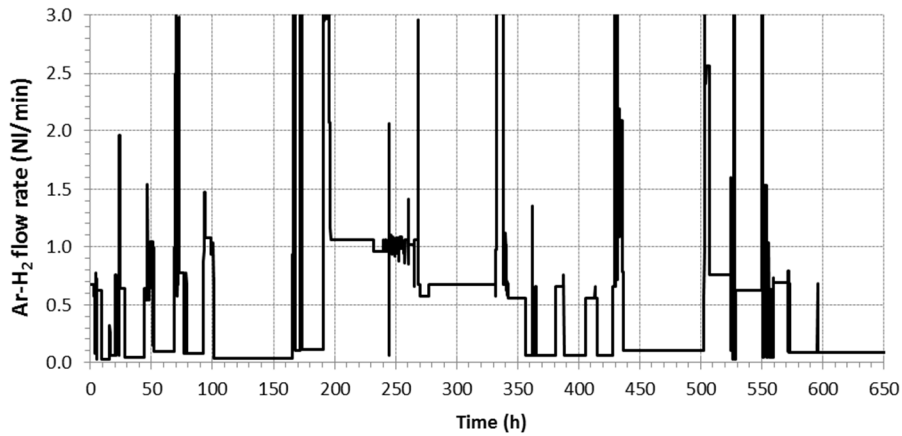


Fig. 6.20: Ar-3%H₂ gas flow rate supplied by the injection system into the riser column of NACIE-UP loop.

6.3.4 Results

Total oxygen reduction

The behaviour of the electric potential of Cu/Cu₂O sensor over the 650 hours of Ar-3%H₂ injection in NACIE-UP loop is shown in Fig. 6.21. The measured electric potential underwent a substantial increase from time 0 to 650 hours, meaning that the oxygen concentration in the LBE was deeply reduced (see Fig. 6.19 for the comparison). Comparing the sensor output of the first 25 hours with the output of the last 50 hours, an increase of the electric potential of about 0.3 V for almost the same temperature can be observed. At the beginning, the oxygen sensor measured an electric potential of 0.17 V at 240°C, which corresponds to an oxygen concentration of about 10⁻⁶ % wt. (near the electric potential associated to the oxygen saturation). Conversely, the electric potential at the end of the test reached 0.5 V at 250°C, corresponding to an oxygen concentration of about 10⁻¹² % wt. It is worth noting that the major contribution in the deoxygenation was given by the continuous injection of the Ar-3%H₂ at about 400°C between 200 and 500 hours. Here, a continuous increase of the electric potential (from 0.26 to 0.6 V) occurred when the LBE temperature was stably set at 400°C and H₂ continuous supplied to the LBE. This is likely ascribable to the speed-up of the deoxygenation reaction under the effect of the high temperature and continuous H₂ supply.

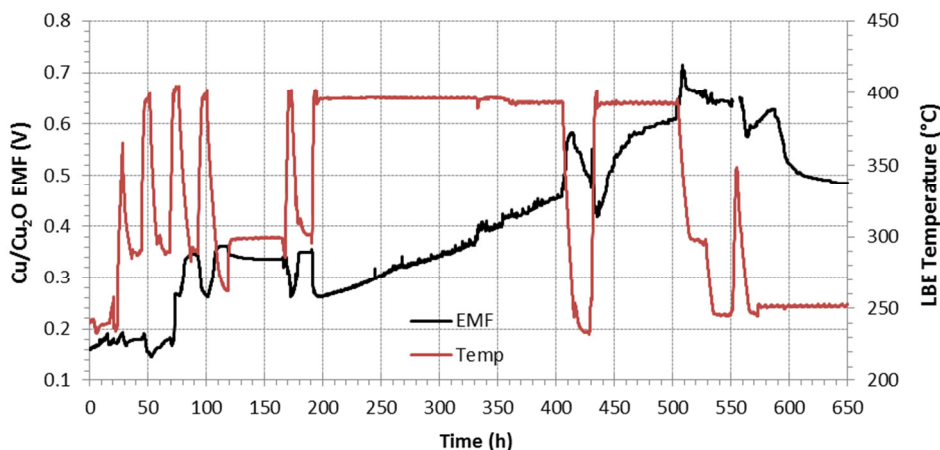


Fig. 6.21: Cu/Cu₂O electric potential over time as a function of the temperature in NACIE-UP expansion vessel.

Despite the monitoring of the oxygen concentration was performed only in the expansion vessel, the high level of circulation induced by the gas injection in the riser column should certainly ensure a

good mixing of the LBE so it is possible to affirm that the oxygen concentration was globally reduced in the whole loop and not only in the riser column. The confirmation of the global deoxygenation in the loop was given by the measurement of the LBE flow rate with the mass flowmeter placed in the lower horizontal leg (see Fig. 6.22): no evidence of flow degradation was noticed (the LBE flow follows the trend of the Ar-H₂ injection) and so no deposition of coolant oxides should have occurred. The future installation of oxygen sensors in other positions in the loop (e.g. in the dynamic horizontal hot and cold leg) will help in having a better understanding of the oxygen behaviour during the operation.

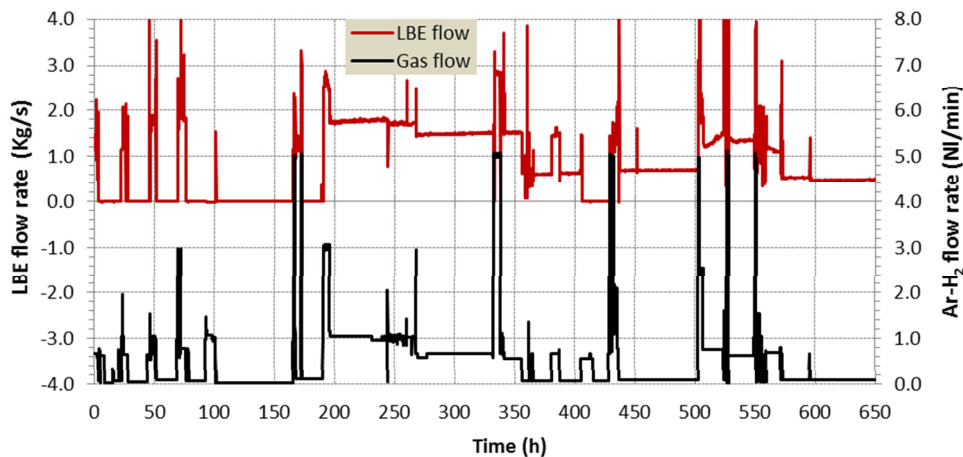


Fig. 6.22: LBE and Ar-H₂ mass flow rate over time in NACIE-UP loop during gas injection.

The in-loop deoxygenation confirmed the interpretation discussed in section 6.2.3 about the effect of the HLM mixing on the deoxygenation. Good HLM deoxygenation can be obtained with gas mixture with low H₂ concentration if a good HLM mixing is ensured in the system, so that the diffusion of the dissolved oxygen towards the gas/liquid interface is promoted.

However, it is important to note that the oxygen concentration in the LBE was not controlled in such deoxygenation experiment. Indeed, the oxygen concentration which should ensure steels oxidation and protection in LBE should be around 10⁻⁸ % wt. in the range 200-400°C (according to Fig. 6.14) whereas the oxygen concentration monitored in the loop was around 10⁻¹² % wt. Assuming that the oxygen concentration was almost the same in the whole loop, such concentration has to be considered too low for an effective self-protection of structural steels in HLM experimental facility and future HLM-cooled reactor. Unfortunately, only the injection of Ar-3%H₂ gas mixture was available in the loop during the experiment and it was not possible to make any correction of the oxygen concentration with oxygen supply methods such as Ar-O₂ injection or PbO particles dissolution (PbO mass exchanger). Thus, a complete oxygen control system including both an oxygen removal and oxygen supply system (such as a PbO mass exchanger) will be implemented in the loop in future to balance the oxygen concentration to the correct value.

Effect of metal impurities on oxygen control

A careful observation of the trend in Fig. 6.21 revealed that the sensor electric potential was likely affected by metal/metal-oxide equilibria M/M_xO_y established in LBE as a consequence of the dissolution of steels. Dissolution products are due to corrosion phenomenon of loop steel walls as well as protective steel sheath of the oxygen sensor. Indeed, during the temperature variations from 400°C to 230°C the electric potential increased instead of providing electric potentials following a given oxygen iso-concentration line (see Fig. 6.19), meaning that oxygen consume was occurring for the formation of a metal-oxide M_xO_y .

The instauration of M/M_xO_y equilibria in HLMs is not surprising since dissolved metals such as Fe, Ni and Cr are prone to collect in the expansion vessel and float on the HLM free level when their concentrations reach or are close to the saturation level. During an experiment performed in LBE-cooled STELLA loop at CEA, Courouau demonstrated that the electric potential of oxygen sensors is strongly affected by dissolved metal impurities in the flowing LBE [8]. Such metal impurities are already present in the starting Pb alloy and their amount increases over time as a consequence of the corrosion of the loop walls as well as the corrosion of the protective sheath of the oxygen sensor [8].

Fig. 6.23 analyses the behaviour of the oxygen sensor in the time range 0-500 hours: the electric potential was represented as a function of temperature together with oxygen iso-concentration lines and Ni/NiO and Fe_3O_4 equilibria. Ni/NiO equilibrium was calculated considering the following reaction:



The oxygen concentration for the formation of NiO according to Eq. 6.1 was calculated as:

$$\ln C_{O,NiO}^{LBE} = \frac{\Delta G_{NiO}^\circ}{RT} + \ln C_{O,sat}^{LBE} + \ln a_{Pb} \quad (\text{if } a_{Ni} = 1) \quad \text{Eq. 6.2}$$

where standard Gibbs' free energy of formation ΔG_{NiO}° (in j/mol) related to Eq. 6.1 was calculated in the range 127-727°C using the thermodynamic data for NiO available in [9]:

$$\Delta G_{NiO}^\circ = -18009 - 11.8 \cdot T \quad \text{Eq. 6.3}$$

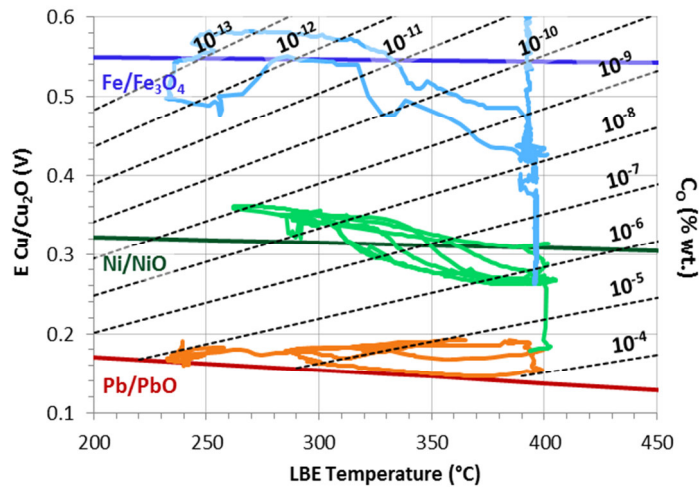
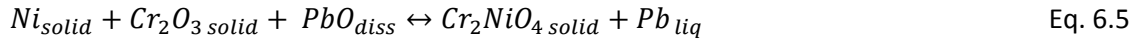
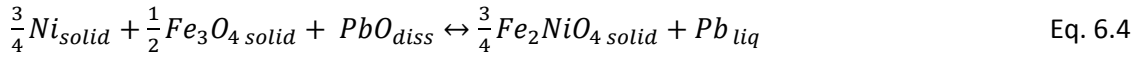


Fig. 6.23: Behaviour over time of Cu/Cu₂O sensor electric potential versus LBE temperature in NACIE-UP expansion vessel (orange 0-72 h, green 75-200 h, blue 200-500 h).

Observing Fig. 6.23, the oxygen sensor gave potential values in accordance with Pb/PbO equilibrium in the first 72 hours (orange line), so the oxygen concentration was at the solubility level or very close to it at the beginning. From 72 to 200 hours the monitored oxygen concentration decreased during the Ar-H₂ injection (green line). The subsequent temperature variation in the range 230-400°C revealed that the electric potential was likely affected by a M/M_xO_y equilibrium placed below the Fe/Fe_3O_4 equilibrium and slightly above the Ni/NiO one. From 200 to 500 hours, the oxygen concentration was significantly reduced at about 400°C (blue line). When the temperature was decreased down to 230°C, the sensor electric potential approximately followed the Fe/Fe_3O_4 equilibrium below 320°C, meaning that magnetite may have formed when Fe saturation in the expansion vessel occurred.

Assuming that only Ni, Fe and Cr elements were dissolved as a consequence of the corrosion process, the likely formation of Fe₂NiO₄ and Cr₂NiO₄ spinel oxides was considered to explain the behaviour of the electric potential in the time range 75-200 hours. Fe₂NiO₄ and Cr₂NiO₄ formation are expressed by the following reactions:



The oxygen concentration for the formation of Fe₂NiO₄ and NiCr₂NiO₄ according to Eq. 6.4 and Eq. 6.5 respectively is expressed as:

$$\ln C_{O,Fe_2NiO_4}^{LBE} = \frac{\Delta G_{Fe_2NiO_4}^\circ}{RT} + \ln C_{O,sat}^{LBE} + \ln a_{Pb} \quad (\text{if } a_{Ni} = 1) \quad \text{Eq. 6.6}$$

$$\ln C_{O,Cr_2NiO_4}^{LBE} = \frac{\Delta G_{Cr_2NiO_4}^\circ}{RT} + \ln C_{O,sat}^{LBE} + \ln a_{Pb} \quad (\text{if } a_{Ni} = 1) \quad \text{Eq. 6.7}$$

where $\Delta G_{Fe_2NiO_4}^\circ$ and $\Delta G_{Cr_2NiO_4}^\circ$ (in J/mol) related to Eq. 6.6 and Eq. 6.7 were calculated in the range 127-727°C by using the thermodynamic data for Fe₂NiO₄ and Cr₂NiO₄ available in [9]:

$$\Delta G_{Fe_2NiO_4}^\circ = -35113 + 4.5 \cdot T \quad \text{Eq. 6.8}$$

$$\Delta G_{Cr_2NiO_4}^\circ = -22746 - 5.2 \cdot T \quad \text{Eq. 6.9}$$

Fig. 6.24 shows in detail the trend of Cu/Cu₂O electric potential as a function of LBE temperature in the time range 72-200h with indication of Ni/NiO, Ni/Fe₂NiO₄ and Ni/Cr₂NiO₄ equilibria. The electric potential seems to follow the Fe₂NiO₄ formation equilibrium, which is more thermodynamically stable than NiO and the most stable among the two Ni spinel oxides. In particular, the electric potential seems to be in good agreement with the Ni/Fe₂NiO₄ equilibrium below 300°C whereas it seems to follow oxygen concentration corresponding to nickel iso-concentration lines ($C_{Ni} = C_{Ni,sat}$) between 250-300°C for higher temperatures, meaning that the spinel oxide may have formed only at low temperature when Ni saturation in the expansion vessel occurred. For the calculation of the nickel iso-concentration lines, the following equation was considered:

$$\ln C_{O,Fe_2NiO_4}^{LBE} = \frac{\Delta G_{Fe_2NiO_4}^\circ}{RT} + \ln C_{O,sat}^{LBE} - \frac{3}{4} \ln C_{Ni}^{LBE} + \frac{3}{4} \ln C_{Ni,sat}^{LBE} + \ln a_{Pb} \quad (a_{Ni} < 1) \quad \text{Eq. 6.10}$$

where nickel solubility was calculated using the following solubility equations from [3] valid in the temperature ranges 255-469°C and 469-900°C respectively:

$$\log C_{Ni,sat}^{LBE} = 4.32 - \frac{2933}{T} \quad \text{Eq. 6.11}$$

$$\log C_{Ni,sat}^{LBE} = 1.74 - \frac{1006}{T} \quad \text{Eq. 6.12}$$

To date, no experimental evidence of Fe₂NiO₄ formation in LBE was observed during the operation of HLM loops. Aerts suggested that Ni is likely prone to form Fe₂NiO₄ spinel oxide instead of NiO single oxide in LBE [10] but further investigations are needed to confirm the hypothesis of its formation (even if thermodynamically favoured).

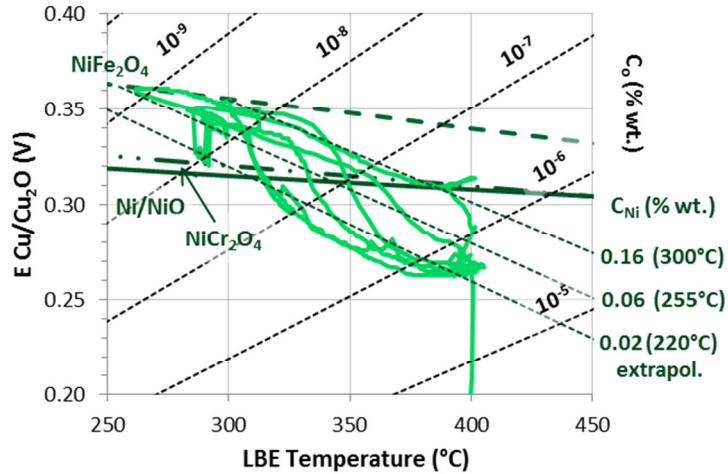


Fig. 6.24: Trend of Cu/Cu₂O sensor electric potential as a function of LBE temperature from 72h to 200h. Ni/NiO, Ni/Fe₂NiO₄ and Ni/Cr₂O₄ equilibria are plotted with oxygen iso-concentration lines and Ni iso-concentration lines from Ni/Fe₂NiO₄ equilibrium.

Beside the uncertainty on the possible formation of Fe₂NiO₄ in LBE during the NACIE-UP operation, the present analysis of the sensor electric potential revealed that oxygen-metal interactions may play a key role on the oxygen concentration control in HLM-cooled systems. Indeed, when cooling is applied to a HLM environment enriched with metal impurities (e.g. during the heat sink in the HX), significant oxygen depletion could be observed as a consequence of the formation and precipitation of a given metal-oxide. This phenomenon was already observed in the LBE corrosion loop CRAFT at SCK-CEN, where Fe₃O₄ dissolution/precipitation equilibrium was responsible of a significant oxygen depletion from 10⁻⁸ % wt. to 10⁻¹⁰ % wt. during some oxygen control tests [11]. This phenomenon is reflected in the oxygen sensor behaviour during NACIE-UP operation in the temperature range 230-400°C as well as during Cu/Cu₂O sensor testing in low oxygen LBE in small experimental capsules (see section 5.3.2), where oxygen concentration decrease due to very low amount of Fe impurity in the fresh LBE was observed and monitored in the temperature range 200-450°C.

6.4 CONCLUSIVE REMARKS

Various deoxygenation tests with Ar-H₂ gas mixtures were performed in HLM in different conditions of temperature, H₂ concentration, HLM amount and fluid-dynamic regime with the primary purpose to operate with low oxygen concentration and avoid PbO formation both in static (small capsules and HLM storage tank) and flowing condition (loop facility). The tests performed were very useful in identifying the factors influencing the deoxygenation process from a qualitative point of view.

The deoxygenation tests of small amount of Pb (750 g) in steel capsules gave preliminary interesting results. When the static melts were treated with gas with 3 % vol. of H₂, the deoxygenation process was apparently so slow that a good level of deoxygenation was not reached in reasonable times. To the opposite, deep and fast deoxygenation was obtained in the Pb using high H₂ concentrations in the gas (from 10 to 20 % vol.). To have gas mixtures with high H₂ concentration, a gas control system based on H₂ electrolytic generator was implemented to supply flexible gas mixtures in safe conditions. A similar gas control system was also implemented for the HLM deoxygenation in HELENA storage tank.

The deoxygenation tests in storage tank were performed with success in Pb (385 L) with different H₂ concentrations in the gas (from 4.8 to 26.7 % vol.) and two HLM temperatures (480 and 420°C). Here the gas flow rate was kept at high level (1 NL/min) to provide good HLM mixing even in static condition. As for tests performed in small capsules, the increase of H₂ concentration in the gas

promoted the deoxygenation reaction for a given temperature. In addition, a deoxygenation test in cover gas mode was performed to discriminate the effect of the HLM mixing. The comparative analysis of tests in the storage tank (bubbling and cover gas mode) and in the steel capsules (bubbling mode) seems to confirm that the deoxygenation process with H₂ gas is limited by poor HLM mixing (resistance in HLM phase). Indeed, successful HLM deoxygenation occurred in the storage tank even with low H₂ concentration (4.8 % vol.) and at low temperature (420°C).

Finally, a deoxygenation test in flowing condition was performed in LBE-cooled NACIE-UP loop facility (200 L) in the temperature range 200-400°C. For the purpose, an adequate LBE filling procedure in the primary loop was put in place to reduce the starting oxygen contamination ascribable to PbO in the HLM and O₂ gas traces in the system. Then injection of argon gas with 3 % vol. of H₂ was performed in the hot leg of the loop for 650 hours in the temperature range 230-400°C and the oxygen concentration over time monitored with Cu/Cu₂O oxygen sensor installed in the expansion vessel. A deep deoxygenation of the LBE occurred in 650 hours and a very low oxygen concentration of 10⁻¹² % wt. was achieved. The in-loop deoxygenation test confirmed the results obtained in small capsules and in HELENA storage tank: HLM deoxygenation with H₂ in static condition is limited by poor HLM mixing or turbulence and deep deoxygenation can be obtained even with low H₂ concentration in loop systems where HLM mixing is high. A deeper investigation accompanied by further experimental tests are anyway needed to confirm this interpretation also from a quantitative point of view. The in-loop deoxygenation showed also the need to implement a full oxygen control system which includes both oxygen removal device (such as the Ar-H₂ injection) and oxygen supply device (such as the Ar-O₂ injection or the PbO mass exchanger). A system so implemented will be able to balance correctly the oxygen concentration to the target level (around 10⁻⁸ % wt. for NACIE-UP loop) and correct any deviations. Finally, the analysis of the sensor output during the in-loop experiment showed that the sensor behaviour have been affected by dissolved metal impurities which are prone to collect in the expansion vessel. As local effects are expected in the expansion vessel as a consequence of the static condition, the installation of oxygen sensors also in other positions (e.g. the flowing leg) will be put in place in NACIE-UP loop to monitor an oxygen concentration representative of the whole loop.

The results about the deoxygenation in NACIE-UP loop with Ar-H₂ gas mixtures underlined the need of an oxygen supply device in addition to the oxygen removal one, in order to balance the oxygen concentration at the desired level. According to these results, NACIE-UP facility will be implemented in future with a gas control system able to supply both H₂ and O₂ for the oxygen balance.

6.5 REFERENCES

- [1] M.N. Arnol'dov, M.N. Ivanovskii , A.V. Milovidova, V.A. Morozov, "The permeability and solubility of hydrogen in a lead-bismuth melt of eutectic composition", *High Temperature* Vol. 42, No. 5 (2004) 715-719.
- [2] OECD/NEA, "Handbook on Lead-bismuth Eutectic Alloy and Lead Properties, Materials Compatibility, Thermal-hydraulics and Technologies", 2015.
- [3] B. Gonzalez Prieto, J. Lim, K. Rosseel, J. A. Martens, A. Aerts, "Polonium evaporation from liquid lead-bismuth eutectic with different oxygen content", *J Radioanal. Nucl. Chem.* 309 (2016) 597-605.
- [4] S. Gossé, "Thermodynamic assessment of solubility and activity of iron, chromium, and nickel in lead bismuth eutectic", *J. Nucl. Mater.* 449 (2014) 122-131.
- [5] J-L. Courouau, S. Sellier, F. Balbaud, K. Woloshun, A. Gessi, P. Schuurmans, M. Ollivier, C. Chabert, "Initial start-up operations chemistry analysis for MEGAPIE", 5th MEGAPIE Technical Review Meeting, 2004, Nantes, France.

- [6] I. Di Piazza, M. Angelucci, R. Marinari, M. Tarantino, N. Forgione, "Heat transfer on HLM cooled wire-spaced fuel pin bundle simulator in the NACIE-UP facility", *Nucl. Eng. Des.* 300, (2006) 256-267.
- [7] W. Ambrosini, M. Azzati, G. Benamati, G. Bertacci, L. Cinotti, N. Forgione, F. Oriolo, G. Scaddozzo, M. Tarantino, "Testing and qualification of CIRCE instrumentation based on bubble tubes", *J. Nucl. Mater.* 335 (2004) 293-298.
- [8] J.-L. Courouau, C. Chabert, L. Pignoly, L. Gicquel, K. Ginestar, L. Brissonneau, "Demonstration of the effect of impurities on the long term behaviour of electrochemical oxygen sensor during the STELLA 2006 tests", *Proceeding of the 1st International Workshop on Technology and Components of Accelerator Driven Systems*, 2010, Karlsruhe, Germany.
- [9] I. Barin, G. Platzki, "Thermochemical data of pure substances", 3rd Ed., Weinheim; New York: VCH, 1995.
- [10] A. Aerts, K. Gladinez, B. Gonzalez, J. Lim, G. Manfredi, A. Marino, K. Rosseel, "Sources of impurities and mass transfer in HLM", *ESNII+ Workshop on Coolant Quality Control, Physico-Chemistry & Dosimetry*, Oct. 2016, UJV Rez, Prague.
- [11] A. Aerts, S. Gavrilov, G. Manfredi, A. Marino, K. Rosseel, J. Lim, "Oxygen-iron interaction in liquid lead-bismuth eutectic alloy", *Phys. Chem. Chem. Phys.* 18 (2016), 19526-19530.

7. CONCLUSIONS AND FUTURE WORK

The present PhD thesis focused on the chemical behaviour of HLMS, which are candidate coolants in LFR and ADS systems. Specifically, the work focalized on the development and calibration of oxygen sensors for HLMS and the developed sensors were used to study the issue of the oxygen control via deoxygenation with H₂ containing gas. The sensors developed in this work gave also useful information about the oxygen interactions with metal impurities dissolved in the melt.

The **baseline study on different oxygen sensors** was performed to understand the effect of the type of reference system (Pt-air, Bi/Bi₂O₃, Cu/Cu₂O) as well as the solid electrolyte (YPSZ and YTSZ) used in the manufacturing. The performance of the reference system in terms of minimum reading temperature can be summarized as: Cu/Cu₂O (200°C) > Bi/Bi₂O₃ (290°C) > Pt-air (400°C). The use of YTSZ electrolyte instead of YPSZ allows a gain in the minimum reading thanks to the higher ionic conductivity. However, the lower mechanical resistance of YTSZ leads to prefer the use of YPSZ to have high service lifetime capability.

In parallel, an **oxygen sensor prototype**, 1 m long with Pt-air reference and YTSZ electrolyte, was developed for the **application in large HLM pool and storage tanks**. The calibration performed in liquid Pb in HLM storage tank showed good accuracy, no hysteresis in the range 380-450°C as well as satisfying tightness of the configuration at pressure near the atmospheric one. Tests in high over-pressure conditions are required and are going to be performed to assess if the tightness is maintained also during filling procedures in the facility. Furthermore, since the current oxygen sensor prototype is able to measure only down to 380°C, the implementation of the sensor with a new reference (such as Cu/Cu₂O) is going on to have detection capability at low temperature.

Concerning the **oxygen control in HLM**, deoxygenation tests **with Ar-H₂ gas mixtures** were performed in different conditions of temperature, H₂ concentration, HLM amount and fluid-dynamic regime (static and flowing). For this purpose, various tests were carried out first in small experimental capsules, then in HLM storage tank and finally into a loop facility. Gas mixtures with high H₂ concentrations were produced in-situ and safely, using an implemented gas control system based on H₂ electrolytic generator and successfully employed for HLM deoxygenation in experimental capsules and HLM storage tank. A deep deoxygenation was achieved in flowing condition inside NACIE-UP loop in Brasimone by injection of Ar-3%H₂ gas and thanks to adequate LBE filling procedures in the primary loop.

The **tests performed in experimental capsules, storage tank and NACIE-UP loop** were useful in identifying the factors influencing the deoxygenation process from a qualitative point of view. HLM temperature and H₂ concentration in the gas mixture promote the deoxygenation reaction and help in speeding-up the deoxygenation process in static HLM regime with poor mixing. When sufficient HLM mixing is ensured in the system (as in HLM loops), the deoxygenation process is fast enough even in presence of low H₂ concentrations and low HLM temperatures. The results so obtained indicated that the deoxygenation process of Pb with H₂ gas mixtures is characterized by resistance in the HLM phase and a deeper study is needed to confirm this interpretation from a quantitative point of view.

The in-loop experiments highlighted the need to implement an oxygen control system also with an oxygen supply device, to balance correctly the oxygen concentration in the HLM. In fact, a too low oxygen concentration for steel self-protection was achieved in NACIE-UP loop. Regarding this point, a **small pool facility called BID1** (Brasimone gas-Injection Device 1, containing ≈ 150 L of liquid Pb) was **conceptualized and designed with the purpose to investigate the various oxygen control methods**, among that the injection of O₂ containing gas as oxygen supply method. The experimental campaigns carried out in this new experimental facility will allow to investigate qualitatively and quantitatively the processes influencing the control of the oxygen concentration. Furthermore, the implementation

of a complete oxygen control system including Ar-H₂ and Ar-O₂ injection will be performed in NACIE-UP loop facility.

Finally, the analysis of the sensor electric potential during experiments in static and flowing HLM showed that the **sensor output is often affected by dissolved metal impurities**. In fact, during temperature variations the sensor electric potential tends to follow metal/metal-oxide equilibria rather than to follow oxygen iso-concentration lines. Since the formation of a given oxide involves the consumption of dissolved oxygen, such oxygen-metal interactions may have a fundamental role in the control of the oxygen concentration, arising issues in keeping constant the oxygen concentration in HLM-cooled systems. In this context, quantitative prediction of the impurities forming over time as a consequence of corrosion of piping and components, and subsequent plant implementation with cold traps and filters, has to be carried out to keep under control the amount of impurities in the HLM-cooled system.

LIST OF PUBLICATIONS

Papers

S. Bassini, A. Antonelli, I. Di Piazza, M. Tarantino, "Oxygen sensors for Heavy Liquid Metal coolants: Calibration and assessment of the minimum reading temperature", *J. Nucl. Mater.* 486 (2017) 197-205.

S. Bassini, I. Di Piazza, A. Antonelli, M. Angelucci, V. Sermenghi, G. Polazzi, M. Tarantino, "In-loop oxygen reduction in HLM thermal-hydraulic facility NACIE-UP", *submitted to Ann. Nucl. Energy*.

F. García Ferré, A. Mairov, D. Iadicicco, M. Vanazzi, S. Bassini, M. Utili, M. Tarantino, M. Bragaglia, F.R. Lamastra, F. Nanni, L. Ceseracciu, Y. Serruys, P. Trocellier, L. Beck, K. Sridharan, M.G. Beghi, F. Di Fonzo, "Corrosion and radiation resistant nanoceramic coatings for Lead Fast Reactors", *submitted to Corros. Sci.*

M. Carmona Gazquez, S. Bassini, T. Hernandez, M. Utili, "Al₂O₃ coating as barrier against corrosion in Pb-17Li", *submitted to Fusion Eng. Des.*

Conference Proceedings

S. Bassini, M. Tarantino, A. Antonelli, D. Martelli, "Design of an oxygen control system for CIRCE HLM pool", Proceedings of the SEARCH/MAXSIMA 2014 International Workshop, 7-10 October 2014, Karlsruhe, Germany.

F. García Ferré, A. Mairov, M. Vanazzi, S. Bassini, M. Utili, M. Tarantino, L. Ceseracciu, Y. Serruys, L. Beck, M.G. Beghi, K. Sridharan, F. Di Fonzo, "Ceramic coatings for innovative nuclear systems", Proceedings of NEA International Workshop on Structural Materials for Innovative Nuclear Systems, 11-14 July 2016, Manchester, UK.

S. Bassini, I. Di Piazza, A. Antonelli, M. Angelucci, V. Sermenghi, G. Polazzi, M. Tarantino, "In-loop oxygen reduction procedure in the HLM thermal-hydraulic facility NACIE-UP", *submitted to the 25th International Conference on Nuclear Engineering (ICONE-25)*, 2-6 July 2017, Shanghai, China.

D. Martelli, S. Bassini, M. Tarantino, I. Di Piazza, "CIRCE-ICE experimental activities in support of LMFR Design", *submitted to the 17th International Conference on Fast Reactors and Related Fuel Cycles: Next Generation Nuclear Systems for Sustainable Development (FR17)*, 26-29 June 2017, Yekaterinburg, Russian Federation.

Oral Contributions

S. Bassini, "Design of an oxygen control system for CIRCE HLM pool", SEARCH/MAXSIMA International Workshop, 7-10 October 2014, Karlsruhe, Germany.

S. Bassini, "Strategia per il controllo della chimica nei sistemi LFR. Stato attuale e futuri sviluppi", Workshop ADP ENEA-MiSE (PAR2013-LP2) "LFR-GEN IV: Stato attuale della tecnologia e prospettive di sviluppo", 15-16 January 2015, ENEA Bologna.

S. Bassini, "Prove di corrosione in piombo stagnante e fluente e controllo dell'ossigeno in impianti a piombo", Workshop ADP ENEA-MiSE (PAR2014-LP2) "LFR-GEN IV: Stato attuale della tecnologia e prospettive di sviluppo", 19-20 November 2015, ENEA Brasimone.

S. Bassini, "LFR: chemistry of liquid lead alloys (source of impurities, instrumentations for control)", ESNII+ Workshop on Coolant Quality Control, Physico-Chemistry & Dosimetry, 5-7 October 2016, ÚJV Řež, Prague.

S. Bassini, "Monitoring of oxygen impurity in HLM with potentiometric sensors", ESNII+ Workshop on Coolant Quality Control, Physico-Chemistry & Dosimetry, 5-7 October 2016, ÚJV Řež, Prague.

S. Bassini, "Cleaning of components of HLM facility", ESNII+ Workshop on Coolant Quality Control, Physico-Chemistry & Dosimetry, 5-7 October 2016, ÚJV Řež, Prague.

Poster

S. Bassini, A. Antonelli, I. Di Piazza, M. Tarantino, "Development of a Cu/Cu₂O Sensor for Oxygen Detection in Heavy Liquid Metals", 5th International Conference on Nuclear and Renewable Energy Resources (NURER 2016), 18-21 September 2016 Hefei, Anhui, China.

Project Deliverables

S. Bassini, "Prove di corrosione su materiali strutturali ricoperti in piombo stagnante", ADP ENEA-MiSE PAR2013, Deliverable Report RdS/PAR2013/069 (2014).

S. Bassini, "Concettualizzazione di un impianto per il monitoraggio del rateo di corrosione su materiali strutturali operanti in piombo", ADP ENEA-MiSE PAR2013, Deliverable Report RdS/PAR2013/070 (2014).

S. Bassini, "Prove di corrosione su materiali strutturali ricoperti in piombo stagnante in funzione del tenore di ossigeno", ADP ENEA-MiSE PAR2014, Deliverable Report RdS/PAR2014/098 (2015).

S. Bassini, "Report sulle prove di corrosione in piombo fluente mediante impianto LECOR", ADP ENEA-MiSE PAR2014, Deliverable Report RdS/PAR2014/099 (2015).

M. Tarantino, D. Martelli, S. Bassini, "Final report on oxygen control system for HLM large pool system", SEARCH 7th FP Project, Deliverable Report CI-T-R-152 (2015).

S. Bassini, M. Tarantino, D. Martelli, I. Di Piazza, "Final report on oxygen control system for large HLM pool systems", MAXSIMA 7th FP Project, Deliverable Report LR-D-S-233 (2016).

S. Bassini, "Studio di elementi metallici come oxygen getters per piombo liquido. Implementazione impianto di prova per la chimica del refrigerante BID1", ADP ENEA-MiSE PAR2015, Deliverable Report RdS/PAR2015/131 (2016).

S. Bassini, "Implementazione di un OCS per impianti a metallo liquido pesante", ADP ENEA-MiSE PAR2015, Deliverable Report RdS/PAR2015/132 (2016).